# Engineering microenvironments to control stem cell fate from 2D to 3D

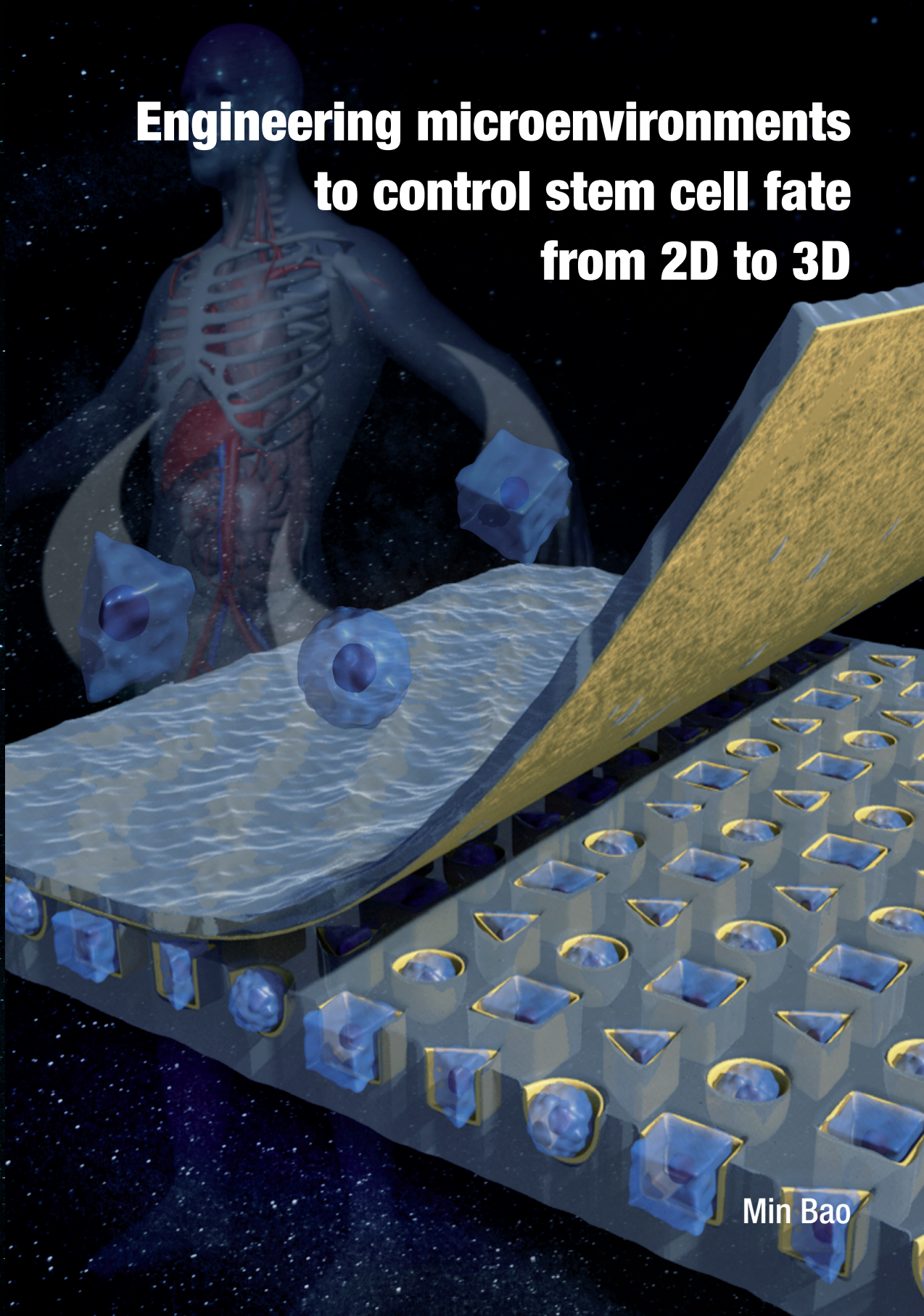

Min Bao

# Engineering microenvironments to control stem cell fate from 2D to 3D

Min Bao

The research presented in this thesis was performed at the Department of Physical-Organic Chemistry, Institute for Molecules and Materials(IMM), Radboud University, Nijmegen, The Netherlands. The described work was supported by Radboud Nanomedicine Alliance. Several of the presented chapters have been submitted or accepted for publication at different scientific journals. Therefore, minor stylistic differences might occur amongst chapters.

**ISBN**: 9789492679482

**Printed by**: Print Service Ede, The Netherlands
**Lay-out**: Print Service Ede
**Cover design:** Min Bao

# Engineering microenvironments to control stem cell fate from 2D to 3D

Proefschrift

ter verkrijging van de graad van doctor
aan de Radboud Universiteit Nijmegen
op gezag van de rector magnificus prof. dr. J.H.J.M. van Krieken,
volgens besluit van het college van decanen
in het openbaar te verdedigen op maandag 8 oktober 2018
om 16.30 uur precies

door

Min Bao
geboren op 29 mei 1990
te Anhui, China

**Promotor:**
Prof. dr. Wilhelm T.S. Huck

**Manuscriptcommissie:**
Prof. dr. Alessandra Cambi
Prof. dr. Erik Danen (Universiteit Leiden)
Dr. Julien Gautrot (Queen Mary University of London, Verenigd Koninkrijk)

**Paranimfen:**
Xinyu Hu
Jing Xie

# Engineering microenvironments to control stem cell fate from 2D to 3D

Doctoral Thesis

To obtain the degree of doctor
from Radboud University Nijmegen
on the authority of the rector magnificus prof. dr. J.H.J.M. van Krieken,
according to the decision of the Council of Deans
to be defended in public on Monday, October 8, 2018
at 16:30 hours

by

Min Bao
Born on May 29, 1990
in Anhui, China

**Supervisor**
Prof. dr. Wilhelm T.S. Huck

**Doctoral Thesis Committee**
Prof. dr. Alessandra Cambi
Prof. dr. Erik Danen (Leiden University)
Dr. Julien Gautrot (Queen Mary University of London, UK)

**Paranymphs:**
Xinyu Hu
Jing Xie

## Table of Contents

# Chapter 1

## Recent Advances in Engineering the Stem Cell Microniche in 3D

Parts of this chapter have been published as:
Bao, M., Xie, J., & Huck, W. T. Recent Advances in Engineering the Stem Cell Microniche in 3D." Advanced Science, **2018**, 1800448.

## Abstract

Conventional 2D cell culture techniques have provided fundamental insights into key biochemical and biophysical mechanisms responsible for various cellular behaviors, such as cell adhesion, spreading, division, proliferation and differentiation. However, 2D culture in vitro does not fully capture the physical and chemical properties of the native microenvironment. There is a growing body of research that suggests that cells cultured on 2D substrates differ greatly from those grown in vivo. In this review, we focus on recent progress in using bio-inspired 3D matrices that recapitulate as many aspects of the natural extracellular matrix as possible. We will review a range of techniques for the engineering of 3D microenvironment with precisely controlled biophysical and chemical properties, and the impact of these environments on cellular behavior. Finally, we provide an outlook on future challenges for engineering the 3D microenvironment and how such approaches would further our understanding of the influence of the microenvironment on cell function.

## 1.1 Introduction

In vivo, stem cells reside in a complex, specialized and dynamic microenvironment, or microniche"[1-5]. Although these microenvironments are extremely diverse, they share a number characteristic features of function and composition[6]. The microenvironment serves as a structural support for cells, but also offers various biochemical (e.g. cell-cell contact, cell adhesion sites and insoluble factors) and biophysical (e.g., topography, porosity and rigidity) cues that together regulate cell behavior, including cell spreading, migration, differentiation, and self-renewal.

The extracellular matrix (ECM), a key constitutive part of the microniche, plays an essential role in regulating cell behavior[7, 8], and supports cell or organ development, function and repair. The physical properties of the ECM (topography, porosity, rigidity) all impact on biological functions that are related to cell spreading, division, migration or tissue polarity. In addition, the ECM provides biochemical signaling cues that regulate cell phenotype (**Figure 1.1**).

Stem cells, including pluripotent stem cells (PSCs), embryonic stem cells (ESCs), mesenchymal stem cells (MSCs), hematopoietic stem cells (HSCs) and neural stem cells (NSCs), have been widely used for investigating fundamental interactions between cells and ECM, and have potential applications in translated regenerative medicine or stem cell therapy. Thus, controlling stem cell fate (the ability to maintain the stemness, or differentiate into different cell types) through engineered microniches is becoming particularly important in cell biology and tissue engineering field. Recently, numerous studies have shown that engineered microniches that mimic different aspects of the native stem cell niche can promote to maintain stem cell quiescence (which is necessary for long-term culture of stem cells to generate disease models),[9, 10] facilitate stem cell expansion (which is needed for stem cell delivery and stem cell therapy),[11] and regulate stem cell differentiation (which can be used for tissue engineered constructs).[12, 13]

In this review, we will discuss the role of the microniche in controlling cell function, with a specific emphasis on the importance of the role of the ECM. We will start with a short overview on different properties of the ECM that regulate cell fate, and then examine the differences between 2D and 3D cell culture. We will also provide an overview of the techniques used for investigating the interactions between ECM and stem cells in 3D, and discuss current advances toward designing 3D engineered niches.

## 1.2 The stem cell microniche

The stem cell niche consists of a myriad of interacting components (**Figure 1.1**), which may include the ECM, other cells, growth factors, and heterologous cell types (e.g., endothelial cells). These components provide biophysical and biochemical inputs that regulate cell behavior such as adhesion, spreading, migration, division, self-renewal, quiescence, and differentiation. This section reviews recent progress in studying the effect of different ECM properties on regulating cell fate determination and engineering approaches to control the stem cell microenvironment.

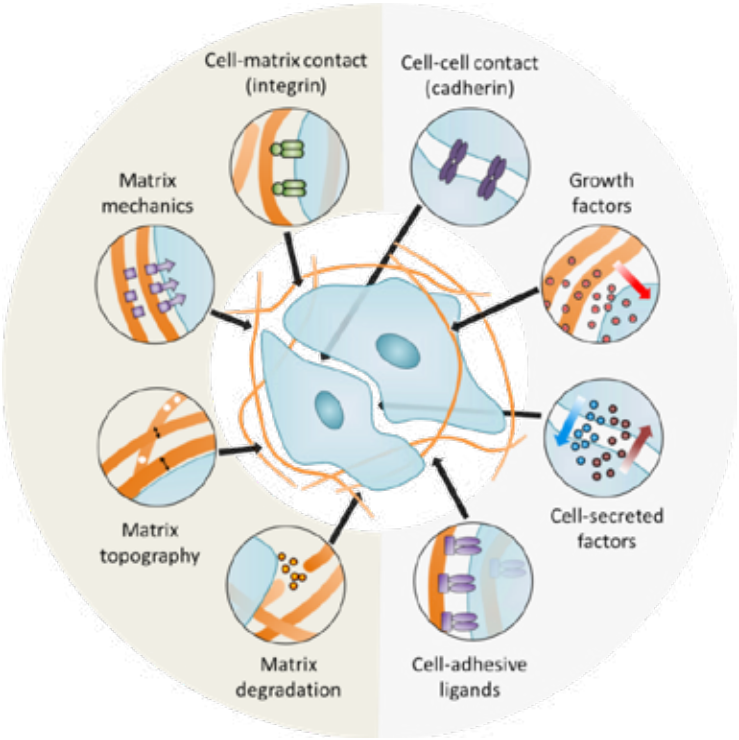


**Figure 1.1. Niche interactions known to modulate stem cell phenotype.** The biochemical composition, mechanical properties, and microstructure of the ECM are all known to modulate stem cell behavior, with optimal properties dependent on both the stem cell type of interest and the desired phenotypic output.

### 1.2.1 Extracellular matrix mechanics

The native ECM is a network of fibrillar proteins and polysaccharides that anchors cells within their specific microenvironment. Cells are mechanically coupled to the ECM through transmembrane proteins known as integrins[14]. These integrins bind specific cell-adhesive ligands presented by ECM proteins, connecting the ECM to the intracellular actin cytoskeleton. During cell spreading and growth, the ECM can be mechanically

deformed and remodeled by cells[15], the mechanical properties of the ECM alter the ability of cells to generate tension, modulating cell spreading, nuclear shape, and intercellular signaling pathways. Different types of mechanics can influence cell behavior in different ways, including bulk stiffness, local stiffness, strain-stiffening, and stress-relaxation.

### 1.2.1.1 Bulk Stiffness

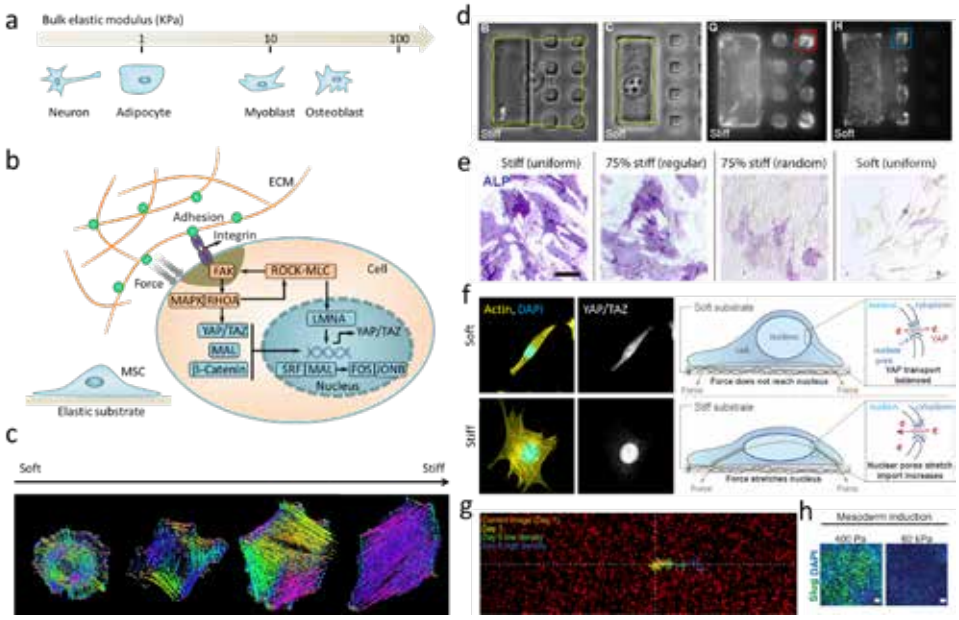


**Figure 1.2. Bulk stiffness regulates stem cell fate.** a) The differentiation of MSCs towards particular lineages is regulated by substrates with stiffness that is similar to native tissues. b) Mechanotransduction pathways inside cells regulate cell fates. c) Actin cytoskeleton organization depends on substrate stiffness. The different colors indicate different orientations of actin filaments[16]. d) A micropatterned platform that limits cells to a stiff region stimulates durotaxis[17]. e) Spatially patterned matrix elasticity directs stem cell differentiation[18]. f) Stiffness triggers nuclear YAP localization by regulating transport across nuclear pores[19]. g) Stiffness gradient affect cell migration, cells can migrate from soft to stiff[20]. h) Stiffness determines embryonic stem cell differentiation[21].

Substrate stiffness, typically characterized by the elastic, or Young's modulus, has emerged as one of the most important mechanical features in controlling cell fate. This means that cells can sense the resistance of the substrate (typically a hydrogel) towards deformation. Modifications to the bulk stiffness of ECM-coated hydrogels give rise to a range of responses in stem cells. On 2D substrates, mesenchymal stem cells typically show differentiation towards osteoblasts on stiff substrates while lineage selection on soft substrates favors adipocytes[12]. (**Figure 1.2a**).

During mechanotransduction, mechanical stimuli such as stretching, shear stress, or substrate rigidity, are converted into chemical signals that control cell fate[22]. Key

in this process are focal adhesions (FAs)[23] and cell-cell interactions (involving, among others, β1-integrin[14] and E-cadherin[24]), mechano-sensors (such as talin[22]) and nuclear signaling elements (for example, YAP/TAZ[25] and lamin A/C[26]), which together act to modify protein and gene expression profiles (**Figure 1.2b**). Until now, substrates with stiffnesses ranging from a few hundred Pa to MPa have been prepared in a range of model substrates, including natural material such as chitosan, hyaluronic acid, gelatin, alginate and agarose, or synthetic hydrogels such as PEG, PV, or polyacrylamide. Cells cultured on these hydrogels are responsive to the degree of stiffness by altering their adhesion, spreading, morphology, and migration characteristics. For instance, fibroblasts or endothelial cells cultured on a relatively stiff substrate (> 2–3 kPa) display significant spreading and generate greater actin stress fibers compared with those on a relatively soft substrate (< 2–3 kPa)[27]. The orientations of actin filaments strongly depends on substrate stiffness, with stiffer substrates can leading to more aligned actin filaments (**Figure 1.2c**)[16]. Cell spreading is also affected by stiffness, and by preparing a rigid domain of one large adhesive island, adjacent to a soft area of small adhesive islands grafted in an otherwise non-adhesive soft hydrogel, researchers have shown that cells spread and probe substrate stiffness by using filopodia extensions (**Figure 1.2d**)[17]. Matrix stiffness often shows local heterogeneities at different length scales within the natural niche[18, 28]. Chun et al. fabricated a hydrogel with regions of spatially varied and distinct mechanics, and they found that hMSCs cultured on hydrogels with higher concentrations of stiff regions, showed more spread, elongated cell morphologies, higher nuclear YAP localization, and higher osteoblast differentiation, indicating that local variations in the underlying substrate mechanical properties might regulate cell adhesion, spreading, and nuclear transcription effectors (**Figure 1.2e**)[18]. The effect of stiffness of cell function can often be related to the activity of certain nuclear transcription factors (Yes-associated protein, YAP/TAZ)[25], and it was shown recently that stiffer substrates give rise to nuclear flattening, thereby stretching nuclear pores, and reducing their mechanical resistance to molecular transport, and finally increasing YAP nuclear import and localization (**Figure 1.2f**)[19]. In addition, cell migration is also affected by stiffness[20, 29-31]. When subjected to a stiffness gradient, cells display directed migration toward stiffer regions. The anisotropic mechanical properties lead to directional epithelial growth and trigger cells to migrate at the direction where the stiffness is larger, a behavior termed durotaxis, which is considered to contribute to the repair of tissue (**Figure 1.2g**)[20]. It has been shown that matrix stiffness also guides the spreading and differentiation of embryonic stem cells (ESCs) (**Figure 1.2h**)[21], where softer substrates enhance mesoderm differentiation of human ESCs.

However, much of our knowledge about stiffness-induced stem cell differentiation on 2D cell cultures cannot be directly translated to a 3D environment. For example, it was recently reported that hMSCs encapsulated in a stiff crosslinked hyaluronic acid

hydrogel, showed reduced cell spreading and nuclear localization of YAP/ TAZ[32]. These results indicate that mechanotransduction signaling in a 3D environment is not merely regulated by bulk stiffness, but is sensitive to other parameters such as dimensionality and degradability of the gel.

### 1.2.1.2 Local microenvironments

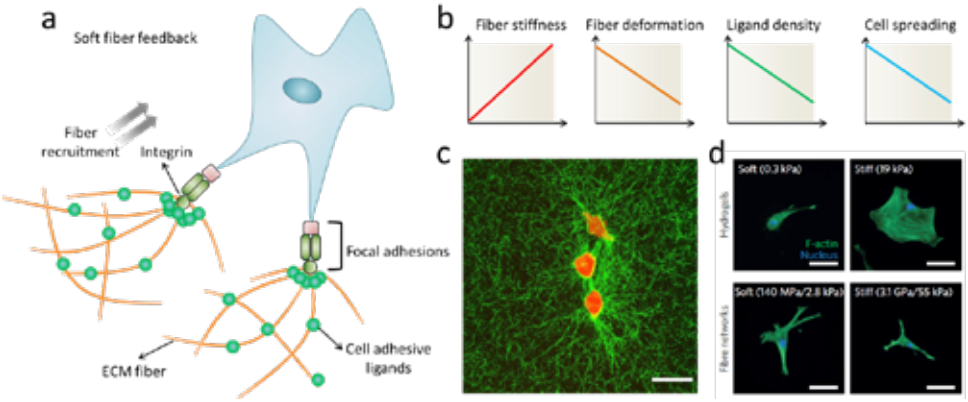


**Figure 1.3. Cells response to local fiber stiffness.** a) Schematic image shows how cell response to soft fibers. b) Soft local stiffness increases ability of cells to deform and recruit fibers, thus enhancing concentration of local ligand and activating FAs and related cellular signals to induce cell spreading. c) Cells deform collagen fibers to form bundled structure[33]. d) Cells failed to spread on substrate with low bulk stiffness, in contrast, increasing fiber stiffness suppressed cell spreading[34].

Since the local microenvironment is quite different from the bulk ECM, researchers have started to realize the importance of the local microenvironment of cells. Unlike bulk stiffness, where increased stiffness always promotes cell spreading, materials with soft local stiffness have greater flexibility in changing their conformations to optimize cell contact, and thereby inducing the formation of FAs and relevant cellular signals to trigger cell spreading (**Figure 1.3a**). If the fiber stiffness is higher, the transfer of cellular traction forces to nearby fibers will be limited. Consequently, cells are not able to build up sufficient tension, which may suppress cell spreading and migration (**Figure 1.3b**). The fibrous nature of the ECM creates a unique microenvironment that enables long range mechanical cell-cell communication via cell-induced remodeling of the network (**Figure 1.3c**)[33, 35-38]. Recently, Baker et al. fabricated a synthetic fibrous material with tunable fiber mechanics by using electrospinning. They found a critical role for fiber recruitment in the cellular response to fibrous materials, where lower fiber stiffness promoted cellular tension to deform and recruit surrounding fibers, greatly increasing the ligand density around the surface of cells, facilitating the formation of FAs and subsequent signaling events (**Figure 1.3d**)[34].

Cells are capable of sensing and responding to local mechanical properties in a 3D microenvironment. Recent efforts have focused on producing collagen materials with tunable properties. By controlling the collagen gelation temperature, collagen hydrogels of different fiber stiffnesses can be prepared[39-41]. Collagen fiber bundling and diameter can be increased by decreasing the gelation temperature, which results in increasing local fiber stiffness. It was shown that increased local fiber stiffness can withstand the repetitive contractile pulling at cell adhesion sites, which reinforces the stability of cellular adhesion and maturation of human foreskin fibroblasts[41]. By adding gold nanorods into collagen hydrogels, the nanoscale stiffness of the collagen hydrogel can be tuned without changing the bulk mechanical properties, and increased local collagen stiffness was shown to upregulate β1-integrin-mediated signaling pathways[42]. These emerging insights into how cells respond to local stiffness rather than bulk stiffness have critical implications for the development of new biomaterials for engineering the cell microenvironment in 3D.

### 1.2.1.3 Strain-stiffening

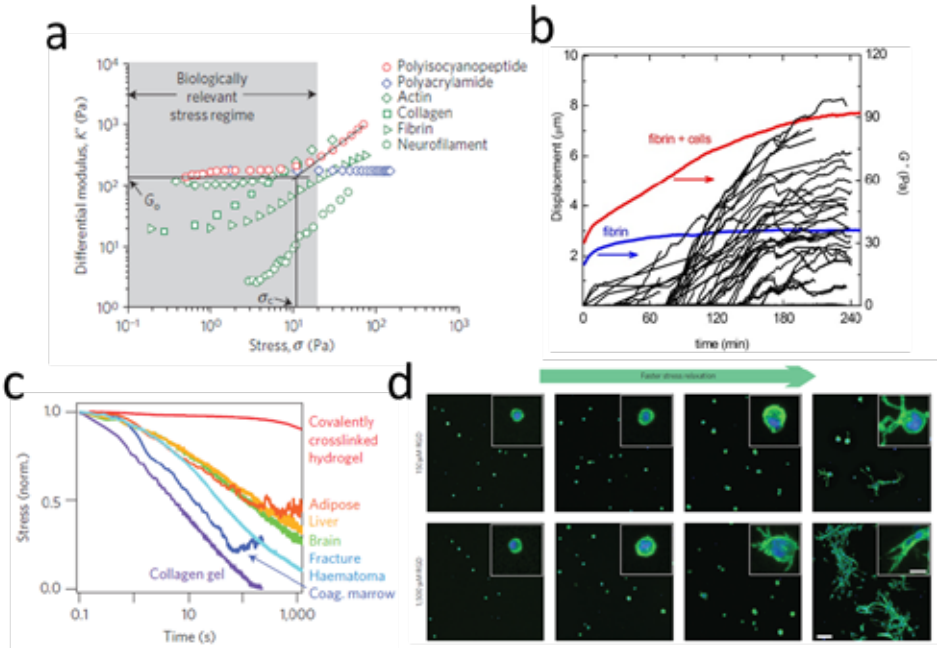


**Figure 1.4. Non-linear mechanical properties determine cell fate.** a) An overview of strain-stiffening properties for different materials[43]. b) Cells can generate cell traction forces to actively stiffen fibrin gel[44]. The traction strain was quantified by measuring the displacements of embedded fluorescent beads inside the fibrin hydrogel (black lines). The elastic modulus was measured by real time rheology (red line). The blue curve shows elastic modulus for a pure fibrin gel without cells. c) An overview of stress-relaxation properties for different materials (including hydrogels and tissues)[13]. d) Hydrogels with faster stress relaxation property can promote cell spreading and proliferation[13].

Many filamentous biopolymers (fibrin, F-actin, microtubules or vimentin) display nonlinear elasticity, typically strain stiffening (when the applied strain to the matrices is increased beyond the critical strain, the materials become stiffer with increasing strain) (**Figure 1.4a**). However, the effects of nonlinear elasticity mechanical properties on cell behavior have barely been studied. Recently, it was shown that hydrogels with nonlinear elasticity facilitate long-distance communication between cells[45], regulate the ways of 3D cell migration[46], and control stem cells differentiation[43]. For example, Janmey and co-workers demonstrated that fibroblasts and hMSCs displayed an elongated morphology when cultured on soft fibrin gels, indicating that the gels can be deformed by cell traction force, allowing access to the high strain moduli in the regimes of strain stiffening[45, 47]. Shear rheology measurements showed that the cells increased the stiffness of the fibrin gels (**Figure 1.4b**)[44]. In a recent study, hydrogels based on the polyisocyanopeptide (PIC) were produced with precisely controlled strain-stiffening behavior. The critical strain of the PIC hydrogels was increased by increasing the PIC polymer chain length, while the adhesion-ligand density and the stiffness of PIC bulk hydrogel were kept constant. When cells were cultured in 3D PIC hydrogels, hMSCs preferred to differentiate into osteoblasts when the critical strain was increased, a process apparently mediated by microtubule-associated protein DCAMKL[43]. Taken together, these results highlight the strain-stiffening property as an important element in fabricating 3D microenvironments.

#### 1.2.1.4 Stress relaxation

The natural ECM is not an ideal elastic solid. Most hydrogels and soft tissues that are based on biopolymers display viscoelastic (or dissipative) properties[48]. These hydrogels show stress relaxation (the stress decreases in response to the constant applied strain with increasing time) or creep (the strain increases in response to the constant applied stress with increasing time)[49, 50]. **Figure 1.4c** shows stress-relaxation tests for different materials, including hydrogels and native tissues. Living tissues all exhibit stress relaxation behavior. However, the effects of stress relaxation properties on cell behavior have often been overlooked. In recent years, a number of groups have designed hydrogels with tunable stress relaxation properties by changing the hydrogel composition or concentration[50], molecular weight[51], crosslink type or density[52], and degradation[53, 54]. Recent studies demonstrated that hydrogel stress relaxation properties could have significant effects on cell fate decisions. For example, Cooper-White et al. found that hMSCs morphology, proliferation and differentiation were influenced by modifications to substrate creep[55]. Chaudhuri et al. prepared alginate matrices with controllable viscoelastic or elastic features through covalent or ionic cross-linking, and it was found that when hMSCs encapsulated in the 3D alginate hydrogels with faster relaxation properties, showed enhanced spreading, proliferation and osteogenic differentiation. (**Figure 1.4d**). It is thought that integrin signaling, ECM ligand bundling, cell contractility, and nuclear YAP localization all play a role in these processes[13, 56].

Since most biopolymers show both stress-relaxation and strain-stiffening properties, it should be noted that changes in viscoelasticity and nonlinear elasticity are often coupled, which makes it difficult to decouple the two. Chaudhuri et al. found that collagen and fibrin hydrogels exhibited both stiffening and faster stress relaxation upon increasing the strain, an effect attributed to the dissolution of weak cross-links that are dependent on the force[57]. Thus, future studies are needed to engineer the 3D cell microenvironment with purely nonlinear elasticity or viscoelasticity behavior, and explore potential applications of these hydrogels in tissue engineering and regenerative medicine.

### 1.2.2 Surface receptors

Several recent papers have argued that mechanical feedback of the linkage between ECM substrate and cell surface receptors, could influence cell adhesion, spreading and differentiation[58-62]. For example, Trappmann et al. found that cell spreading and differentiation were unaffected by the stiffness of PDMS substrates, but was strongly dependent on the modulus of PAAm. The authors proposed that soft PAAm hydrogels were more porous than stiff gels and this will lead to differences in anchoring densities, thereby altering the mechanical feedback of the collagen[59]. Recently, Cavalcanti-Adam and Roca-Cusachs and coworkers developed a hydrogel with precisely controlled rigidity and nanometre-scale distribution of ECM ligands. They found that when cells were cultured on low-rigidity substrates, FAs formation could be upregulated by increasing the spacing between ligands, while on high-rigidity substrates, adhesion collapsed. Moreover, disordered ligand distribution on the substrates significantly increased the stability of adhesion formation, but reduced the rigidity threshold for adhesion collapse[62]. On the one hand, these results show that the precise nature of the mechanical properties of the link between cells and the substrate must be taken into account when designing substrates for regulating cell fate. On the other hand, cells are very complex systems, and how exactly insoluble physical cues from the cellular environment affect cell behavior, still poses a considerable challenge.

### 1.2.3 Degradability

Many natural materials, such as collagen or fibrin hydrogels, are enzymatically degradable, enabling cells to degrade and remodel their microenvironment. The effect of degradation has a significant effect on cell behavior, especially in 3D microenvironments. Lutolf and co-workers[63] highlighted the importance of matrix degradability in studies of cellular invasion into degradable and adhesive synthetic hydrogels. Khetan and Burdick[64] have shown that cell spreading was limited in hydrogels with a high density of non-degradable crosslinks. They further demonstrated that in 3D covalently crosslinked hyaluronic acid hydrogels, the differentiation of hMSCs was regulated by the generation of degradation-mediated cellular traction force, independent of matrix mechanics or cell morphology[65]. Heilshorn and colleagues recently investigated the effect of degradation and stiffness on neural progenitor cell stemness in a 3D hydrogel. The hydrogel was made from elastin like protein

and functioned with cell-adhesive peptide. By changing the protein concentration and crosslinking density, the stiffness and degradability of hydrogels could be independently tuned. They found that neural progenitor cell stemness did not depend on gel stiffness, but strongly related with degradability. Degradability could increase cell-mediated matrix remodelling and then enhance neural progenitor cell self-renewal and potency. This study provided an evidence for the important role of degradability in maintaining neural progenitor cell in 3D microenvironments[10]. These results highlight the important role of degradability in regulating cell fate. It should be noted thought that controlling the degradation kinetics and the formation of degradation byproducts remains challenging, especially since degradation leads to softening of the ECM, and thus making it harder to present cells with ECM of the right stiffness.

### 1.2.4 Confinement

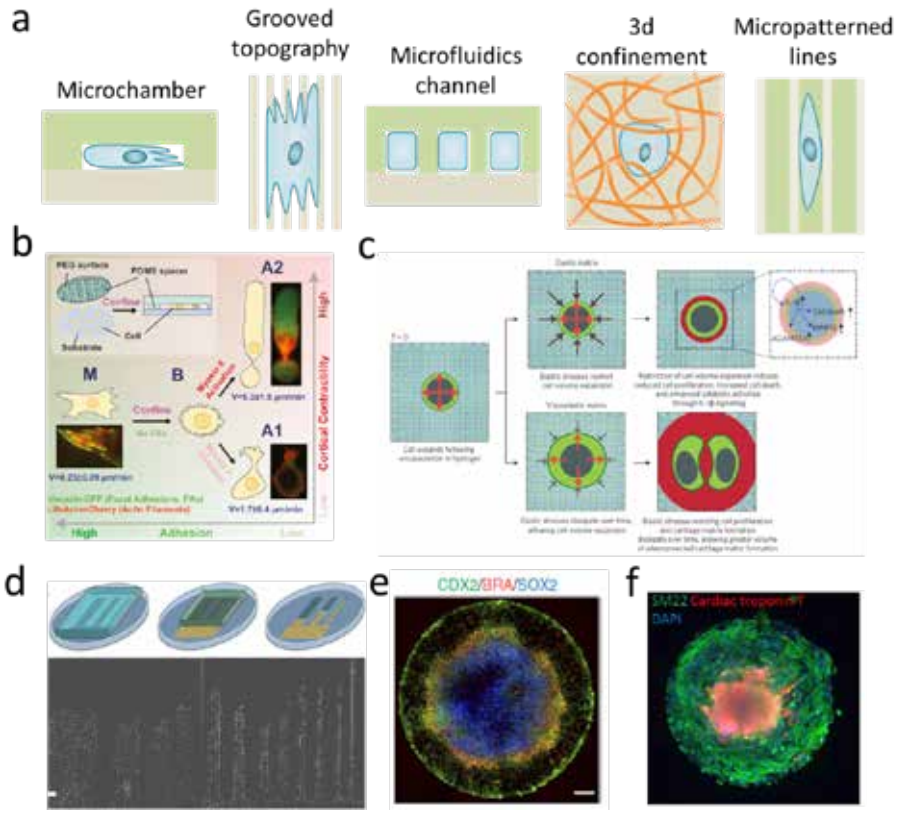


**Figure 1.5. The effect of confinement on cell behavior.** a) Schematics of engineered models of confining microenvironments. b) Cells migrate fast in confined environments because of low adhesion[66]. c) Mechanical confinement regulates cartilage matrix formation by chondrocytes[67]. d) Confinement affects cell migration[29]. e) Confinement environment is sufficient to induce self-organization of embryonic stem cells[68]. f) Geometric confinement induce self-organizing human cardiac microchambers[69].

Cells in the body are confined by other cells or by components of the ECM. Therefore, studying the cellular response to confinement is very important for fundamentally understanding the interactions between cells and the ECM. Recently, a lot of in vitro models, including microchambers, grooved substrates, microfluidic channels, microcontact printed substrates, and 3D hydrogels, have been engineered to study the effect of confined environment on cell spreading, migration and signaling[29, 30, 66-72] (**Figure 1.5a**).

Cell confinement has been used in a number of different studies, including, for example, studies into the relationship between cell cytoskeleton and cell polarity[30, 73, 74] and cell migration under confinement[72, 73, 75-78]. On 2D substrates, cells can form distinct FAs and stress fibers to spread and migrate. Conversely, cells in confined environments typically show fewer FAs and suppressed stress fiber formation[73]. Furthermore, cytoskeletal structures and nuclear elongation are aligned with the confining axis. For example, actin accumulation and stress fibers formation were suppressed under confinement environment, regardless of substrate stiffness[30, 73, 74, 78]. Confinement can also alter the type and morphology of cell adhesions. The homogeneous expression of pFAK and p-paxillin will be inhibited under increased confinement[73]. Similarly, when cells are limited to 1D fibronectin lines that are generated by microcontact printing, FAs will be distributed along the cell body[79]. Vinculin will be also homogeneously dispersed over the cell body in cells that are vertically confined[66]. (**Figure 1.5b**). By culturing cells in 3D hydrogels, Lee et al. found that when chondrocytes were cultured in hydrogels with slower stress-relaxation, cell volume expansion was limited by the spatial confinement, resulting in lower cell proliferation rate (**Figure 1.5c**)[67]. The influence of confinement on cell migration behavior has also been extensively studied. Cells migration in confinement is typically straight (**Figure 1.5d**)[29], and migration speed is significantly higher in microchannels than on 2D substrates[73, 80]. Fully confined cells display a sliding migration[66, 73, 81], but it remains unclear whether vertical and lateral confinement affect cell migration equally. Geometric confinement can also influence stem cell differentiation. For example, when human embryonic stem cells colonies were geometrically confined on circular Matrigel micropatterns, they reproducibly differentiated into an outer trophectoderm-like ring, an inner ectodermal circle and a ring of mesendoderm that expresses primitive-streak markers (**Figure 1.5e**)[68]. Ma et al. exploited confinement conditions to link spatial cell-fate specification and the formation of a beating 3D cardiac microchamber, which can be used to mimic certain aspects of early stage heart development (**Figure 1.5f**)[69]. Taken together, these studies clearly show that confinement gives rise to marked changes in the cellular cytoskeleton structure, cellular adhesion distributions, cell migration behavior and stem cell differentiation, indicating that cells are responsive to physical confinement.

### 1.2.5 Geometrical cues

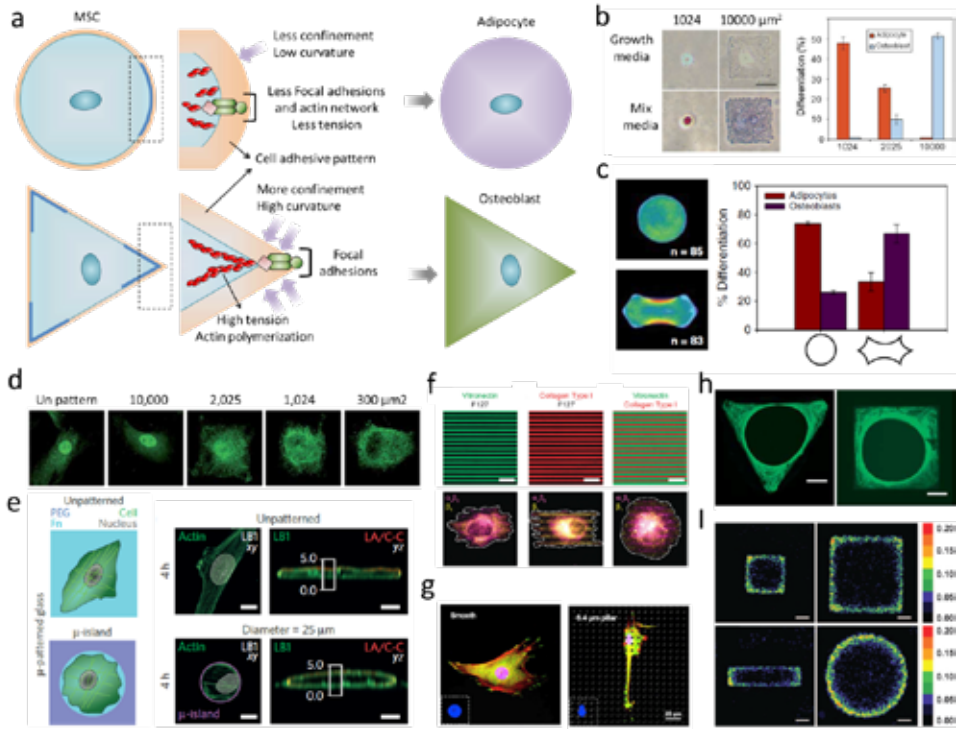


**Figure 1.6. The effect of geometry and topography on cell fate decisions.** a) Schematic image shows how cells sense sharp curvature. b) Cell spreading area determines stem cell differentiation[82]. c) Differentiation of hMSCs is determined by cell contractility triggered by different geometries[83]. d) Cell spreading area directs YAP/TAZ localization[25]. e) Cell spreading area determines nuclear lamin localization[26]. f) Substrates with spatially organized multiple adhesive ligands patterns can be used for investigating the effect of various integrin bindings on cell adhesion and migration[84]. g) With the increase of pillar height, nucleus was deformed, FAs and actin cytoskeletons were densely distributed around the micropillars and became obscure[85]. h) Geometry determines tissue growth rate[86]. I) Geometric cues affect cell proliferation rate[87].

In native tissue, different cell types vary greatly in their size and shape, and these geometrical cues are important factors in cell fate regulation. These influence of these cues can be studied by culturing cells on micro patterned ECM (for example, collagen, fibronectin, lamin, Matrigel) islands of defined geometries, which can be fabricated with various techniques, for example, micro-contact printing/stamping, microwells with different geometries and sizes, and cell printing. When culturing cells on these 2D ECM islands, the cells generate tension forces, and spread until they arrive at the island perimeter[88]. Cells prefer to generate larger tension at curvature, partially because of the confinement[89], and this will lead to upregulation of FAs and actin formation (**Figure 1.6a**). The molecular mechanism of cell-geometry-dependent regulation of differentiation have been elucidated in some cases[90]. A recent study suggested that cell geometry regulates

cell signaling via modulation of plasma membrane order. Changes in plasma membrane order due to geometric cues affect stem cell fate through a newly identified signaling mechanism involving the serine/threonine kinase Akt/protein kinase B (PKB)[91]. Studies on cell geometry have shown that cell fate can be guided between apoptosis, growth and differentiation by altering the extent to which the cell can physically expand and flatten (**Figure 1.6b**)[82, 92, 93]. Recent studies demonstrated that the differentiation of MSCs could be switched between osteoblast and adipocytes in a shape-dependent manner (**Figure 1.6c**)[83], which is partially dependent on the localization of YAP/TAZ (**Figure 1.6d**)[25, 94]. Cell geometry also plays a very important role in nuclear events. It has been shown that confining cells on patterned surfaces could significantly alter the structural organization of the nuclear lamina compared with cells on flat surfaces (**Figure 1.6e**)[26]. Substrate topography (e.g. grooves, steps, pits, etc.) also strongly controls MSC shape and lineage selection. For example, Desai et al. fabricated a substrate with spatially organized multiple adhesive ligands patterns, and found that cells can sense surface geometry by segregating single integrins on the surface of cells to regulate ECM-specific binding[84]. (**Figure 1.6f**) Cell geometry can also regulate nuclear geometry, which may generate a new way to control stem cell lineage commitment on the subcellular level[85, 95, 96] (**Figure 1.6g**). Apart from single cells, tissue growth is also strongly affected by the geometrical features of the matrix. Human epidermal stem cells seeded on 100-μm-diameter circular collagen-coated disks, self-assembled into a stratified microepidermis. Like the small islands that accommodate single cells, larger islands with a non-adhesive center still supported microepidermis assembly[97].

Cells in microtissues detect and respond to radii of curvature and when grown in polygonal channels, new tissue started in the corners (**Figure 1.6h**)[86]. The tissue in sharp corners (for example, triangular channel) was thicker than those in square and hexagonal channels, following the decrease of local curvature and indicating that increasing local curvature can increase the rate of proliferation (**Figure 1.6l**)[87]. Although the idea of 3D micropatterned systems is not novel, technical limitations of these endeavors have limited the feasibility of studying single cell behavior in 3D microenvironments. Recently, we demonstrate the first method to constrain stem cell size and geometry in a systematic and quantitative manner, by encapsulating cells in 3D hyaluronic acid hydrogel microniches[98]. This method differs from previous studies on 2D micropatterned substrates and microwells, as it can provide cells with a completely non-polarized microenvironment of precisely defined volume, and it also allows for rapid acquisition of confocal microscopy images on large numbers of individual cells in identical microenvironments. By using this method, we found that cytoskeletal organization in cells in 3D microniches has a preferred size and geometry. Furthermore, we found that key proteins and mRNA concentrations were diluted in larger cells.

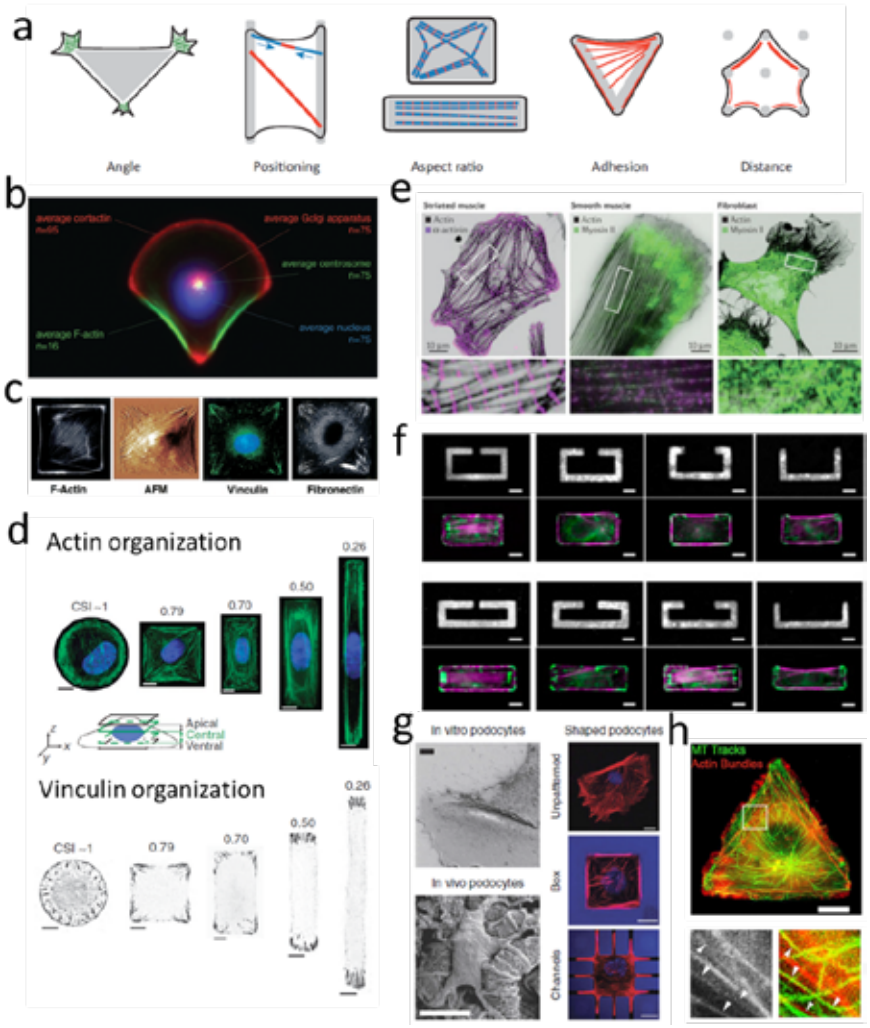


**Figure 1.7. The effect of geometrical cues on actin organization.** a) Schematic image showing how geometry directs cytoskeleton organization[99]. b) Organization of polarity is governed by cell adhesive microenvironment[100]. c) Organization of the stress fibers, FAs and ECM within cells on a patterned square ECM island[101]. d) Cell aspect ratio changes affect organization of actin stress fibres and FAs[102]. e) Actin, myosin II and α-actinin staining for different cell types[103]. f) Dissipation of elastic energy in severed stress fibers depends on fiber length[104]. g) (Left) SEM images show in vivo podocytes with branched structure; (Right) F-actin staining for cells cultured on glass, box, and microchannels[105]. h) Microtubule growth trajectories are correlated with F-actin bundles controlled by cell geometry[106].

Separate studies show that geometrical cues also affect the orientation of cell motility, initiated by the formation of actin filaments, lamellipodia and filopodia (**Figure 1.7a**)[99]. Polarity axes as defined by the internal and cortical cell asymmetry were controlled by the adhesive geometry (**Figure 1.7b**)[100]. When cells were cultured on ECM islands with square or rectangle geometry, FAs and actin stress fibers would be inclined to situate along the

cell's diagonal axes (**Figure 1.7c, d**)[101, 102]. The alignment of stress fibers and FAs is partially a result of actomyosin contractility (**Figure 1.7e**)[103]. Moreover, it was found that all fibers were connected to each other instead of being isolated and cell relaxation was induced by means of local ablation of one fiber (**Figure 1.7f**)[104]. The cell shape within tissue can reflect the past physical and chemical signals that the cells have run into, and the cellular phenotype can also be controlled by the cell shape information. Ron et al. used micro fabricated 3D biomimetic chips to demonstrate that 3D cell shape can control cell phenotype via cell tension(**Figure 1.7g**)[105]. In addition, it appears that the interplay between actin and microtubuli arrangement plays an important role in cell polarization. In cells spreading on either soft, ECM-coated gels, or stiff cadherin-modified substrates, the rearward actomyosin (partially) prevents microtubuli penetration at the leading edge on both soft and stiff substrates[106]. In contrast, when cells were allowed to spread unconstrained on stiff ECM-coated substrate, microtubuli aligned in parallel with actin stress fibers, and reached all the way to the leading edge of the cell(**Figure 1.7h**)[107].

A range of techniques have been used control geometric cues on substrates and study their influence on stem cells cultured on such substrates. However, challenges remain. Firstly, it is necessary to assess the influence of geometrical control, after long-term culture when the cells produce their own ECM and loose direct links with micro- or nanoscale geometrical cues. Secondly, it remains unclear whether findings on 2D substrates can be applied to 3D. Finally, the underlying molecular mechanisms by which cells sense and respond to the geometric cues, and how the mechanical properties of cells result in the cytoskeleton tension and contractility of cells, are not fully understood.

### 1.3 Taking dimensionality into consideration: from 2D to 3D

As mentioned above, different properties of ECM can be designed to regulate cell fate determination. However, most of these studies involved 2D platforms, which present, by necessity, grossly oversimplified environments compared to the in vivo 3D scenario. In 3D, cells form adhesive connections on all sides, providing an un-polarized environment for cells to grow. The polarized environment and extremely asymmetric distribution of adhesions on 2D substrates may lead to unnatural apical–basal cell polarity and corresponding alterations in cell functions. Besides, cell spreading and adhesion on 2D substrate are unlimited, which allows free spreading and migration of cells without any physical limits. Those fully embedded cells are sterically hindered when they spread and migrate as they are confined by the surrounding matrix. Cells must penetrate the matrix pores, or degrade the matrix around them, before spreading and migration become possible. On 2D substrates, the speed of migration is determined by the actin polymerization, integrin-mediated adhesion and myosin-mediated cellular contraction. However, in a 3D matrix, the contribution effectors to cell migration is very complex, involving, for example, the activation of the nuclear piston[108], local ECM stiffness[41], membrane tethered protease degradation[39, 109], the ability to squeeze

the nucleus through matrix pores[110], and microtubule dynamics[111]. As a result, the speed of cell migration and its response to stiffness are quite different in 2D compared to 3D. Furthermore, on 2D substrates, cell culture medium, soluble factor and cell-secreted factors can undergo free diffusion, whereas in 3D matrices, diffusion of oxygen, proteins and small molecules can be limited, resulting in gradients.

It is likely that cells cultured in 3D display behavior more relevant to in vivo conditions. Sudhir et al. demonstrated that when hMSCs were cultured in covalently crosslinked HA hydrogels, hMSCs differentiation was controlled by the generation of cellular traction forces mediated by hydrogel degradation, regardless of cell morphology and hydrogel stiffness. These outcomes emphasize the critical role of degradability in 3D as a parameter separate from the influence of cell morphology or substrate[65]. Recent efforts[112] on 3D tumor spheroids aimed at recapitulating the natural tumor microenvironment, showed that 3D tumor spheroids better mimic tumor cell development than traditional 2D monolayer models. Zernicka-Goetz's group has shown that by culturing embryonic and extraembryonic stem cells inside a 3D Matrigel, the cells self-organized into a synthetic embryo, whose development and structure were very similar to those of the natural embryo[113].

### 1.4 Technologies to engineer 3D stem cell niches

As discussed above, cells can sense and respond to myriad signals from their 3D microenvironment. Over the past decades, a wide range of sophisticated in vitro cell culture platforms have been developed that control the presentation of biochemical and mechanical cues in 3D. One of the key points to consider in the fabrication of a 3D environment for cells, is to allow oxygen and nutrients reach to the compartmentalized cells, while excreted waste products are released. A broad range of fabrication approaches have been employed to control cell-matrix and cell-cell interactions in 3D (**Figure 1.8**). In this section, we discuss recent work on bioengineering approaches for controlling interaction between cells and the microenvironment in 3D.

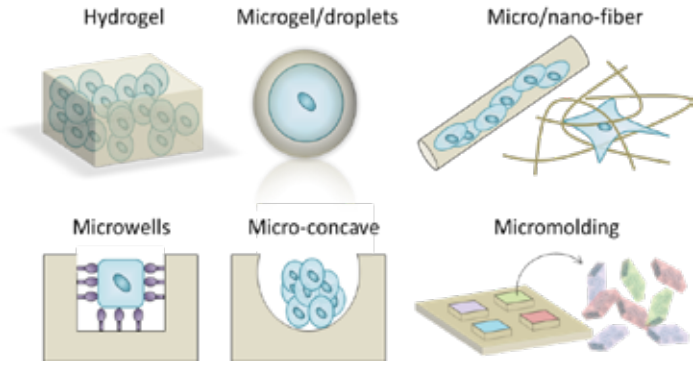


**Figure 1.8.** Schematic overview of the major methods used to achieve 3D cell culture

### 1.4.1 Hydrogel-based technology

Hydrogels, which are water-swollen crosslinked polymeric systems, can be prepared from a variety of natural biomaterials and synthetic polymers (**Table 1.1**), presenting a wide range of mechanical and chemical features. Many methods can be used to regulate the physical and chemical properties of hydrogels[6, 114-118].

Naturally-derived hydrogels for cell culture are mainly made of proteins and ECM elements, for example, collagen, fibrin, hyaluronic acid or Matrigel, as well as materials derived from other biological sources such as chitosan, alginate, gelatin, agarose or dextran. Most of these hydrogels are inherently biocompatible and bioactive since they are naturally-derived. Some of them (for example, collagen, fibrin and Matrigel) have binding sites for cells to interact with, and such interactions have some benefits for the viability, proliferation, cell migration, differentiation and remodeling of the gel matrix. However, hydrogels made from those natural materials have some disadvantages in isolating certain cell responses and determining exactly which signals are promoting cellular function. For example, Matrigel is comprised of entactin, laminin and collagen, but also contains a variable and uncharacterized fraction of growth factors. Furthermore, it is difficult to independently tune the physical and chemical properties for these natural hydrogels. For example, there is no way to regulate the stiffness of collagen or fibrin gels without changing the adhesive ligand density, pore size and porosity of the hydrogel. Finally, the shape and size of individual cells cannot be controlled inside hydrogels, and we cannot use hydrogels to make direct comparisons with the outcomes on 2D substrates.

Alternatively, hydrogels composed of synthetic polymers, for example PEG, can be used for long term cell culture, and allow for ECM deposition as they degrade, suggesting that synthetic gels can be used as 3D cell culture platforms, even there is no integrin-binding ligands. Hydrogels made from those synthetic materials are highly reproducible, the mechanical properties can be easily adjusted, and can be conveniently processed. However, they lack the endogenous factors that facilitate cell behavior. These synthetic scaffolds offer a minimalist approach with which the mammalian cells can be cultured in vitro for the purpose of clinical applications and the basic researches of cell physiology.

The ECM is a very dynamic system. To properly mimic the native ECM, some of its complexity (for example dynamics) must be taken into consideration when designing these hydrogels. Recently, instead of mimicking the static aspects of the cellular microenvironment, researchers started to adopt more dynamic hydrogels. External stimuli can be used to change the chemical and physical properties of hydrogels to better mimic the dynamic native cellular microenvironment. For instance, mechanically dynamic hydrogels that can be stiffened[119], softened[120], or reversibly stiffened and

**Table 1.1 Representative materials that can be used for 3D cell culture studies**

| Materials | Gelation method | Featured properties | Ref |
|---|---|---|---|
| | **Natural-derived materials** | | |
| Collagen | Raising the temperature and the pH can initiate collagen fibril self-assembly | Fibrous structure<br>Exhibits structural and mechanical properties (strain-stiffening) reminiscent of native tissues<br>Displays native cell adhesion ligands | 33, 36, 57, 74 |
| Fibrin | Thrombin can initiate self-assembly of insoluble polypeptide chains of fibrinogen into a fibrillar network | Fibrous structure<br>Enzymatically degradable<br>Strain-stiffening property | 44, 122 |
| Gelatin | Gelatin gel can be formed by lowing the temperature or photo-crosslinking (for methacrylated gelatin, GelMA) | Stiffness can be controlled<br>Enzymatically degradable | 123 |
| Alginate | Alginate hydrogels can be formed by cooperative binding with divalent cations such as $Ca^{2+}$ or $Ba^{2+}$ | Should be functioned with adhesive proteins for cell adhesion and spreading<br>Stress-relaxation property | 13, 67, 124 |
| Hyaluronic acid | Modified HA can form gels by photo-crosslinking or enzymatically crosslinking | It contains a high degree of chemical modification that enables considerable tunability | 65, 125, 126 |
| Chitosan | Gels can be formed by adjusting the pH | Excellent biocompatibility and immunostimulatory activities | 127 |
| Dextran | Dextran gels can be formed by chemically crosslinking | commercially available<br>Crosslinked dextran can be act as a microcarrier | 128 |
| Agarose | Cooling initiates the aggregation of double helices by the entanglement of anhydro bridges | Tunable elastic moduli<br>Viscoelastic properties | 129-131 |
| Matrigel | Gels can be formed irreversibly and rapidly between<br>24 °C and 37 °C | Gelling speed depends on the concentration and gelation temperature<br>A heterogeneous composition | 132 |
| | **Synthetic materials** | | |
| Polyethylene glycol (PEG) | PEG gels can be formed under both physiological pH and temperature | Can be engineered to present different adhesive ligands and to degrade via passive, proteolytic, or user-directed modes | 133 |
| Poly(vinyl alcohol) (PVA) | Modified PVA can form gels under photo-crosslinking | Satisfactory biocompatibility and sufficient mechanical properties | 134 |

softened[121], have been developed to investigate the effect of stiffness changes on cellular responses. These mechanically dynamic substrates enable us to study the effect of mechanical dosing on cell fate decisions, which is of particular interest for the mechanobiology community.

### 1.4.2 Microwell-based technology

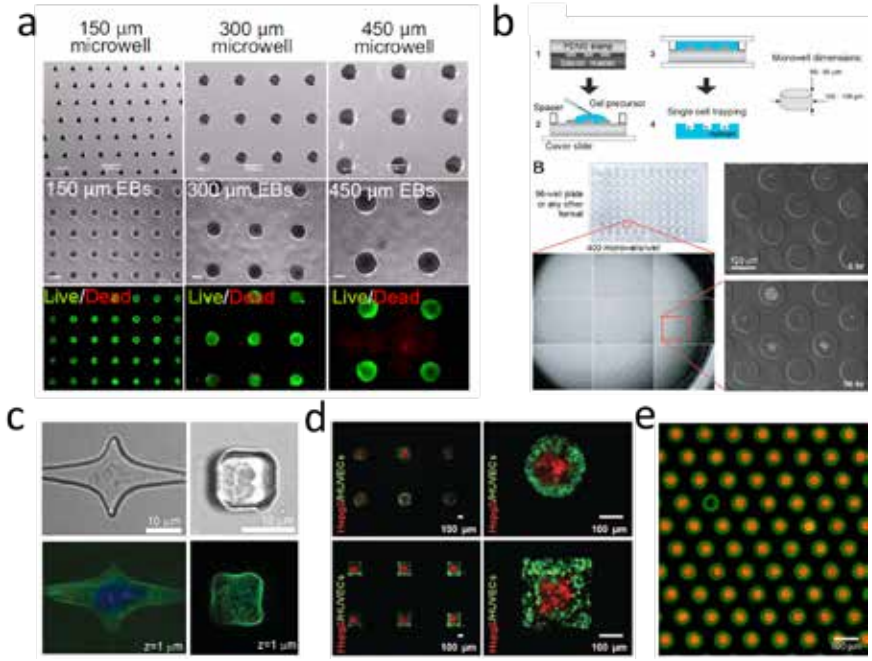


**Figure 1.9. Microwells in cell biology studies.** a) ES cells cultured in PEG microwells with different diameters for 7 days[71]. b) High-throughput platform based PEG microwells for investigating single cell fate[135]. c) Confocal images show cells cultured in PDMS microwells with different shapes[136]. d) Controlling spatial organization of multiple cell types in microwells with certain 3D geometries[137]. e) Microwells can be used for creating microparticle arrays with complex building blocks, green particles are assembled before red particles[138].

Microwells are a widely used and simple platform to structurally engineer the 3D cell microenvironment. Microwell arrays can be produced by means of direct etching into silicon, or by photolithography, or through molding of hydrogel materials using soft-lithography. Many different cell types (such as human hepatoblastoma cells, fibroblasts, adipose-derived stem cells, embryonic stem cells)[71, 139-141] can be cultured in microwells to form cell spheroids in a high-throughput manner. For example, embryonic stem cell aggregates can be formed inside microwells of different sizes (**Figure 1.9a**)[71]. People found that cardiogenesis was enhanced in larger embryoid bodies (for example, 450 µm in diameter), while the differentiation of endothelial cells was increased in smaller embryoid bodies (for example, 150 µm in diameter). These cell spheroids can be taken as components for bottom-up tissue engineering applications or serve as efficient 3D in vitro models for research on drug toxicity or cancer invasion. Lutolf *et al.*[135] modified and functionalized inside surfaces of microwells with different biomolecules to examine in vitro self-renewal of hematopoietic stem cells as well as the regulation of this process

by recombinant protein signals (**Figure 1.9b**). Furthermore, cell density, porosity and mechanics of the hydrogel as well as the concentration of coated ECM components can be combinatorically regulated in these microwells, which enables a study on the effect of cell-cell interactions as well as hydrogel stiffness on the fate of MSCs[142].

Changing the sizes and geometric features of microwells can provide tunable confined spaces for controlling cell differentiation. Moreover, by culturing cells in microwells, the influence of cell shape, substrate stiffness and dimensionality can be decoupled (**Figure 1.9c**). For example, Tsurkan et al.[143] fabricated microwells and microchannels with defined architectures using microlens array photopatterning technology, and they identified that neural precursor cell differentiation is dependent on the degree of spatial confinement. However, most reported microwell cultural systems are immobile, limiting their possibilities to actively operate encapsulated individual cells. Recently, microwells with varied dynamically adjustable geometries have been designed by using biocompatible polymers that are responsive to temperature, such as PCL[144]. The dynamic alterations in microwell geometries resulted in dramatically changes in the cytoskeletal architecture and differentiation patterns of stem cells. Halil et al. prepared dynamic microwells with tunable shape transformation properties under different temperatures by using poly(*N*-isopropylacrylamide), a thermo-responsive polymer. This feature was exploited to pattern multiple cell types at different temperatures in dynamic circular and square microwells[137]. (**Figure 1.9d**)

Cellular microwell arrays can provide high throughput platforms for deconstructing the multicomponent cues that regulate cell function, and can be used to create large-scale microparticle arrays with complex motifs[138] (**Figure 1.9e**). However, the limitation of using microwells for cell culture is that they are pseudo-3D models that cannot really mimic the in vivo 3D environment, therefore, more advanced and integrative technologies should be developed to engineer the biophysical microenvironment of cells.

### 1.4.3 Microgels-based technology

Inspired by observing different organs or tissues that consist of repetitive building blocks (think of hepatic lobules or nephron architecture), microgels have been fabricated for 3D cell encapsulation. To date, microgels have been fabricated with different shapes and sizes by using different methods. For example, a patterned photomask could be used to fabricate microgels with an array of shapes. By expanding this method, Fan et al.[145] presented a two-step method based on photolithography technology to encapsulate single neuron cells in gelatin microgels, and found that axonal circles formed in these hydrogel rings mimicking self-synapse diseases. Another common approach to create microgels involves the use of a micropatterned mold. For example, by using a patterned PDMS stamp, HA microgels containing the cells could be molded under UV crosslinking[146].

By using the same method, more complex 3D cell microenvironments over multiple size scales can be fabricated[147]. Recently, Ma et al. engineered a hyaluronic acid microgel that contains fibrinogen by using droplet-based microfluidics[148, 149]. The microgels serve as a 3D microenvironment for culturing of single hMSCs, and could be cultured up to 4 weeks with different stiffness (0.9–9.2 kPa)[150]. One recent study from Mooney's group[151] shows that by using microfluidic technology, single cells could be encapsulated in 3D alginate microgels, and cells remained viable in microgels over three days. It was found that the osteogenic differentiation of encapsulated cells was determined by the cell density or gel stiffness, and the work also demonstrated that by injecting the singly encapsulated marrow stromal cells intravenously into the mice, the clearance kinetics were postponed and the donor-derived soluble factors in vivo were maintained. Therefore, encapsulation of individual cells in microgels might be useful in the field of regenerative medicine applications and tissue design.

### 1.5 Content of the thesis

The interactions between cells and materials are dynamic and complex. Cells can sense a wide variety of signals provided by materials such as stiffness, topography, geometry and matrix ligand density, and then respond to these signals through multiple ways including mechanical forces exerted on the materials by the cells. Cells convert stimuli information through intracellular signal transduction cascades to modify gene expression and cell fate decisions. Recently, advances in micro-engineered biomaterials to direct stem cell fate decisions have focused on designing biomimetic materials that mimic the "in vivo" microenvironments' ability to interact with cells. However, designing tailored biomaterials that present multiple signals is challenging, especially since the precise roles of physical and biochemical cues in coordinating cellular processes such as spreading, proliferation, and differentiation remains difficult to dissect.

The natural extracellular matrix is made of a complex mixture of fibrillar proteins, where the architecture and mechanical properties of the protein fibrils vary considerably in various tissues. We use model collagen hydrogel systems in **Chapter 2** to study the importance of local microarchitecture in determinng cell behavior. Particularly we show how mechanical properties of collagen fibers affect stem cell differentiation.

In addition to mechanical properties, cell geometry and dimensionality is considered an important property of the cell microenvironment which direct cell fate decisions. In **chapter 3**, I first present a robust method to fabricate 3D microniches of controlled shape, size and tunable mechanical properties. We will then show how the volume and shape of single hMSCs can be controlled in these 3D microniches.

Our 3D microniches can provide cells with a completely non-polarized microenvironment

of precisely defined volume, and it also allows for rapid acquisition of confocal microscopy images on large numbers of individual cells in identical microenvironments. In **chapter 4**, I investigate how stem cell volume and shape in 3D regulate cell behavior including stress fiber formation, actomyosin activity, focal adhesion formation, nuclear structure, protein and mRNA level of mechanotransduction factors, and cell differentiation. I will show how cell volume plays a determinant role.

In addition to single cells studies, I also explore how multicellular architectures organize within geometrically well-defined 3D microniches. Morphogenesis, the self-organization of the embryo into geometrically organized tissues with three different germ layers, is a remarkable demonstration of biology's ability to organize matter in time and space. In **Chapter 5**, I will show how we can replicate this embryonic spatial ordering in vitro by using 3D microniches. By systematically modulating the shapes and aspect ratios of 3D microniches, we will explore how gradients of mechanical forces can drive patterning of lineages.

Finally, in **chapter 6**, I will provide a summary of this thesis, and an outlook for future work based on the achievements provided in this thesis.

## 1.6 References


1. Schofield, R. The relationship between the spleen colony-forming cell and the haemopoietic stem cell. *Blood cells* **4**, 7-25 (1978).
2. Morrison, S.J. & Spradling, A.C. Stem cells and niches: mechanisms that promote stem cell maintenance throughout life. *Cell* **132**, 598-611 (2008).
3. Voog, J. & Jones, D.L. Stem cells and the niche: a dynamic duo. *Cell stem cell* **6**, 103-115 (2010).
4. Scadden, D.T. The stem-cell niche as an entity of action. *Nature* **441**, 1075 (2006).
5. Spradling, A., Drummond-Barbosa, D. & Kai, T. Stem cells find their niche. *Nature* **414**, 98-104 (2001).
6. Huang, G. *et al.* Functional and Biomimetic Materials for Engineering of the Three-Dimensional Cell Microenvironment. *Chemical reviews* **117**, 12764-12850 (2017).
7. Rozario, T. & DeSimone, D.W. The extracellular matrix in development and morphogenesis: a dynamic view. *Dev. Biol.* **341**, 126-140 (2010).
8. Watt, F.M. & Huck, W.T. Role of the extracellular matrix in regulating stem cell fate. *Nat. Rev. Mol. Cell Biol.* **14**, 467-473 (2013).
9. Lay, K., Kume, T. & Fuchs, E. FOXC1 maintains the hair follicle stem cell niche and governs stem cell quiescence to preserve long-term tissue-regenerating potential. *Proc. Natl. Acad. Sci.* **113**, E1506-E1515 (2016).
10. Madl, C.M. *et al.* Maintenance of neural progenitor cell stemness in 3D hydrogels requires matrix remodelling. *Nat. Mater.* **16**, 1233 (2017).
11. Huebsch, N. *et al.* Matrix elasticity of void-forming hydrogels controls transplanted-stem-cell-mediated bone formation. *Nat. Mater.* **14**, 1269 (2015).
12. Engler, A.J., Sen, S., Sweeney, H.L. & Discher, D.E. Matrix elasticity directs stem cell lineage specification. *Cell* **126**, 677-689 (2006).
13. Chaudhuri, O. *et al.* Hydrogels with tunable stress relaxation regulate stem cell fate and activity. *Nat. Mater.* **15**, 326-334 (2016).
14. Wang, N., Tytell, J.D. & Ingber, D.E. Mechanotransduction at a distance: mechanically coupling the extracellular matrix with the nucleus. *Nat. Rev. Mol. Cell Biol.* **10**, 75-82 (2009).
15. Galbraith, C.G. & Sheetz, M.P. Forces on adhesive contacts affect cell function. *Curr. Opin. Cell Biol.* **10**, 566-571 (1998).
16. Gupta, M. *et al.* Adaptive rheology and ordering of cell cytoskeleton govern matrix rigidity sensing. *Nat. Commun.* **6** (2015).
17. Wong, S., Guo, W.-H. & Wang, Y.-L. Fibroblasts probe substrate rigidity with filopodia extensions before occupying an area. *Proc. Natl. Acad. Sci.* **111**, 17176-17181 (2014).
18. Yang, C. *et al.* Spatially patterned matrix elasticity directs stem cell fate. *Proc. Natl. Acad. Sci.* **113**, E4439-E4445 (2016).

19. Elosegui-Artola, A. *et al.* Force triggers YAP nuclear entry by regulating transport across nuclear pores. *Cell* **171**, 1397-1410. e1314 (2017).
20. Hadden, W.J. *et al.* Stem cell migration and mechanotransduction on linear stiffness gradient hydrogels. *Proc. Natl. Acad. Sci.* **114**, 5647-5652 (2017).
21. Przybyla, L., Lakins, J.N. & Weaver, V.M. Tissue mechanics orchestrate Wnt-dependent human embryonic stem cell differentiation. *Cell Stem Cell* **19**, 462-475 (2016).
22. Iskratsch, T., Wolfenson, H. & Sheetz, M.P. Appreciating force and shape [mdash] the rise of mechanotransduction in cell biology. *Nat. Rev. Mol. Cell Biol.* **15**, 825-833 (2014).
23. Critchley, D.R. Focal adhesions–the cytoskeletal connection. *Curr. Opin. Cell Biol.* **12**, 133-139 (2000).
24. Takeichi, M. Cadherins: a molecular family important in selective cell-cell adhesion. *Annu. Rev. Biochem.* **59**, 237-252 (1990).
25. Dupont, S. *et al.* Role of YAP/TAZ in mechanotransduction. *Nature* **474**, 179-183 (2011).
26. Ihalainen, T.O. *et al.* Differential basal-to-apical accessibility of lamin A/C epitopes in the nuclear lamina regulated by changes in cytoskeletal tension. *Nat. Mater.* **14**, 1252-1261 (2015).
27. Yeung, T. *et al.* Effects of substrate stiffness on cell morphology, cytoskeletal structure, and adhesion. *Cytoskeleton* **60**, 24-34 (2005).
28. Ma, H., Killaars, A.R., DelRio, F.W., Yang, C. & Anseth, K.S. Myofibroblastic activation of valvular interstitial cells is modulated by spatial variations in matrix elasticity and its organization. *Biomaterials* **131**, 131-144 (2017).
29. Vedula, S.R.K. *et al.* Emerging modes of collective cell migration induced by geometrical constraints. *Proc. Natl. Acad. Sci.* **109**, 12974-12979 (2012).
30. Pathak, A. & Kumar, S. Independent regulation of tumor cell migration by matrix stiffness and confinement. *Proc. Natl. Acad. Sci.* **109**, 10334-10339 (2012).
31. Saez, A., Ghibaudo, M., Buguin, A., Silberzan, P. & Ladoux, B. Rigidity-driven growth and migration of epithelial cells on microstructured anisotropic substrates. *Proc. Natl. Acad. Sci.* **104**, 8281-8286 (2007).
32. Caliari, S.R., Vega, S.L., Kwon, M., Soulas, E.M. & Burdick, J.A. Dimensionality and spreading influence MSC YAP/TAZ signaling in hydrogel environments. *Biomaterials* **103**, 314-323 (2016).
33. Kim, J. *et al.* Stress-induced plasticity of dynamic collagen networks. *Nat. Commun.* **8**, 842 (2017).
34. Baker, B.M. *et al.* Cell-mediated fibre recruitment drives extracellular matrix mechanosensing in engineered fibrillar microenvironments. *Nat. Mater.* **14**, 1262-1268 (2015).
35. Sarvestani, A.S. & Picu, C.R. Network model for the viscoelastic behavior of polymer

nanocomposites. *Polymer* **45**, 7779-7790 (2004).
36. Aghvami, M., Barocas, V. & Sander, E. Multiscale mechanical simulations of cell compacted collagen gels. *J. Biomech. Eng.* **135**, 071004 (2013).
37. Wang, H., Abhilash, A., Chen, C.S., Wells, R.G. & Shenoy, V.B. Long-range force transmission in fibrous matrices enabled by tension-driven alignment of fibers. *Biophys. J.* **107**, 2592-2603 (2014).
38. Xie, J., Bao, M., Bruekers, S.M. & Huck, W.T. Collagen gels with different fibrillar microarchitectures elicit different cellular responses. *ACS Appl. Mater. Interfaces* **9**, 19630–19637 (2017).
39. Wolf, K. *et al.* Physical limits of cell migration: control by ECM space and nuclear deformation and tuning by proteolysis and traction force. *J. Cell Biol.* **201**, 1069-1084 (2013).
40. Raub, C.B. *et al.* Noninvasive assessment of collagen gel microstructure and mechanics using multiphoton microscopy. *Biophys. J.* **92**, 2212-2222 (2007).
41. Doyle, A.D., Carvajal, N., Jin, A., Matsumoto, K. & Yamada, K.M. Local 3D matrix microenvironment regulates cell migration through spatiotemporal dynamics of contractility-dependent adhesions. *Nat. Commun.* **6**, 8720 (2015).
42. Li, Y. *et al.* AuNP–Collagen Matrix with Localized Stiffness for Cardiac-Tissue Engineering: Enhancing the Assembly of Intercalated Discs by β1-Integrin-Mediated Signaling. *Adv. Mater.* **28**, 10230-10235 (2016).
43. Das, R.K., Gocheva, V., Hammink, R., Zouani, O.F. & Rowan, A.E. Stress-stiffening-mediated stem-cell commitment switch in soft responsive hydrogels. *Nat. Mater.* **15**, 318-325 (2016).
44. Jansen, K.A., Bacabac, R.G., Piechocka, I.K. & Koenderink, G.H. Cells actively stiffen fibrin networks by generating contractile stress. *Biophys. J.* **105**, 2240-2251 (2013).
45. Winer, J.P., Oake, S. & Janmey, P.A. Non-linear elasticity of extracellular matrices enables contractile cells to communicate local position and orientation. *PloS one* **4**, e6382 (2009).
46. Petrie, R.J., Gavara, N., Chadwick, R.S. & Yamada, K.M. Nonpolarized signaling reveals two distinct modes of 3D cell migration. *J. Cell Biol.* **197**, 439-455 (2012).
47. Solon, J., Levental, I., Sengupta, K., Georges, P.C. & Janmey, P.A. Fibroblast adaptation and stiffness matching to soft elastic substrates. *Biophys. J.* **93**, 4453-4461 (2007).
48. Gong, Z. *et al.* Matching material and cellular timescales maximizes cell spreading on viscoelastic substrates. *Proc. Natl. Acad. Sci.*, 201716620 (2018).
49. Babaei, B., Abramowitch, S.D., Elson, E.L., Thomopoulos, S. & Genin, G.M. A discrete spectral analysis for determining quasi-linear viscoelastic properties of biological materials. *J. R. Soc. Interface* **12**, 20150707 (2015).
50. Okay, O. & Oppermann, W. Polyacrylamide– Clay Nanocomposite Hydrogels: Rheological and Light Scattering Characterization. *Macromolecules* **40**, 3378-3387 (2007).

51. Park, Y.D., Tirelli, N. & Hubbell, J.A. Photopolymerized hyaluronic acid-based hydrogels and interpenetrating networks. *Biomaterials* **24**, 893-900 (2003).
52. Zhao, X., Huebsch, N., Mooney, D.J. & Suo, Z. Stress-relaxation behavior in gels with ionic and covalent crosslinks. *J. Appl. Phys.* **107**, 063509 (2010).
53. Müller, C., Müller, A. & Pompe, T. Dissipative interactions in cell–matrix adhesion. *Soft Matter* **9**, 6207-6216 (2013).
54. Schultz, K.M., Kyburz, K.A. & Anseth, K.S. Measuring dynamic cell–material interactions and remodeling during 3D human mesenchymal stem cell migration in hydrogels. *Proc. Natl. Acad. Sci.* **112**, E3757-E3764 (2015).
55. Cameron, A.R., Frith, J.E. & Cooper-White, J.J. The influence of substrate creep on mesenchymal stem cell behaviour and phenotype. *Biomaterials* **32**, 5979-5993 (2011).
56. Lou, J., Stowers, R., Nam, S., Xia, Y. & Chaudhuri, O. Stress relaxing hyaluronic acid-collagen hydrogels promote cell spreading, fiber remodeling, and focal adhesion formation in 3D cell culture. *Biomaterials* **154**, 213-222 (2018).
57. Nam, S., Hu, K.H., Butte, M.J. & Chaudhuri, O. Strain-enhanced stress relaxation impacts nonlinear elasticity in collagen gels. *Proc. Natl. Acad. Sci.* **113**, 5492-5497 (2016).
58. Wen, J.H. *et al.* Interplay of matrix stiffness and protein tethering in stem cell differentiation. *Nat. Mater.* **13**, 979-987 (2014).
59. Trappmann, B. *et al.* Extracellular-matrix tethering regulates stem-cell fate. *Nat. Mater.* **11**, 642-649 (2012).
60. Choi, C.K.K. *et al.* Substrate coupling strength of integrin-binding ligands modulates adhesion, spreading, and differentiation of human mesenchymal stem cells. *Nano letters* **15**, 6592-6600 (2015).
61. Ye, K. *et al.* Matrix stiffness and nanoscale spatial organization of cell-adhesive ligands direct stem cell fate. *Nano letters* **15**, 4720-4729 (2015).
62. Oria, R. *et al.* Force loading explains spatial sensing of ligands by cells. *Nature* **552**, 219 (2017).
63. Lutolf, M. *et al.* Synthetic matrix metalloproteinase-sensitive hydrogels for the conduction of tissue regeneration: engineering cell-invasion characteristics. *Proc. Natl. Acad. Sci.* **100**, 5413-5418 (2003).
64. Khetan, S. & Burdick, J.A. Patterning network structure to spatially control cellular remodeling and stem cell fate within 3-dimensional hydrogels. *Biomaterials* **31**, 8228-8234 (2010).
65. Khetan, S. *et al.* Degradation-mediated cellular traction directs stem cell fate in covalently crosslinked three-dimensional hydrogels. *Nat. Mater.* **12**, 458-465 (2013).
66. Liu, Y.-J. *et al.* Confinement and low adhesion induce fast amoeboid migration of slow mesenchymal cells. *Cell* **160**, 659-672 (2015).

67. Lee, H.-p., Gu, L., Mooney, D.J., Levenston, M.E. & Chaudhuri, O. Mechanical confinement regulates cartilage matrix formation by chondrocytes. *Nat. Mater.* **16**, 1243 (2017).
68. Warmflash, A., Sorre, B., Etoc, F., Siggia, E.D. & Brivanlou, A.H. A method to recapitulate early embryonic spatial patterning in human embryonic stem cells. *Nat. Methods* **11**, 847-854 (2014).
69. Ma, Z. *et al.* Self-organizing human cardiac microchambers mediated by geometric confinement. *Nat. Commun.* **6** (2015).
70. Deglincerti, A. *et al.* Self-organization of human embryonic stem cells on micropatterns. *Nat. Protoc.* **11**, 2223-2232 (2016).
71. Hwang, Y.-S. *et al.* Microwell-mediated control of embryoid body size regulates embryonic stem cell fate via differential expression of WNT5a and WNT11. *Proc. Natl. Acad. Sci.* **106**, 16978-16983 (2009).
72. Tarle, V. *et al.* Modeling collective cell migration in geometric confinement. *Phys. Biol.* **14**, 035001 (2017).
73. Balzer, E.M. *et al.* Physical confinement alters tumor cell adhesion and migration phenotypes. *FASEB J.* **26**, 4045-4056 (2012).
74. Kraning-Rush, C.M., Carey, S.P., Lampi, M.C. & Reinhart-King, C.A. Microfabricated collagen tracks facilitate single cell metastatic invasion in 3D. *Integr. Biol.* **5**, 606-616 (2013).
75. Faure-André, G. *et al.* Regulation of dendritic cell migration by CD74, the MHC class II-associated invariant chain. *Science* **322**, 1705-1710 (2008).
76. Paul, C.D., Mistriotis, P. & Konstantopoulos, K. Cancer cell motility: lessons from migration in confined spaces. *Nat. Rev. Cancer* **17**, 131-140 (2017).
77. Irimia, D. & Toner, M. Spontaneous migration of cancer cells under conditions of mechanical confinement. *Integr. Biol.* **1**, 506-512 (2009).
78. Jiang, X., Bruzewicz, D.A., Wong, A.P., Piel, M. & Whitesides, G.M. Directing cell migration with asymmetric micropatterns. *Proc. Natl. Acad. Sci. U. S. A.* **102**, 975-978 (2005).
79. Doyle, A.D., Wang, F.W., Matsumoto, K. & Yamada, K.M. One-dimensional topography underlies three-dimensional fibrillar cell migration. *J. Cell Biol.* **184**, 481-490 (2009).
80. Stroka, K.M. *et al.* Water permeation drives tumor cell migration in confined microenvironments. *Cell* **157**, 611-623 (2014).
81. Rolli, C.G., Seufferlein, T., Kemkemer, R. & Spatz, J.P. Impact of tumor cell cytoskeleton organization on invasiveness and migration: a microchannel-based approach. *PLoS One* **5**, e8726 (2010).
82. McBeath, R., Pirone, D.M., Nelson, C.M., Bhadriraju, K. & Chen, C.S. Cell shape, cytoskeletal tension, and RhoA regulate stem cell lineage commitment. *Dev. Cell* **6**, 483-495 (2004).

83. Kilian, K.A., Bugarija, B., Lahn, B.T. & Mrksich, M. Geometric cues for directing the differentiation of mesenchymal stem cells. *Proc. Natl. Acad. Sci.* **107**, 4872-4877 (2010).
84. Desai, R.A., Khan, M.K., Gopal, S.B. & Chen, C.S. Subcellular spatial segregation of integrin subtypes by patterned multicomponent surfaces. *Integr. Biol.* **3**, 560-567 (2011).
85. Liu, X. *et al.* Subcellular cell geometry on micropillars regulates stem cell differentiation. *Biomaterials* **111**, 27-39 (2016).
86. Rumpler, M., Woesz, A., Dunlop, J.W., van Dongen, J.T. & Fratzl, P. The effect of geometry on three-dimensional tissue growth. *J. R. Soc. Interface* **5**, 1173-1180 (2008).
87. Nelson, C.M. *et al.* Emergent patterns of growth controlled by multicellular form and mechanics. *Proc. Natl. Acad. Sci. U. S. A.* **102**, 11594-11599 (2005).
88. Tan, K.Y. *et al.* Decoupling geometrical and chemical cues directing epidermal stem cell fate on polymer brush-based cell micro-patterns. *Integr. Biol.* **5**, 899-910 (2013).
89. Werner, M. *et al.* Surface curvature differentially regulates stem cell migration and differentiation via altered attachment morphology and nuclear deformation. *Adv. Sci.* **4** (2017).
90. Connelly, J.T. *et al.* Actin and serum response factor transduce physical cues from the microenvironment to regulate epidermal stem cell fate decisions. *Nat. Cell Biol.* **12**, 711 (2010).
91. von Erlach, T.C. *et al.* Cell-geometry-dependent changes in plasma membrane order direct stem cell signalling and fate. *Nat. Mater.*, 1 (2018).
92. Chen, C.S., Mrksich, M., Huang, S., Whitesides, G.M. & Ingber, D.E. Geometric control of cell life and death. *Science* **276**, 1425-1428 (1997).
93. Singhvi, R. *et al.* Engineering cell shape and function. *Science*, 696-696 (1994).
94. Totaro, A. *et al.* YAP/TAZ link cell mechanics to Notch signalling to control epidermal stem cell fate. *Nat. Commun.* **8** (2017).
95. Jain, N., Iyer, K.V., Kumar, A. & Shivashankar, G. Cell geometric constraints induce modular gene-expression patterns via redistribution of HDAC3 regulated by actomyosin contractility. *Proc. Natl. Acad. Sci.* **110**, 11349-11354 (2013).
96. Makhija, E., Jokhun, D. & Shivashankar, G. Nuclear deformability and telomere dynamics are regulated by cell geometric constraints. *Proc. Natl. Acad. Sci.* **113**, E32-E40 (2016).
97. Gautrot, J.E. *et al.* Mimicking normal tissue architecture and perturbation in cancer with engineered micro-epidermis. *Biomaterials* **33**, 5221-5229 (2012).
98. Bao, M., Xie, J., Piruska, A. & Huck, W.T. 3D microniches reveal the importance of cell size and shape. *Nat. Commun.* **8**, 1962 (2017).
99. Vignaud, T., Blanchoin, L. & Théry, M. Directed cytoskeleton self-organization.

*Trends Cell Biol.* **22**, 671-682 (2012).
100. Théry, M. *et al.* Anisotropy of cell adhesive microenvironment governs cell internal organization and orientation of polarity. *Proc. Natl. Acad. Sci.* **103**, 19771-19776 (2006).
101. Parker, K.K. *et al.* Directional control of lamellipodia extension by constraining cell shape and orienting cell tractional forces. *FASEB J.* **16**, 1195-1204 (2002).
102. Versaevel, M., Grevesse, T. & Gabriele, S. Spatial coordination between cell and nuclear shape within micropatterned endothelial cells. *Nat. Commun.* **3**, 671 (2012).
103. Murrell, M., Oakes, P.W., Lenz, M. & Gardel, M.L. Forcing cells into shape: the mechanics of actomyosin contractility. *Nat. Rev. Mol. Cell Biol.* **16**, 486-498 (2015).
104. Kassianidou, E., Brand, C.A., Schwarz, U.S. & Kumar, S. Geometry and network connectivity govern the mechanics of stress fibers. *Proc. Natl. Acad. Sci.*, 201606649 (2017).
105. Ron, A. *et al.* Cell shape information is transduced through tension-independent mechanisms. *Nat. Commun.* **8**, 2145 (2017).
106. Plestant, C. *et al.* Adhesive interactions of N-cadherin limit the recruitment of microtubules to cell–cell contacts through organization of actomyosin. *J. Cell Sci.* **127**, 1660-1671 (2014).
107. Huda, S. *et al.* Microtubule guidance tested through controlled cell geometry. *J. Cell Sci.* **125**, 5790-5799 (2012).
108. Petrie, R.J., Harlin, H.M., Korsak, L.I.T. & Yamada, K.M. Activating the nuclear piston mechanism of 3D migration in tumor cells. *J. Cell Biol.* **216**, 93-100 (2017).
109. Wolf, K. & Friedl, P. Extracellular matrix determinants of proteolytic and non-proteolytic cell migration. *Trends Cell Biol.* **21**, 736-744 (2011).
110. Irianto, J. *et al.* Nuclear constriction segregates mobile nuclear proteins away from chromatin. *Molecular biology of the cell* **27**, 4011-4020 (2016).
111. Watanabe, T., Noritake, J. & Kaibuchi, K. Regulation of microtubules in cell migration. *Trends Cell Biol.* **15**, 76-83 (2005).
112. Gu, L. & Mooney, D.J. Biomaterials and emerging anticancer therapeutics: engineering the microenvironment. *Nat. Rev. Cancer* **16**, 56-66 (2016).
113. Harrison, S.E., Sozen, B., Christodoulou, N., Kyprianou, C. & Zernicka-Goetz, M. Assembly of embryonic and extraembryonic stem cells to mimic embryogenesis in vitro. *Science* **356**, eaal1810 (2017).
114. Thiele, J., Ma, Y., Bruekers, S., Ma, S. & Huck, W.T. 25th Anniversary article: designer hydrogels for cell cultures: a materials selection guide. *Adv. Mater.* **26**, 125-148 (2014).
115. Peppas, N.A., Hilt, J.Z., Khademhosseini, A. & Langer, R. Hydrogels in biology and medicine: from molecular principles to bionanotechnology. *Adv. Mater.* **18**, 1345-1360 (2006).

116. Zhang, Y.S. & Khademhosseini, A. Advances in engineering hydrogels. *Science* **356**, eaaf3627 (2017).
117. Caliari, S.R. & Burdick, J.A. A practical guide to hydrogels for cell culture. *Nat. Methods* **13**, 405-414 (2016).
118. Annabi, N. *et al.* 25th anniversary article: Rational design and applications of hydrogels in regenerative medicine. *Adv. Mater.* **26**, 85-124 (2014).
119. Guvendiren, M. & Burdick, J.A. Stiffening hydrogels to probe short-and long-term cellular responses to dynamic mechanics. *Nat. Commun.* **3**, 792 (2012).
120. Kloxin, A.M., Kasko, A.M., Salinas, C.N. & Anseth, K.S. Photodegradable hydrogels for dynamic tuning of physical and chemical properties. *Science* **324**, 59-63 (2009).
121. Stowers, R.S., Allen, S.C. & Suggs, L.J. Dynamic phototuning of 3D hydrogel stiffness. *Proc. Natl. Acad. Sci.* **112**, 1953-1958 (2015).
122. Liu, J. *et al.* Soft fibrin gels promote selection and growth of tumorigenic cells. *Nat. Mater.* **11**, 734-741 (2012).
123. Zhao, X. *et al.* Photocrosslinkable gelatin hydrogel for epidermal tissue engineering. *Adv. Healthcare Mater.* **5**, 108-118 (2016).
124. Chaudhuri, O. *et al.* Substrate stress relaxation regulates cell spreading. *Nat. Commun.* **6**, 6365 (2015).
125. Kim, I.L., Khetan, S., Baker, B.M., Chen, C.S. & Burdick, J.A. Fibrous hyaluronic acid hydrogels that direct MSC chondrogenesis through mechanical and adhesive cues. *Biomaterials* **34**, 5571-5580 (2013).
126. Gerecht, S. *et al.* Hyaluronic acid hydrogel for controlled self-renewal and differentiation of human embryonic stem cells. *Proc. Natl. Acad. Sci.* **104**, 11298-11303 (2007).
127. Lee, S. *et al.* Enhanced therapeutic neovascularization by CD31-expressing cells and embryonic stem cell-derived endothelial cells engineered with chitosan hydrogel containing VEGF-releasing microtubes. *Biomaterials* **63**, 158-167 (2015).
128. Trappmann, B. *et al.* Matrix degradability controls multicellularity of 3D cell migration. *Nat. Commun.* **8**, 371 (2017).
129. Balgude, A., Yu, X., Szymanski, A. & Bellamkonda, R. Agarose gel stiffness determines rate of DRG neurite extension in 3D cultures. *Biomaterials* **22**, 1077-1084 (2001).
130. Rivron, N.C. *et al.* Tissue deformation spatially modulates VEGF signaling and angiogenesis. *Proc. Natl. Acad. Sci.* **109**, 6886-6891 (2012).
131. Wood, D.K., Weingeist, D.M., Bhatia, S.N. & Engelward, B.P. Single cell trapping and DNA damage analysis using microwell arrays. *Proc. Natl. Acad. Sci.* **107**, 10008-10013 (2010).
132. Poincloux, R. *et al.* Contractility of the cell rear drives invasion of breast tumor cells in 3D Matrigel. *Proc. Natl. Acad. Sci.* **108**, 1943-1948 (2011).
133. Tibbitt, M.W. & Anseth, K.S. Hydrogels as extracellular matrix mimics for 3D cell culture. *Biotechnol. Bioeng.* **103**, 655-663 (2009).

134. Schmedlen, R.H., Masters, K.S. & West, J.L. Photocrosslinkable polyvinyl alcohol hydrogels that can be modified with cell adhesion peptides for use in tissue engineering. *Biomaterials* **23**, 4325-4332 (2002).
135. Lutolf, M.P., Doyonnas, R., Havenstrite, K., Koleckar, K. & Blau, H.M. Perturbation of single hematopoietic stem cell fates in artificial niches. *Integr. Biol.* **1**, 59-69 (2009).
136. Ochsner, M. *et al.* Micro-well arrays for 3D shape control and high resolution analysis of single cells. *Lab Chip* **7**, 1074-1077 (2007).
137. Tekin, H. *et al.* Controlling spatial organization of multiple cell types in defined 3D geometries. *Adv. Mater.* **24**, 5543-5547 (2012).
138. Kim, J.J., Bong, K.W., Reátegui, E., Irimia, D. & Doyle, P.S. Porous microwells for geometry-selective, large-scale microparticle arrays. *Nat. Mater.* **16**, 139 (2017).
139. Khademhosseini, A. *et al.* Co-culture of human embryonic stem cells with murine embryonic fibroblasts on microwell-patterned substrates. *Biomaterials* **27**, 5968-5977 (2006).
140. Bernard, A.B., Lin, C.-C. & Anseth, K.S. A microwell cell culture platform for the aggregation of pancreatic β-cells. *Tissue Eng. Part C* **18**, 583-592 (2012).
141. Fukuda, J. *et al.* Micromolding of photocrosslinkable chitosan hydrogel for spheroid microarray and co-cultures. *Biomaterials* **27**, 5259-5267 (2006).
142. Gobaa, S. *et al.* Artificial niche microarrays for probing single stem cell fate in high throughput. *Nat. Methods* **8**, 949-955 (2011).
143. Tsurkan, M.V. *et al.* Photopatterning of multifunctional hydrogels to direct adult neural precursor cells. *Adv. Healthcare Mater.* **4**, 516-521 (2015).
144. Gong, T. *et al.* Dynamically tunable polymer microwells for directing mesenchymal stem cell differentiation into osteogenesis. *J. Mater. Chem. B* **3**, 9011-9022 (2015).
145. Fan, Y., Xu, F., Huang, G., Lu, T.J. & Xing, W. Single neuron capture and axonal development in three-dimensional microscale hydrogels. *Lab Chip* **12**, 4724-4731 (2012).
146. Khademhosseini, A. *et al.* Micromolding of photocrosslinkable hyaluronic acid for cell encapsulation and entrapment. *J. Biomed. Mater. Res. Part A* **79**, 522-532 (2006).
147. Eng, G. *et al.* Assembly of complex cell microenvironments using geometrically docked hydrogel shapes. *Proc. Natl. Acad. Sci.* **110**, 4551-4556 (2013).
148. Ma, S. *et al.* Monodisperse collagen–gelatin beads as potential platforms for 3D cell culturing. *J. Mater. Chem. B* **1**, 5128-5136 (2013).
149. Ma, S. *et al.* Fabrication of Microgel Particles with Complex Shape via Selective Polymerization of Aqueous Two-Phase Systems. *Small* **8**, 2356-2360 (2012).
150. Ma, Y., Neubauer, M.P., Thiele, J., Fery, A. & Huck, W. Artificial microniches for probing mesenchymal stem cell fate in 3D. *Biomater. Sci.* **2**, 1661-1671 (2014).
151. Mao, A.S. *et al.* Deterministic encapsulation of single cells in thin tunable microgels for niche modelling and therapeutic delivery. *Nat. Mater.* **16**, 236 (2017).

# Chapter 2

## Physical cues from the fibrillar microenvironment of collagen gels impact on cell behavior

This chapter has been published in:
Xie, J.[†], Bao, M.[†], Bruekers, S.M. & Huck, W.T. Collagen gels with different fibrillary microarchitectures elicit different cellular responses. ACS Applied Materials & Interfaces, **2017**, 9(23), 19630–19637. ([†]equally contribution)

## Abstract

The extracellular matrix consists of a complex mixture of fibrillar proteins, where the architecture and mechanical properties of the protein fibrils vary considerably in various tissues. How the mechanical properties of these fibers impact on cellular behavior is poorly understood, not least because most studies into mechanotransduction are carried out on flat, homogeneous hydrogel materials. In this chapter, we systematically polymerized collagen gels at different temperatures, providing substrates with tunable mechanics and defined local micro-architecture. We studied the dependence of spreading dynamics, proliferation, migration and differentiation of human mesenchymal stem cells (hMSCs) on the fibrillar properties as compared to the bulk properties of the matrix. We found that high fiber stiffness together with limited connectivity between bundles due to short fiber lengths limited the transfer of cellular traction forces to nearby fibers, resulting in cells devoid of long-range and continuous force transmission, and suppressed cell spreading, proliferation and migration. Cells on such fibers also showed limited focal adhesion formation. Our results indicated that fiber recruitment dynamically increased collagen density around cells and promoted cell spreading, proliferation, migration and osteogenic differentiation. Morphological characterization of cells indicates that the cellular response to the changes in substrate properties are mediated through upregulation of focal adhesions formation and related signaling pathways. Such insight contributes to the further elucidation of the mechanotransduction process as well as to the design and development of biomimetic environments for tissue engineering applications.

## 2.1 Introduction



Cells can sense and transduce physical properties of the extracellular matrix (ECM) into intercellular signals which can further influence cell response[1-5]. Significant progress has been made in understanding these mechanosensing and mechanotransduction processes by studying cells on flat hydrogel substrates with tailored mechanical properties[2, 6-9]. However, what cells are actually sensing, especially in the context of the native fibrillar ECM, has remained elusive[10-12]. The native ECM is a complex and heterogeneous system, making it very difficult to correlate specific materials properties of the ECM to cellular responses. Furthermore, as the ECM is composed of fibrous proteins (e.g., collagen, elastin, fibronectin and laminin)[13, 14], there is often a much higher local stiffness (~1 MPa at the individual-fiber level) compared to the bulk matrix (~100 Pa at the bulk-matrix level)[15, 16].

Baker et al.[17] recently designed a synthetic fibrous material with tunable mechanics and user-defined architecture, that mimics key aspects of the fibrillar nature of the ECM. They found that lower fiber stiffness permitted cellular forces to recruit nearby fibers, thereby dynamically increasing ligand density at the cell surface and promoting the formation of focal adhesions (FAs) and related signaling. In contrast, networks of stiff fibers seemed to limit cell spreading. This is somewhat counterintuitive to the generally accepted notion that cells on softer surfaces often form fewer FAs and spread much less compared to stiff substrate. Baker et al. highlighted the importance of microstructure in synthetic fibrillar microenvironments. The aim of this work is to establish whether a similar mechanism holds true for matrices composed of fibrillar proteins instead of synthetic polymers, in order to gain a deeper understanding of how local differences in structure and mechanics of the native ECM influence cell behavior.

Type I collagen is the predominant structural protein in the native ECM and can form fibrillar structure in various connective tissues such as tendons, ligaments and skin[18, 19]. However, the structural and mechanical properties of collagen fibers vary depending upon their location in different tissues. For example, in areolar tissue, collagen fibers exhibit a loose arrangement and run in random directions. Compared to areolar tissue, the structure of tendons is completely different, as collagen fibers bunch up to form dense, rope-like bundles. In addition, collagen fibers localized in various tissues also differ greatly in mechanical properties, they are rigid in bone, compliant in skin or have a gradient from rigid to compliant in cartilage[20-23]. A number of studies have reported detailed protocols to control the fiber thickness, stiffness and length of collagen fibers, primarily by changing collagen concentration and polymerization temperature or pH[24-26]. Here, we expand these methods and study the response of human mesenchymal stem cells (hMSCs) that are cultured on collagen gels composed of different fibers.

## 2.2 Results and discussion

### 2.2.1 Formation of collagen gels with different physical properties

In order to investigate how cells sense local fibrillar microenvironments with different physical cues, we tuned the collagen gel microarchitecture by varying the polymerization temperature while maintaining the collagen concentration at 3 mg/mL, as previously reported[24, 27]. This method ensures that ligand density, mechanical properties, and local topography can be precisely controlled, and varied independently of each other. We do note that changing the polymerization temperature leads to a change in physical parameters, including fiber stiffness and topography. As shown in **Figure 2.1a~c**, collagen fibers formed at higher temperature exhibited a more compact structure and thinner fibers compared to those formed at lower temperature. Specifically, compared to collagen gels polymerized at 21 °C and 37 °C (denoted as Col-21 and Col-37), at 4 °C polymerization temperature (denoted as Col-4), fiber diameter and pore size were the largest (1.7 ± 0.4 μm and 6.9 ± 1.9 μm, respectively), while the length of fibers appeared to be the shortest (about 30.6 ± 3.7 μm). Bulk stiffness all of these three collagen gels were very soft with stiffness ranging from 16.4 to 151.5 Pa (**Figure 2.1d**). However, the

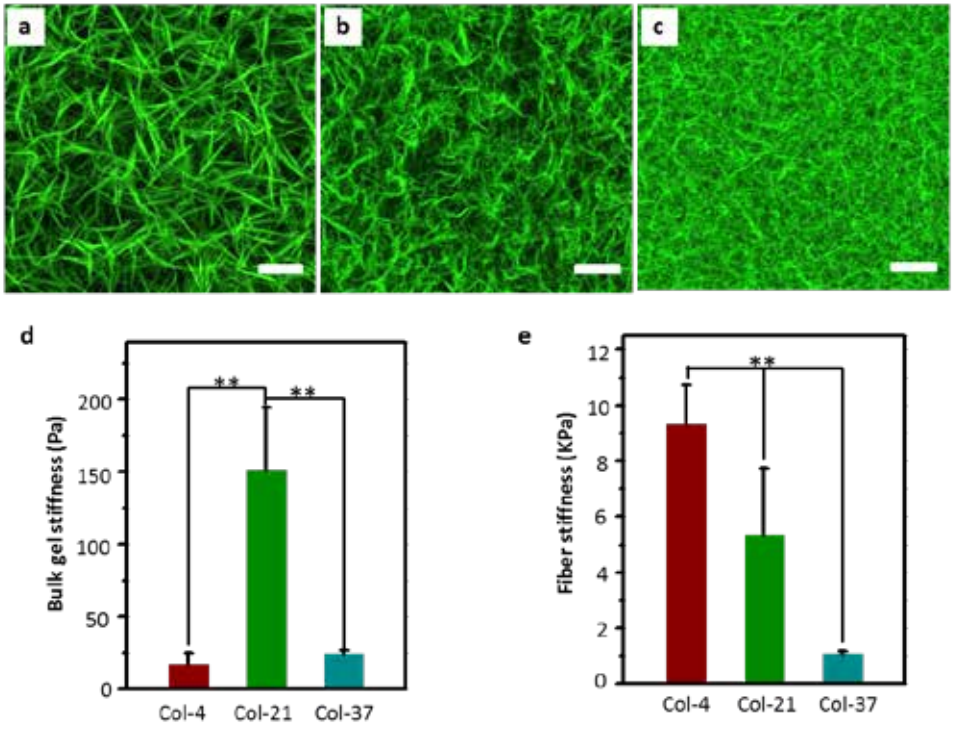


**Figure 2.1. Collagen gels polymerized at different temperature with tunable mechanical and architectural features.** a-c) Morphologies of Alexa-Fluor 488-labelled collagen gels polymerized at 4, 21 and 37°C, respectively. d) Stiffness of bulk gels; N=4. e) Stiffness of local fibers; N=4, n=5. Scale bars: 20 μm. ***P<0.01*.

local fiber stiffness measured by AFM revealed that fiber stiffness was much higher and varied over a much wider range (from 1.1 to 9.3 kPa), by simply decreasing the polymerization temperature from 37 to 4°C. (**Figure 2.1e**). In natural tissues, bulk stiffness ranges from several pascals (Pa) to many kilopascals (kPa), while the stiffness of the protein fibers that these tissues are composed of, is often much higher, in the megapascal (MPa) range[28]. By changing polymerization temperature without changing the density of collagen, we could alter fiber stiffness dramatically while the bulk stiffness remained more or less constant, yielding substrates that mimic different fibrillar properties of the native ECM.

### 2.2.2 Microarchitectures influence cell spreading and proliferation

These structural and mechanical differences led us to investigate the effects of physical properties of fibrillar microenvironment on cell behavior. hMSCs, an often-used cell type for mechanotransduction studies,[2, 29, 30] were seeded at a relatively low cell density (1250 cells/cm$^2$) to observe cellular responses (spreading, proliferation, migration and differentiation) that are primarily determined by the local ECM differences, keeping the contribution of cell-cell interactions to a minimum. Representative cell spreading morphologies on Col-4, Col-21 and Col-37 at different time points within 24 h incubation are presented in **Figure 2.2a**. Spreading of hMSCs on Col-21 and Col-37 started with the formation of small protrusions at 2 h after seeding. However, cells on Col-4 exhibited a round state and failed to spread until 5 h culture time. Quantification of cell perimeter and spreading area on Col-21 and Col-37 (**Figure 2.2b and c**) showed a rapid increase after cell seeding, then followed by a steady state around 15 h incubation. On Col-4, cell spreading occurred at a later stage (around 5 h) and it took more time for cells to reach a steady state (around 24 h). At steady state, cells on all gels adopted a similar spindle-like morphology and cell perimeters were comparable on all substrates (**Figure 2.2b**), however, the spreading area was significantly lower for cells cultured on Col-4 (**Figure 2.2c**). Cell proliferation over 48 h culture was measured by EdU test and revealed the same tendency with spreading area. Cell proliferation on Col-37 with soft fibers was 1.7-fold higher compared to Col-4 with stiff fibers (**Figure 2.2d**). It suggested that characteristics of local microenvironment have an important effect on both cell spreading and proliferation.

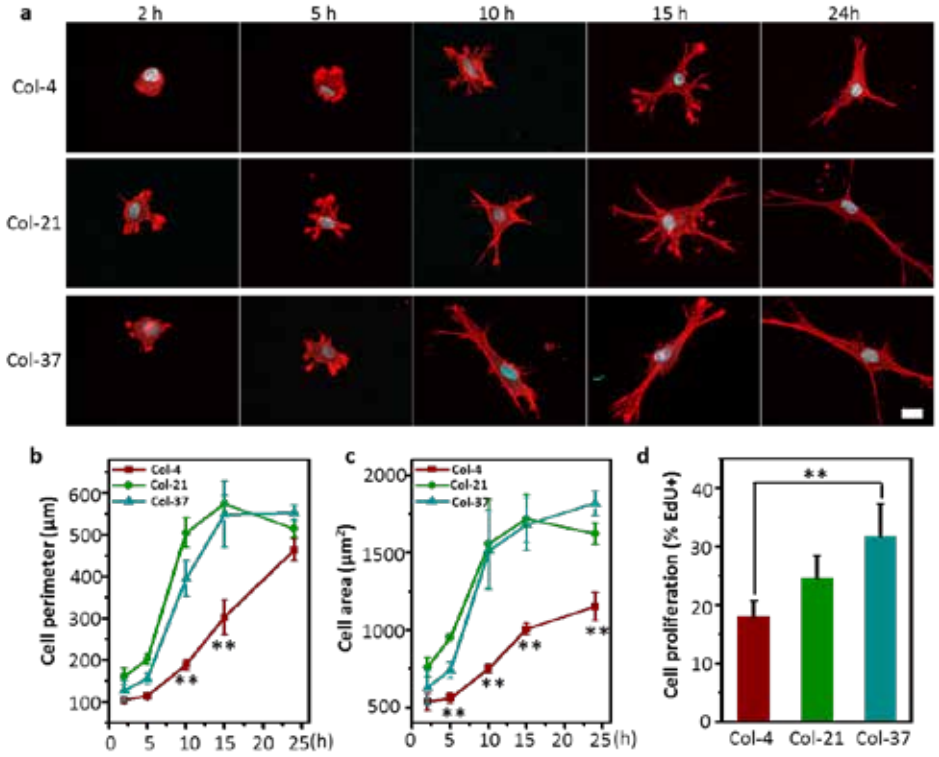


**Figure 2.2. Cell spreading dynamics and proliferation.** a) Morphology of representative cells at different time points, cell skeleton staining with phalloidin (red), nucleus staining with DAPI (blue). b) Quantification of cell perimeter at different time points. c) Quantification of cell area at different time points. d) Proliferation of cells over 48 h as determined by EdU test. N=3, n≥ 80. Scale bars: 20 μm. ***P<0.01*.

### 2.2.3 Cell-mediated remodeling of fibrillar microenvironment shows positive correlation with cells spreading

Fibre recruitment has been described as a mechanism by which cells probe and respond to mechanics in fibrillar matrices. We hypothesized that different physical properties of collagen gels have significant effects on the ability of cells to remodel the surrounding matrix. In order to observe this phenomenon, we prepared fluorescently labeled collagen hydrogels on which we cultured the hMSCs.

Interestingly, we observed that the remodeling on Col-37 and Col-21 started at very early stages around 5 h after seeding, and deformed networks and collagen fiber alignments between cells were clearly observed (**Figure 2.3a**). However, cells on Col-4 showed an immobile state without any pulling. A closer look at the interaction between cells and surrounding matrix demonstrated that cells on Col-37 and Col-21 formed protrusions and pulled the surrounding fibers directionally along the protrusions into bundled, aligned, condensed matrix (**Figure 2.3a**). After culturing hMSCs for 15 h on collagen

gels, cells on all substrates were able to remodel their surrounding matrix and this kind of reorganization was more pronounced. However, compared with cells on Col-37 and Col-21, less formation of long collagen lines between cells of Col-4 was observed (**Figure 2.3b**), and it resulted in no continuous force transmission between cell and matrix.

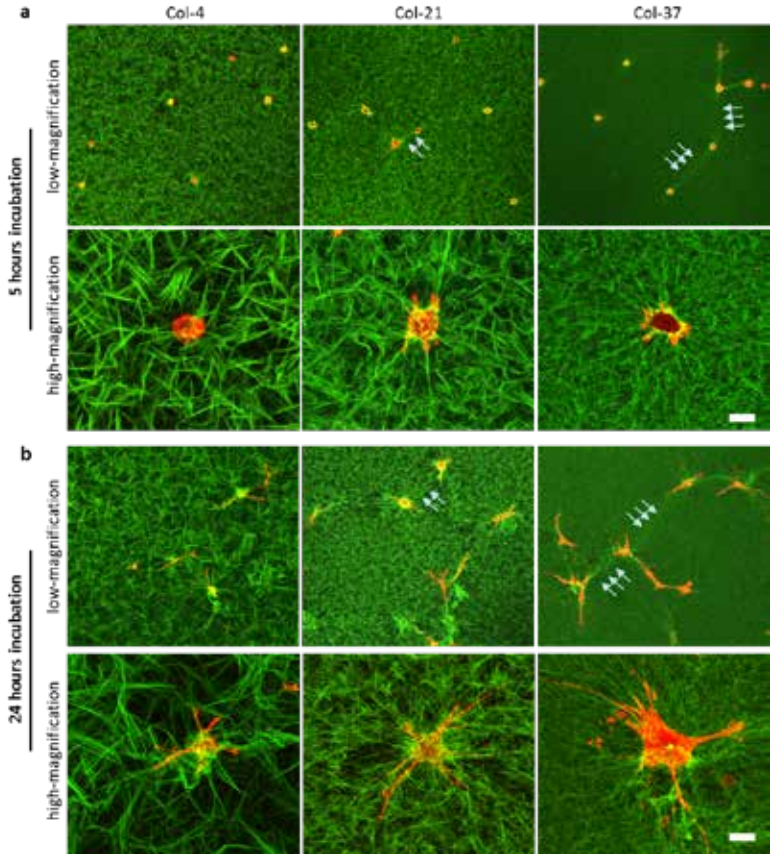


**Figure 2.3. Mechanical remodeling of fibrillar microenvironment by hMSCs.** a) Cell-mediated initial recruitment after 5 h incubation. b) Collagen fibers became gradually disorganized after 15 h incubation. Actin cytoskeleton is stained with phalloidin (red), collagen fiber is labelled with collagen antibody (green). Arrows indicate collagen lines formed between cells. Scale bars are 200 μm for images at low-magnification (top) and 20 μm for images at high-magnification (bottom).

### 2.2.4 Recruitment of collagen fibers activates β-integrin and related pathway through myosin-mediated cellular contractility

Immunostaining for activated β1 integrin (major integrin involved in collagen binding) [31, 32] revealed that compared with cells on Col-4, higher levels of β1 integrin were found in cells cultured on Col-37 (**Figure 2.4a**). Also, on Col-37, FAs frequently occur as clusters along cell protrusions , and are located primarily at the cell periphery. In contrast, no clear

focal adhesion signals were found on Col-4 (**Figure 2.4b**). Taken together, the compact structure of Col-37 provides more anchoring sites and effective mechanical feedback, which can promote cell spreading through integrin-mediated FAK pathway[5]. In addition, in order to transmit force, integrin, via FAs, couples to actomyosin motors, which mediate cell contraction to mechanically pull on adhesion sites and promote cell spreading[33, 34].

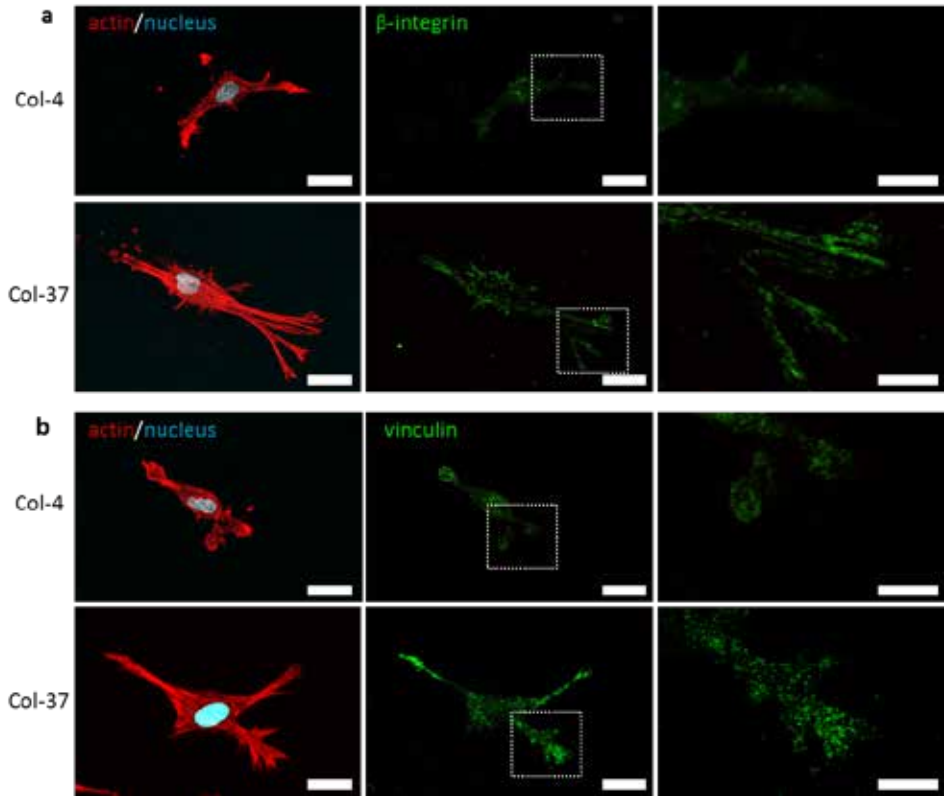


**Figure 2.4. Mechanical remodeling of fibrillar microenvironment activates β-integrin and promotes FAs formation.** a) β-integrins and b) FAs formation of representative hMSCs on Col-4 and Col-37 after 24 h culture. Merged images (left, scale bars: 20 μm). Single-channel images at low- and high-magnification overview (middle, scale bars: 20 μm; right, scale bars: 100 μm).

To test if a complete loss of contractility would result in different cell behavior, cells were treated with Blebbistatin (Bleb), an inhibitor of myosin II–mediated contractility but not adhesion to the collagen substrate[35, 36]. Interestingly, significantly reduced fiber recruitment (**Figure 2.5a**) and local stiffness were observed after Bleb treatment (**Figure 2.5b**). These results confirm that local force generation, fiber recruitment and strain stiffening by spreading cells, depend upon the β1 integrin–collagen interaction, focal adhesion assembly, and myosin II-mediated contractility.

These findings are in line with literature reports that have highlighted that the role of ECM fibers in long-range force transmission.[37-40] Despite these studies, little is known about the effect of fiber mechanics on force transmission. Our study has shown that soft fiber of collagen gel can facilitate long-range force transmission, while cells on stiff fibers could not, because the fiber is too stiff and short. Due to limitations of fiber recruitment and force transmission, the population of β-integrin and FAs undergoing retraction at the leading edge were reduced. Via integrin-based adhesion sites, cells can mechanically sense physical surroundings and adjust mechanisms of migration,[41, 42] through the process of protrusion, adhesion, translocation and retraction. Thus, on Col-4 because of fewer FAs, the formation of leading edge protrusions was delayed. The strongly remodeled collagen bundles formed in Col-37 clearly do promote FAs formation and force transmission, and guide cell migration along the bundles.

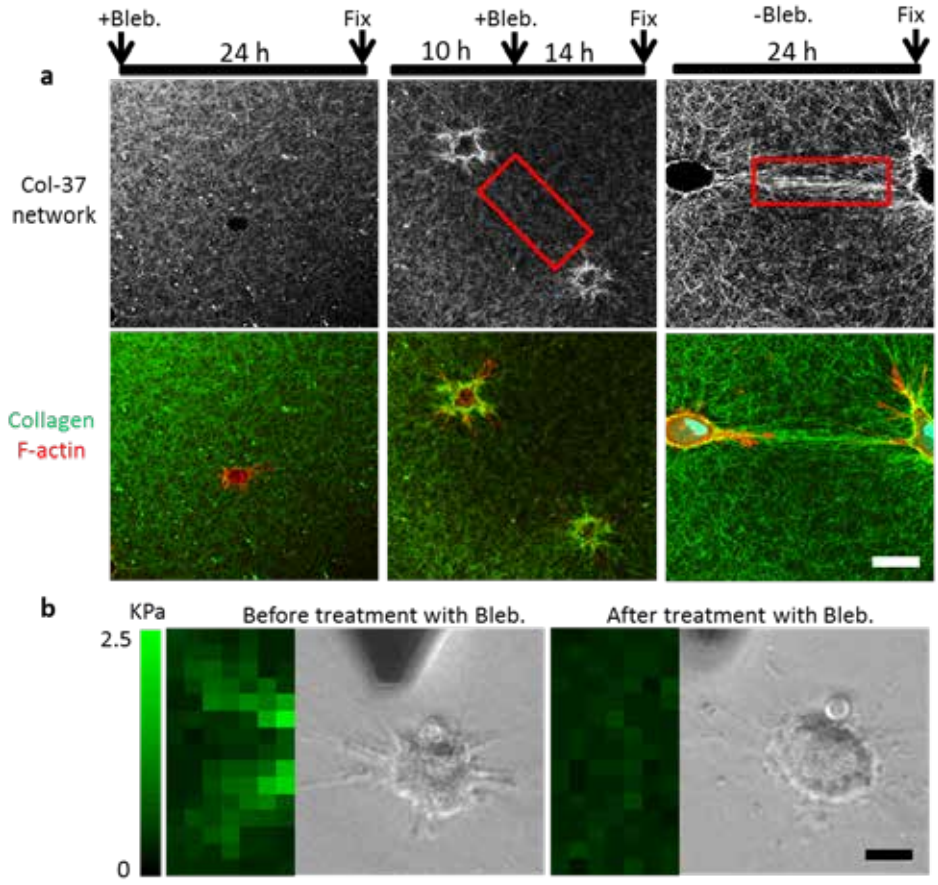


**Figure 2.5. Myosin IIa-mediated cell contractility induces fiber recruitment.** a) Cell spreading after inhibition of Myosin IIa with Bleb. treatment before (left images) or during (middle images) cell culture. Cells without Bleb. treatment are control (right images). Scale bars: 200 μm. b) Local stiffness heatmap of Col-37 before and after Bleb. treatment. Heat maps were generated over the corresponding positions of bright-field images and represent the Young's modulus at each probing position. Scale bars: 20 μm.

### 2.2.5 Physical cues of fibrillar microenvironment influence hMSCs migration and differentiation

Activation of FAK signaling pathway is critical for efficient cell migration[43, 44]. The movement of 30 representative cells was tracked (**Figure 2.6a-c**). Cells demonstrated inactive behavior on Col-4, with delayed spreading and migration. However, on Col-37 and Col-21, cells spread and migrated quickly, and more and more cells appeared in the area under observation. Cells on Col-37 migrated in random directions and over longer distances comparted to other substrates, while most cells on Col-4 showed very limited migration (**Figure 2.6d**).

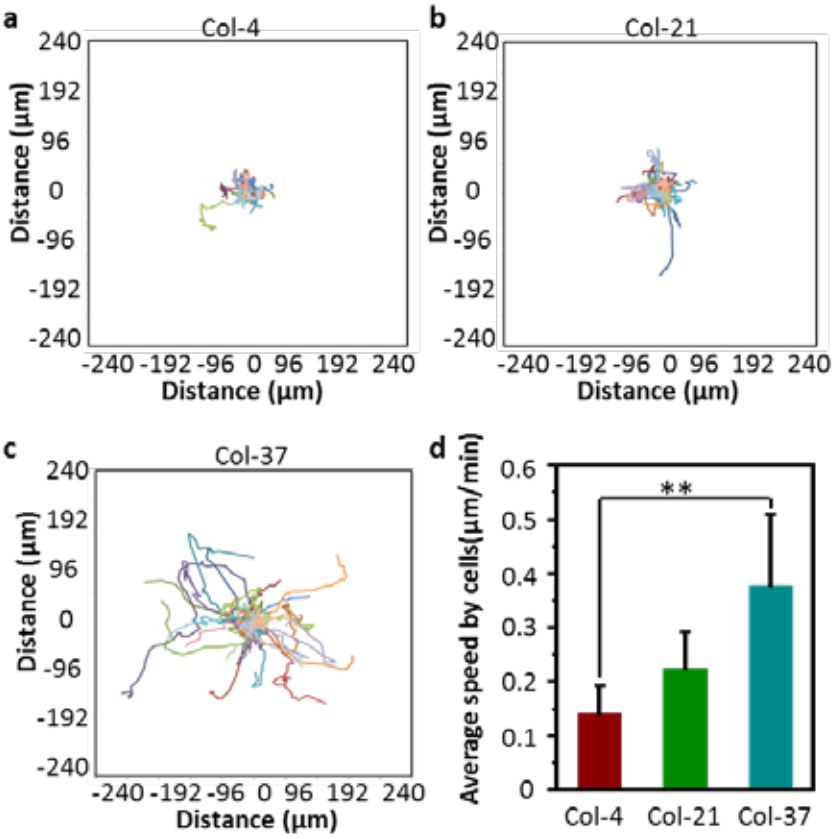


**Figure 2.6. Cell migration influenced by fibrillar properties.** a-c) Movement tracking of 25 representative cells after 15 h culture on gels. d) Average speed of cells on different collagen gels. ***P<0.01*, **P<0.05*; n=25.

Finally we tested the differentiation of hMSCs and found that under medium conditioned with differentiation supplements (**Figure 2.7a**), hMSCs showed very significant differences in ALP and Oil Red O staining when differentiated on 1.1 kPa and 9.3 kPa collagen fibers (**Figure 2.7b and c**). Numerous studies have demonstrated a strong

correlation between hydrogel stiffness and cell differentiation, where stiff substrate promoted stem cells to differentiate into osteoblasts, while cells on soft substrate preferentially differentiated towards adipocytes.[1, 2, 45] However, in our study we used soft gels with bulk stiffness below 200 Pa, and found that more hMSCs differentiated towards osteoblasts on soft fibers (Col-37 gels).

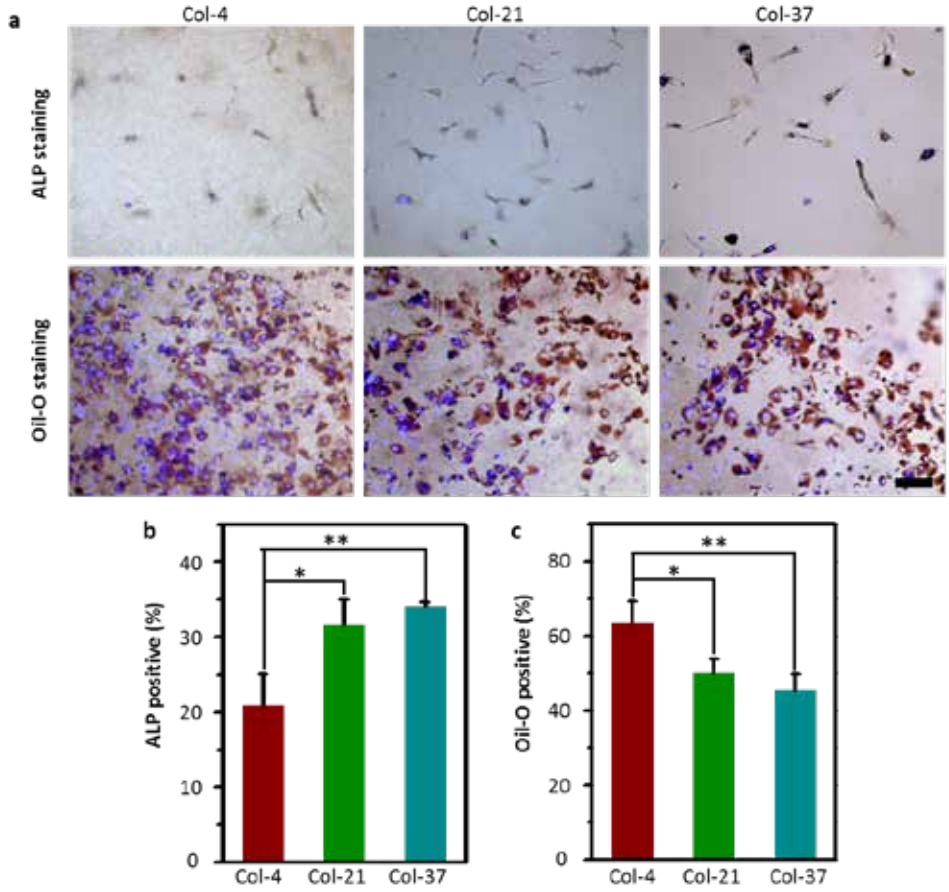


**Figure 2.7. Cells differentiation depends on substrate properties.** a) ALP and Oil-O staining showing osteogenic and adipogenic differentiation of hMSCs. b) Quantitative results of positive osteogenic differentiation. c) Quantitative results of positive adipogenic differentiation. Scale bars: 250 µm. ***P<0.01*, **P<0.05*; N=3,n≥100.

Several earlier studies on synthetic hydrogels surfaces have shown a strong correlation between hydrogel bulk stiffness and cell adhesion, spreading, proliferation and differentiation.[1, 6, 7, 46] In contrast, we found that lower fiber stiffness permitted increased cell area, while stiff fibers suppressed cell spreading. Our results are consistent with Baker's recent study, where fibers made from polymer materials with lower stiffness enabled cells to remodel the surrounding matrix, leading to a larger spreading.[47] In

addition, other research has shown that hMSC spreading, proliferation, and focal adhesion formation are dependent on RGD density, but not on the fiber mechanics of hyaluronic acid hydrogels.[48] However, in that study the fiber stiffness ranged from 1.1 to 8.6 GPa, which is too stiff for cells to recruit. In that case, cell behavior was indeed only regulated by ligand density.

## 2.3 Conclusion

In this study, we investigated how physical cues from the fibrillar microenvironment of collagen gels influence cell behavior. We formed collagen gels with different fibrillary architecture by polymerizing a constant concentration of 3mg/mL collagen at different temperatures. We find that the ability of cells to remodel the gels is a major factor in determining whether cells can spread, proliferate, and migrate on these gels. Lower polymerization temperatures lead to shorter, thicker and stiffer collagen fibers, that appear less able to reorganize over larger length scales as the fibers loose connectivity upon reorganization by cells. As a result, cells show much slower spreading when compared to gels with similar bulk stiffness, but with longer, more flexible fibers that can be easily remodeled. These differences in adhesion and spreading are also apparent in the much lower levels of focal adhesions on gels consisting of short and stiff fibers, and cells tend to differentiate towards adipocytes on these substrates. Our study highlights the importance for a better understanding of the role of fiber architecture of the natural ECM on cellular behavior.

## 2.4 Acknowledgements

Jing Xie is gratefully acknowledged for fabricating collagen gels, performing and analyzing cell experiments as well as many useful discussions. We acknowledge José M. A. Hendrik for assistance with cell cultures, Dr. Liesbeth Pierson for assistance with confocal microscopy.

## 2.5 Experimental section

### 2.5.1 Formation of collagen gels with different physical cues

Collagen gels were prepared as described previously. Briefly, we diluted type I rat tail collagen (BD biosciences) to the desired concentration of 3 mg/mL with DMEM (Gibco), 10 × PBS, $H_2O$ and adjusted pH to 7.4 by addition of 1N NaOH. The ratio of final volume, DMEM and PBS was 20:10:1 and all the solutions were kept on ice. Finally, collagen gels

with different physical cues were generated at different polymerization temperature, 4, 21 and 37°C, and corresponded to polymerization time of overnight, 2 h and 30 min, respectively.

### 2.5.2 Mechanical test

We measured the bulk stiffness of collagen gels using an AR-G2 rheometer (TA instruments, New Castle, DE). First, the polymerization temperature was set, and upon reaching the desired temperature, 700 µL of the gel solution was added to the 35-mm steel parallel plate with 500 µm gap. Measurements were carried out at a controlled temperature of 4°C, 21°C, and 37°C, respectively. After collagen had polymerized (overnight (15 h) at 4°C, 2 h at 21°C and 30 min at 37°C, the shear storage modulus of the gels was measured at 1 % strain at a frequency of 0.1 Hz for 30 min and all results were based on four separate experiments. Local fibers stiffness was measured by AFM (Bruker Nanoscope), using conical-tipped pyramidal cantilevers (NP-S type D, Bruker) at 1 µm resolution, which was as close to the fiber diameter as possible. The "point and shoot" procedure (Nanoscope software, Bruker) was used to measure fiber stiffness, and all the gels were kept in PBS buffer during the measurement. To obtain fiber stiffness values from force curves we used PUNIAS software (http://punias.free.fr). Specifically, multiple force displacement curves (five different locations) were fitted to the conical indenter Sneddon model:

$$F = \frac{2E \tan(\alpha)}{\pi(1 - v^2)} \delta^2$$

where F is the force, E is the Young's modulus, δ is the indentation depth, α=18° is the indenter half-angle and v is the Poisson ratio, which was set to 0.5 on the indentation curve.[49]

### 2.5.3 Morphology of collagen microarchitecture

After collagen gels formation, immunostaining with a fluorescently labeled collagen-antibody allowed us to observe the microarchitecture and the gel reorganization using confocal microscopy. Immunostaining was carried out by first staining with antibody anti-mouse Col (Abcam, ab90395) for 1 h and subsequently by secondary antibody Alexa-Fluor 488 goat-anti-mouse (Thermo Fisher Scientific, R37120) for 1 h. During the experiment, all the antibodies were dissolved in 1% BSA (Sigma). Finally, a Leica SP8 confocal laser scanning microscope (Leica, Germany) was used to take images and monitor reorganization of collagen fibers.

### 2.5.4 Fibrillar structure of gels calculation

To calculate fiber diameter, length and porosity, Alexa-Fluor 488-labelled collagen gels were imaged on an SP8 confocal microscope with a 63x objective. 20 frames of Z-stacks

were captured and merged into a single image by Image 5D - Fiji software. From these images an inverted threshold (dark threshold) was used to calculate the per cent area that was not considered a fiber and used as a per cent porosity measurement. For fiber diameter and length analysis, line segments were drawn across the widths and lengths of fibrils found in merged images for Col-4 using Fiji software. The number of independent experiments (N) was 3, the number of data points (n) was ≥20: more than 20 regions of interest (ROI) from three separate experiments were analyzed.

### 2.5.5 hMSCs culture and seeding

hMSCs were obtained from Lonza and cultured to passage 6 in normal medium containing low glucose DMEM, FBS (Gibco), glutamine and Pen/Strep (Thermo fisher scientific). Then hMSCs (P6) were seeded on the gels at the density of 1250 per $cm^2$ for cellular spreading, proliferation, migration and gel deformation tests, and 2500 or 25000 per $cm^2$ for osteogenic and adipogenic differentiation respectively. Proliferation medium (high glucose DMEM, FBS, glutamine and Pen/Strep) was used to culture cells on different collagen gels, except for differentiation studies; differentiation medium contained proliferation medium with a 1 : 1 combination of osteogenic and adipogenic chemical supplements (Isobutylmethylxanthine, Dexamethason, Glycerophosphate, Insulin, L-Ascorbic acid 2-phosphate, Rosiglitazone, all from Sigma).

### 2.5.6 Time Lapse Imaging

Nikon Diaphot 300 with Hamamatsu C8484-05G CCD Camera and a Leica SP8 confocal microscope were used to monitor cell movements and collagen fibers reorganization. During all experiments, cells were cultured at constant 37 °C, 7.5% $CO_2$ atmosphere and microscopes were used to take images at 10-minute intervals. For cell movements, we used Nikon Diaphot 300 with a 10 × phase contrast objective to track cells over 15 h. Then the movement of single cell was measured by manually clicking on the geometric center of the cell using Image J Manual Tracking Plugin, the xy coordinate corresponding to each clicked pixel was recorded. Trajectory graphs were generated by inputting the data into "Plot_At_Origin" program provided in a previous study.[50] For images of Alexa-Fluor 488-labelled collagen fibers reorganization, 488-nm argon laser of Leica SP8 confocal microscope was used and all of the images were merged by Fiji software.

### 2.5.7 Immunofluorescence staining

Immunofluorescent staining was performed to observe cytoskeletons or focal adhesions. After incubation, cells seeded on the gels were fixed with 4% paraformaldehyde (Sigma) for 10 min, and permeated in 0.2% Triton X-100 (Sigma) for 10 min at room temperature. Subsequently samples were incubated with phalloidin-Atto 633 (Sigma) and DAPI (Millipore) for 1 h for cytoskeletons staining ; for FAs staining, nonspecific binding sites were blocked in 10% BSA solution for 1 h first, followed by incubating with primary

antibody anti-vinculin (Abcam) for 1 h and subsequently with secondary antibody Alexa 488 goat anti-mouse, phalloidin and DAPI for 1 h. The stained cells were imaged using the SP8 and spreading areas were extracted using Fiji software. The stained cells were imaged using the SP8, and spreading areas and perimeter measurements were obtained using Fiji's in-built "Measure" function after drawing a region of interest around cells. More than 80 cells were meaured in three separated experiments.

**2.5.8 Proliferation test**

For proliferation test, EdU labelling which can incorporate into the DNA of cells during replication was performed. Firstly, plate hMSCs on different substrate at the density of 1250 per $cm^2$ and allow them to recover overnight, then treat cells with 1× EdU solution. When the incubation up to 48h, fix and permeabilize cells with 4% PFA and 0.1% Triton X-100 respectively. Following these, samples were treated according to the manufacturer's protocol of Click-iT EdU Alexa Fluor-488 HCS Aaasy (Thermo fisher scientific). All images were collected by a Leica SP2 confocal microscope (Leica, Germany) with filters for DAPI and FITC (Alexa Fluor-488). For quantification, 8 or more low magnification (10 × objective) fields were collected within regions of interest.

**2.5.9 Differentiation assays**

hMSCs were cultured for 7 or 10 days in osteogenic or adipogenic differentiation medium, respectively.Subsequently, all cells were fixed with 4% PFA and penetrated with 0.2% Triton-X 100 for 10 min, respectively. ALP staining was performed by Fast Blue assay (naphthol-AS-MSC phosphate and Fast Blue RR, Sigma) in Tris/HCl buffer (pH 8.9) and incubated at 37 °C for 1 h. Oil Red O staining was performed by incubating cells with 1.8 mg/mL Oil Red O (Sigma) for 30-60 min at room temperature and then rinsing with 60% isopropanol (Sigma). The nuclei were stained with DAPI and images were acquired on a Zeiss inverted microscope (Photometrics, USA).

**2.5.10 Statistics**

Statistical analysis was performed with Origin software and one-way analysis of variance (ANOVA) using a Tukey post-test for more than two variables was carried out. significant difference or very significant. Difference were indicated by *P < 0.05 or **P < 0.01, respectively. All results were expressed as mean ± standard error. Statistical analysis was performed with Origin software and one-way analysis of variance (ANOVA) using a Tukey post-test for more than two variables was carried out. 'Significant' 'very significant' differences were indicated by *P < 0.05 or **P < 0.01, respectively. All results were expressed as mean ± standard error. In each test, the number of independent experiment (N) is more than three, and the number of data points (n) in each experiment is different. Both of N and n are shown in the figure legend.

## 2.6 Reference


1. Discher, D.E., Janmey, P. & Wang, Y.-l. Tissue cells feel and respond to the stiffness of their substrate. *Science* **310**, 1139-1143 (2005).
2. Engler, A.J., Sen, S., Sweeney, H.L. & Discher, D.E. Matrix elasticity directs stem cell lineage specification. *Cell* **126**, 677-689 (2006).
3. Humphrey, J.D., Dufresne, E.R. & Schwartz, M.A. Mechanotransduction and extracellular matrix homeostasis. *Nature reviews Molecular cell biology* **15**, 802-812 (2014).
4. Unadkat, H.V. *et al.* An algorithm-based topographical biomaterials library to instruct cell fate. *Proceedings of the National Academy of Sciences* **108**, 16565-16570 (2011).
5. Trappmann, B. *et al.* Extracellular-matrix tethering regulates stem-cell fate. *Nature materials* **11**, 642-649 (2012).
6. Pelham, R.J. & Wang, Y.-l. Cell locomotion and focal adhesions are regulated by substrate flexibility. *Proceedings of the National Academy of Sciences* **94**, 13661-13665 (1997).
7. Yeung, T. *et al.* Effects of substrate stiffness on cell morphology, cytoskeletal structure, and adhesion. *Cell Motil. Cytoskeleton* **60**, 24-34 (2005).
8. Watt, F.M. & Huck, W.T. Role of the extracellular matrix in regulating stem cell fate. *Nature reviews Molecular cell biology* **14**, 467-473 (2013).
9. Puklin-Faucher, E. & Sheetz, M.P. The mechanical integrin cycle. *Journal of cell science* **122**, 179-186 (2009).
10. Miron-Mendoza, M., Seemann, J. & Grinnell, F. The differential regulation of cell motile activity through matrix stiffness and porosity in three dimensional collagen matrices. *Biomaterials* **31**, 6425-6435 (2010).
11. Pedersen, J.A. & Swartz, M.A. Mechanobiology in the third dimension. *Annals of biomedical engineering* **33**, 1469-1490 (2005).
12. Baker, B.M. & Chen, C.S. Deconstructing the third dimension–how 3D culture microenvironments alter cellular cues. *J. Cell Sci.* **125**, 3015-3024 (2012).
13. Hay, E.D. Extracellular matrix. *The Journal of cell biology* **91**, 205s-223s (1981).
14. Hynes, R.O. The extracellular matrix: not just pretty fibrils. *Science* **326**, 1216-1219 (2009).
15. Storm, C., Pastore, J.J., MacKintosh, F.C., Lubensky, T.C. & Janmey, P.A. Nonlinear elasticity in biological gels. *Nature* **435**, 191-194 (2005).
16. Collet, J.-P., Shuman, H., Ledger, R.E., Lee, S. & Weisel, J.W. The elasticity of an individual fibrin fiber in a clot. *Proceedings of the National Academy of Sciences of the United States of America* **102**, 9133-9137 (2005).
17. Baker, B.M. *et al.* Cell-mediated fibre recruitment drives extracellular matrix mechanosensing in engineered fibrillar microenvironments. *Nature materials* (2015).

18. Gelse, K., Pöschl, E. & Aigner, T. Collagens—structure, function, and biosynthesis. *Advanced drug delivery reviews* **55**, 1531-1546 (2003).
19. Badylak, S.F., Freytes, D.O. & Gilbert, T.W. Extracellular matrix as a biological scaffold material: structure and function. *Acta biomaterialia* **5**, 1-13 (2009).
20. Ushiki, T. Collagen fibers, reticular fibers and elastic fibers. A comprehensive understanding from a morphological viewpoint. *Archives of histology and cytology* **65**, 109-126 (2002).
21. Rho, J.-Y., Kuhn-Spearing, L. & Zioupos, P. Mechanical properties and the hierarchical structure of bone. *Medical engineering & physics* **20**, 92-102 (1998).
22. Kato, Y.P. *et al.* Mechanical properties of collagen fibres: a comparison of reconstituted and rat tail tendon fibres. *Biomaterials* **10**, 38-42 (1989).
23. Silver, F.H., Christiansen, D.L., Snowhill, P.B. & Chen, Y. Role of storage on changes in the mechanical properties of tendon and self-assembled collagen fibers. *Connective tissue research* **41**, 155-164 (2000).
24. Raub, C.B. *et al.* Noninvasive assessment of collagen gel microstructure and mechanics using multiphoton microscopy. *Biophys. J.* **92**, 2212-2222 (2007).
25. Yang, Y.-l., Leone, L.M. & Kaufman, L.J. Elastic moduli of collagen gels can be predicted from two-dimensional confocal microscopy. *Biophysical journal* **97**, 2051-2060 (2009).
26. Rosenblatt, J., Devereux, B. & Wallace, D. Injectable collagen as a pH-sensitive hydrogel. *Biomaterials* **15**, 985-995 (1994).
27. Wolf, K. *et al.* Physical limits of cell migration: control by ECM space and nuclear deformation and tuning by proteolysis and traction force. *J. Cell Biol.* **201**, 1069-1084 (2013).
28. Gautieri, A., Vesentini, S., Redaelli, A. & Buehler, M.J. Hierarchical structure and nanomechanics of collagen microfibrils from the atomistic scale up. *Nano letters* **11**, 757-766 (2011).
29. Huebsch, N. *et al.* Harnessing traction-mediated manipulation of the cell/matrix interface to control stem-cell fate. *Nat. Mater.* **9**, 518-526 (2010).
30. Khetan, S. *et al.* Degradation-mediated cellular traction directs stem cell fate in covalently crosslinked three-dimensional hydrogels. *Nat. Mater.* **12**, 458-465 (2013).
31. Takada, Y., Ye, X. & Simon, S. The integrins. *Genome biology* **8**, 1 (2007).
32. Hynes, R.O. Integrins: bidirectional, allosteric signaling machines. *Cell* **110**, 673-687 (2002).
33. Pasapera, A.M., Schneider, I.C., Rericha, E., Schlaepfer, D.D. & Waterman, C.M. Myosin II activity regulates vinculin recruitment to focal adhesions through FAK-mediated paxillin phosphorylation. *The Journal of cell biology* **188**, 877-890 (2010).
34. Wozniak, M.A., Modzelewska, K., Kwong, L. & Keely, P.J. Focal adhesion regulation of cell behavior. *Biochimica et Biophysica Acta (BBA)-Molecular Cell Research* **1692**, 103-119 (2004).

35. Straight, A.F. *et al.* Dissecting temporal and spatial control of cytokinesis with a myosin II Inhibitor. *Science* **299**, 1743-1747 (2003).
36. Even-Ram, S. *et al.* Myosin IIA regulates cell motility and actomyosin–microtubule crosstalk. *Nat. Cell Biol.* **9**, 299-309 (2007).
37. Shi, Q. *et al.* Rapid disorganization of mechanically interacting systems of mammary acini. *Proc. Natl. Acad. Sci. U. S. A.* **111**, 658-663 (2014).
38. Ma, X. *et al.* Fibers in the extracellular matrix enable long-range stress transmission between cells. *Biophys. J.* **104**, 1410-1418 (2013).
39. Wang, H., Abhilash, A., Chen, C.S., Wells, R.G. & Shenoy, V.B. Long-range force transmission in fibrous matrices enabled by tension-driven alignment of fibers. *Biophys. J.* **107**, 2592-2603 (2014).
40. Hall, M.S. *et al.* Fibrous nonlinear elasticity enables positive mechanical feedback between cells and ECMs. *Proc. Natl. Acad. Sci. U. S. A.* **113**, 14043-14048 (2016).
41. Ridley, A.J. *et al.* Cell migration: integrating signals from front to back. *Science* **302**, 1704-1709 (2003).
42. Lauffenburger, D.A. & Horwitz, A.F. Cell migration: a physically integrated molecular process. *Cell* **84**, 359-369 (1996).
43. Sieg, D.J. *et al.* FAK integrates growth-factor and integrin signals to promote cell migration. *Nature cell biology* **2**, 249-256 (2000).
44. Plotnikov, S.V., Pasapera, A.M., Sabass, B. & Waterman, C.M. Force fluctuations within focal adhesions mediate ECM-rigidity sensing to guide directed cell migration. *Cell* **151**, 1513-1527 (2012).
45. Dupont, S. *et al.* Role of YAP/TAZ in mechanotransduction. *Nature* **474**, 179-183 (2011).
46. Mih, J.D., Marinkovic, A., Liu, F., Sharif, A.S. & Tschumperlin, D.J. Matrix stiffness reverses the effect of actomyosin tension on cell proliferation. *J. Cell Sci.* **125**, 5974-5983 (2012).
47. Baker, B.M. *et al.* Cell-mediated fibre recruitment drives extracellular matrix mechanosensing in engineered fibrillar microenvironments. *Nat. Mater.* **14**, 1262–1268 (2015).
48. Kim, I.L., Khetan, S., Baker, B.M., Chen, C.S. & Burdick, J.A. Fibrous hyaluronic acid hydrogels that direct MSC chondrogenesis through mechanical and adhesive cues. *Biomaterials* **34**, 5571-5580 (2013).
49. Petrie, R.J., Gavara, N., Chadwick, R.S. & Yamada, K.M. Nonpolarized signaling reveals two distinct modes of 3D cell migration. *J. Cell Biol.* **197**, 439-455 (2012).
50. Gorelik, R. & Gautreau, A. Quantitative and unbiased analysis of directional persistence in cell migration. *Nat. Protoc.* **9**, 1931-1943 (2014).

# Chapter 3

## Engineering 3D microniches to control cell size and shape

This chapter has been adapted from:
Bao, M., Xie, J., Piruska, A., & Huck, W. T. 3D microniches reveal the importance of cell size and shape. Nature Communications **2017**, 8(1), 1962.

## Abstract

In addition to rigidity, cell shape and dimensionality is now considered an important property of the cell microenvironment which directs cell behavior. However, available methods for cell culture in two-dimensional (2D) versus three-dimensional (3D) environments are difficult to compare. One major reason for this lack of understanding is rooted in the difficulties of controlling cell geometry in a complex 3D setting and for long periods of culture. Here, we present a robust method to control cell volume and shape of individual human mesenchymal stem cells (hMSCs) inside 3D microniches with a range of different geometries (e.g., cylinder, triangular prism, cubic and cuboid). Our 3D microniches enable fundamental studies into how geometrical cues affect single stem cell fate (i.e. differentiation), and has potential applications in investigating cell-cell or cell-matrix communication in local 3D environment.

## 3.1 Introduction

Stem cells reside *in vivo* in a complex three-dimensional (3D) microenvironment, or niche, where multiple stimuli interact and integrate to regulate cell survival, self-renewal and differentiation[1]. These stimuli include biochemical signals, such as growth factors and signaling molecules, as well as biophysical factors such cell-cell and cell-matrix interactions[2], matrix elasticity[3], and geometry[4-7]. The integration of the various effectors is a complex, but remarkably robust process, as evidenced, for example, by the fact that although different cell types can differ greatly in size and shape, within tissues cells are often strikingly similar[8]. Understanding how biophysical cues in the niche regulate stem cell function and fate is important, as it would lead to a much better insight into how cells develop and maintain their distinctive morphologies, and provide guidance for the design of new materials for tissue and organoid culture. Unfortunately, there are no in vivo methods to control niche geometry independent of changes in growth factors or other intra- and extracellular signaling events. Much of what we know about the influence of biophysical cues on stem cell fate comes from cell culture studies on 2D micro-patterned substrates[4-6, 9-13]. These studies have provided a wealth of insight and have shown that cell geometry and size play an important role in organizing the cytoskeleton and in directing growth, death and differentiation of mesenchymal stem cells (MSCs). However, 2D cell culture does not fully capture the cellular phenotypes found *in vivo*, cell volume cannot be controlled, and the inevitable polarization of cells spreading on adhesive substrates is a strong cue that cannot be decoupled from other parameters in the experiment. Surprisingly, culturing large numbers of individual stem cells fully enclosed in non-polarized and symmetrical 3D microniches with well-defined dimensions has not been achieved and how 3D size and geometry affects cell function remains elusive. To be sure, there has been important progress in capturing physical aspects of the extracellular matrix by culturing cells within hydrogels[14-20], but these gels present no geometrical restrictions on individual cells.

In this chapter, we used photopolymerized methacrylated hyaluronic acid (MeHA) hydrogels to construct artificial single cell 3D microniches with a variety of shapes. Hyaluronic acid (HA) is a naturally derived polysaccharide found abundantly in native tissues, it is biodegradable and can be modified to present a variety of desirable properties for biomedical applications[21]. The elasticity of MeHA hydrogel can be tuned by simply varying the macromer concentration or the fraction of photoinitiator. We first demonstrate the fabrication of MeHA hydrogels with 3D microniches of controlled shape and size, tunable mechanical properties. We will then show how the volume and shape of single hMSCs can be controlled in these 3D microniches.

## 3.2 Results and discussion

### 3.2.1 MeHA hydrogel preparation

Key to the successful design of 3D microniches, is the requirement to fully encapsulate single cells within a matrix material that allows both cell adhesion and permeability of nutrients. HA was selected for several reasons. First, HA can be easily functionalized with proteins such as fibronectin to promote cell adhesion, as well as with cationic polymers such as poly(L-lysine)-graft-poly(ethylene glycol) (denoted as PLL-g-PEG), to create protein-resistant surfaces where required[22]. Second, diffusion of nutrients and oxygen to the cells through the HA hydrogel is rapid enough to support normal cell growth rates[23]. MeHA was synthesized following a previously described procedure (**Figure 3.1a**), The degree of methacrylation of hydroxyl groups on HA was ~15% (confirmed by $^{1}$H NMR). In order to form a hydrogel network, MeHA was crosslinked using UV irradiation in the presence of a photo initiator. By controlling the concentration of MeHA, we could control the mechanical properties of these hydrogels between 1.8 and 36.5 kPa (**Figure 3.1b and c**).

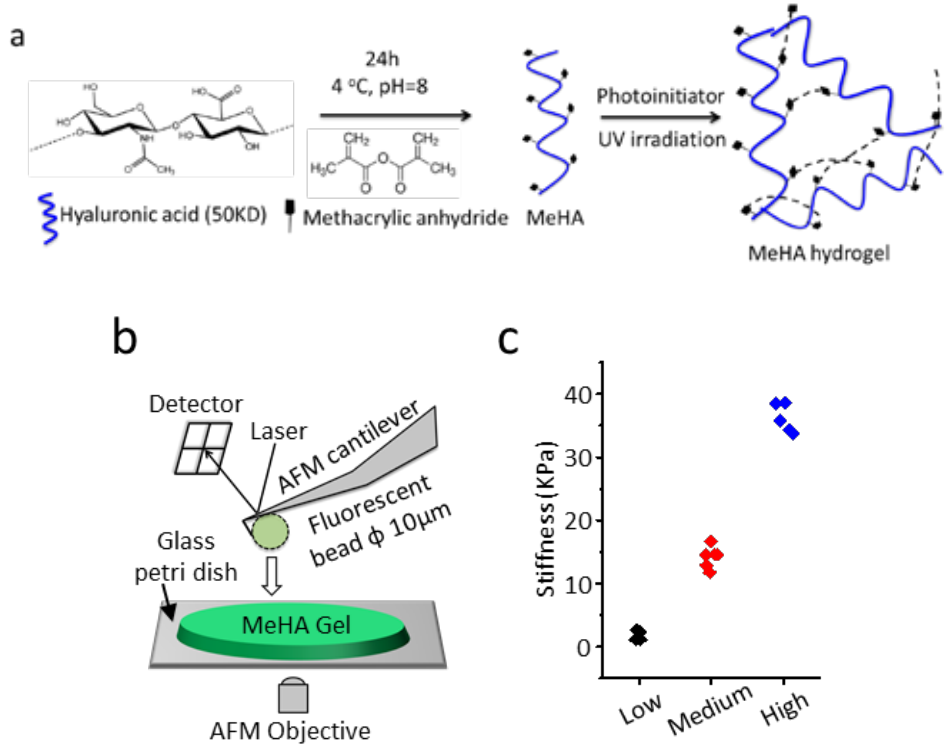


**Figure 3.1. HA hydrogel preparation and mechanical characterization.** a) Schematic of preparing MeHA and photo polymerization of MeHA. b) Experimental setup of AFM-indentation based stiffness measurement for MeHA hydrogel. c) MeHA Hydrogel stiffness with varying macromer concentration (ranging from 2 - 10 wt%).

### 3.2.2 3D microniche preparation and functionalization

**Figure 3.2a** shows our method for compartmentalizing cells in hydrogel niches with well-defined sizes and shapes. First, we formed microwells in hydrogels of MeHA by photo polymerizing MeHA against a silicon master with patterns ranging between 5 and 40 microns in lateral dimensions and 7 to 35 microns in height (**Figure 3.2b**). Prior to seeding the cells, the hydrogel top surface was rendered protein-resistant using PLL-g-PEG, deposited using a wet-stamping technique[12]. Subsequently, we soaked the PLL-g-PEG modified wells with a fibronectin (Fn) solution (100 µg/mL), which binds directly to HA, to promote cell adhesion and spreading[22]. We achieved selective and uniform Fn deposition on the inside surface of the wells, as shown by confocal fluorescence microscopy after staining with a fluorescent antibody against Fn (**Figure 3.2c**). Finally, and most importantly, to complete 3D encapsulation of the cells, we covered the wells with a flat piece (~30 µm thick) of MeHA hydrogel coated with Fn to construct a 3D microniche. The Fn coating is

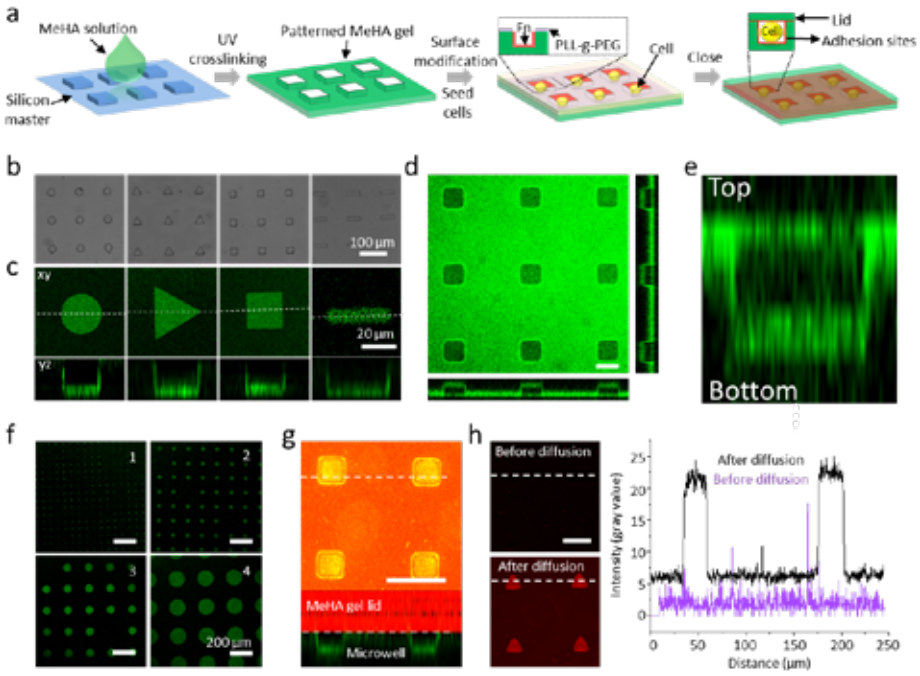


**Figure 3.2. 3D microniche preparation and functionalization**. a) Schematic of method to encapsulate single cells in 3D microniche. b) Phase contrast images of MeHA hydrogel containing microwells of various geometries. c) Maximum intensity projections with different z-stacks and cross-sections of confocal images of microwells coated with Fn. d) Confocal image shows Fn distribution in microwells and on the surface of lid. Scale bar 20 µm. e) Confocal image (at larger magnification) shows homogeneous Fn distribution within 3D microniches from top to bottom. f) Confocal images of different sized microwells, the diameter for size 1: 22.6 µm, size 2: 45 µm, size 3: 70 µm, size 4: 125 µm. g) Confocal image of MeHA hydrogel lid (red fluorescence) on MeHA hydrogel with microwells coated with Fn (green fluorescence), scare bar: 50 µm. h) Fluorescence intensity profiles (gray value) in microwells covered with MeHA hydrogel before and after immersed in GFP contained cell culture medium. Scale bar 50 µm.

also homogeneous within 3D microniches after closing the lid (**Figure 3.2d and e**). **Figure 3.2f** shows that over 96% of cylindrical microniches with different sizes were uniformly coated with Fn. Confocal imaging (**Figure 3.2g**) showed that the MeHA hydrogel lid fully sealed the wells. To confirm the permeability/diffusion of the cell culture medium through the MeHA hydrogel, we monitored diffusion of GFP through the lid. After immersion in cell culture medium with GFP for 10 minutes, the fluorescence intensity of GFP protein inside the niches increased (**Figure 3.2h**), providing strong indication that key components of the cell culture medium could diffuse through the MeHA hydrogel[24].

### 3.2.3 Single cell encapsulation in 3D microniches

Human mesenchymal stem cells (hMSCs) were deposited into the microniches by seeding on top of the patterned gel surface, followed by gentle shaking, and incubation at 37 °C for 10~15 min. Excess cells were removed by gentle washing with cell culture medium several times. To determine the efficiency of the seeding process, we counted cells by staining nuclei with DAPI (**Figure 3.3a**). When the cell density was too high (10000 cells per $cm^2$), cells were present on the surface of the MeHA hydrogel between microniches, requiring extensive washing with medium buffer, risking removal of cells from wells. Cell seeding density at 2500 cells per $cm^2$

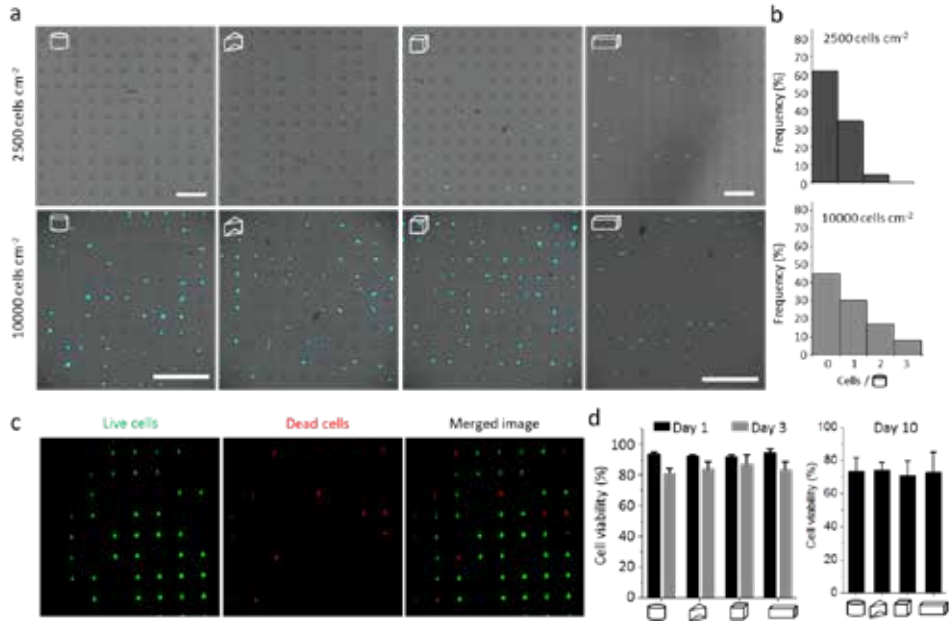


**Figure 3.3. Cell encapsulation in 3D microniches.** (a) Fluorescence image shows nuclear staining of single cells encapsulated in 3D microniche with different geometries at different cell densities (2500 and 10000 cells per $cm^2$), scale bar: 100 µm. (b) Cell encapsulation efficiency at different cell densities in the 3D microenvironment with cylindrical geometry. (c) Representative images of live/dead assay for hMSCs cultured in prismatic 3D microniche. The cells were stained with calcein AM (green) and Ethidium homodimer-1 (red). d) Quantitative analysis of live/dead cell viability of cells cultured in microniches with different geometries after 1, 3 and 10 days. mean ± s.d., n ≥ 4 regions of interest (ROI) with totals of 80-100 cells analyzed.

was optimal, with ~37% of wells filled with cells, and over 95% containing single cells (**Figure 3.3b**). To confirm the biocompatibility of 3D microniches, we measured the viability of hMSCs encapsulated in sealed 3D microniches via live/dead assay (**Figure 3.3c**). After 24 h culture, over 90% cells remained alive in 3D microniches with different geometries (cubical, cylindrical, triangular prismatic and cuboid), and over 80% cells were still alive after 3 days culture. After 10 days culture, over 70% cells were still alive (**Figure 3.3d**). These data confirmed that our 3D microniches maintain cell size and geometry for extended culture times.

### 3.2.4 Cell spreading and proliferation in 3D microniche

**Figure 3.4a and b** shows that the spreading of cells on MeHA gels with and without Fn coating. In consistent with previous finding[22], hMSCs cultured on Fn-coated MeHA hydrogel displayed higher spreading area than on pure MeHA hydrogel. Control experiments also showed that without Fn coating, cells showed significantly less spreading and did not fully occupy the 3D niches (**Figure 3.4c**). These cell spreading results demonstrated the importance of coating the inside to the microniches with Fn.

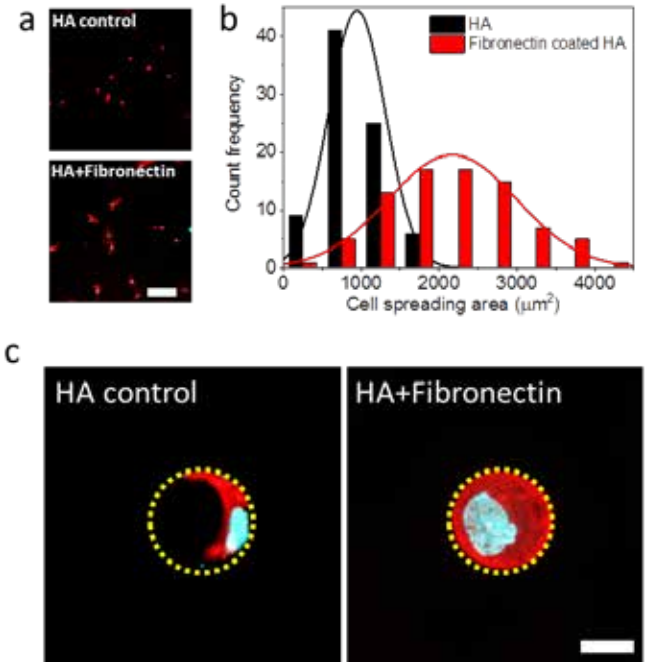


**Figure 3.4. Cell spreading on MeHA gel with and without fibronectin coating.** a) Representative images of hMSCs on flat MeHA and fibronectin coated MeHA substrate. b) Normalized distribution of spreading area of hMSCs on MeHA substrate (n ≈150) and fibronectin coated MeHA substrate (n ≈ 170). c) Representative images of DAPI (blue) and F-actin (red) staining for single hMSCs cultured in 3D microniche for 12 hours. The project area and height of microniche is 400 μm$^2$ and 9 μm respectively.

Since we want to focus on MSC behavior at single cell level, it is an important parameter to only have one cell per well. We performed an EDU proliferation assay after 3 and 10 days culture in 3D microniches with different geometries to test cell proliferation in 3D microniches. Proliferation on flat MeHA hydrogels coated with fibronectin was used as a control. Geometry of cells had no impact on cell proliferation, and quantification of hMSC proliferation as determined by EdU incorporation shows compared with cells on 2D MeHA substrates, cell proliferation within 3D microniches was suppressed (**Figure 3.5a and b**). We calculated the number of cells in microniches with different volumes from DAPI staining after 1 day culture, as shown in **Figure 3.5c**. After 1 day culture, less than 5% microwells contained two cells with different volumes. Even though a higher percentage of two cells can be observed from the largest volume, there is no significant difference in cell numbers per microniches among different volumes after 1 day culture.

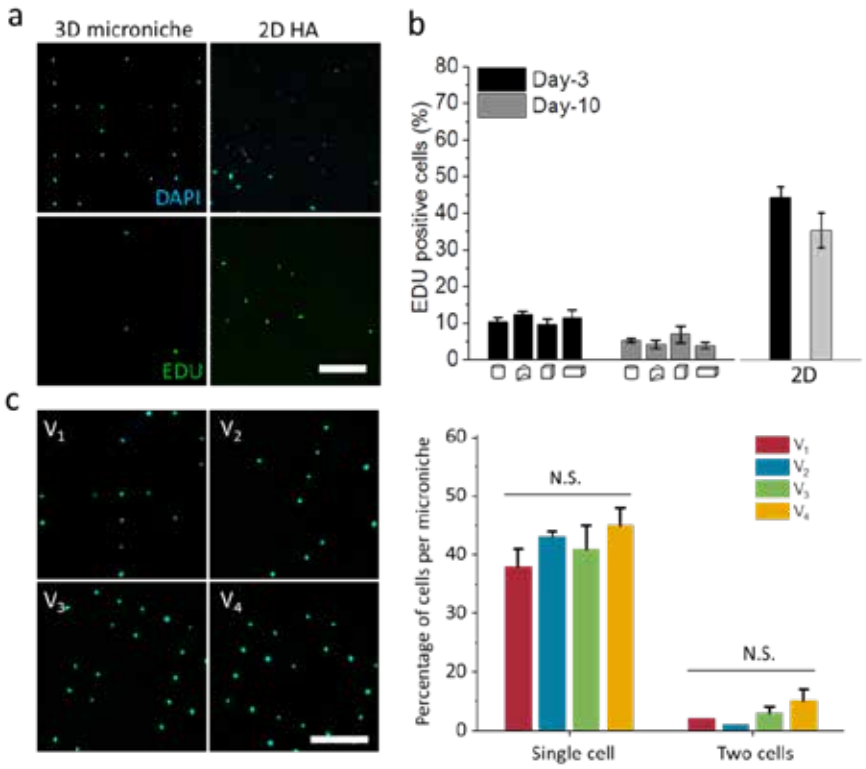


**Figure 3.5. Cell proliferation in 3D microniches.** a) Representative images of EdU assay in hMSCs cultured in 3D microniche and on 2D flat Fn coated MeHA hydrogel after 10 days. b) Proliferation of hMSCs over 3 and 10 days as determined by EdU incorporation. c) Percentage of one cell or two cells per cylindrical microniche with different volumes after 1 day culture. Scale bar 100 µm. mean ± s.d., n ≥ 5 regions of interest (ROI) with totals of 100-150 cells analyzed, $*P < 0.05$, N.S. means no significant differences. Microniches with heights 23, 12, 9, and 7 µm are denoted as $V_1$, $V_2$, $V_3$, and $V_4$, respectively

### 3.2.5 3D Microniche to control single cell volume

We would like to stress the crucial differences between our 3D microniches and previous work on cells cultured in open microwells[16, 25, 26] and 2D patterns[5, 9, 11, 13]. Fluorescence intensity heat maps on cells (n=21 to n=26) cultured in hydrogels with and without lid, show that only in the fully enclosed 3D niches, F-actin filaments were homogenously distributed from top to bottom (**Figure 3.6a**). Fluorescent heatmaps and 3D reconstructions showed that cells completely filled 3D microniches with lids, but without lids, the surface of cells was irregular (**Figure 3.6b and c**), and their volumes never match the volume of the mold (**Figure 3.6d**). This clearly shows that cells in wells without lids will not have uniform volumes, and will polarize due to the lack of integrin binding at the top surface (**Figure 3.6e**); Cells in 3D microniche with lid on top can form integrins from top to bottom. However, no integrin binding at the top surface was observed for cells in microwells without lid on top. therefore such substrates are not suitable for probing the impact of geometry of the 3D microniche on cell behavior.

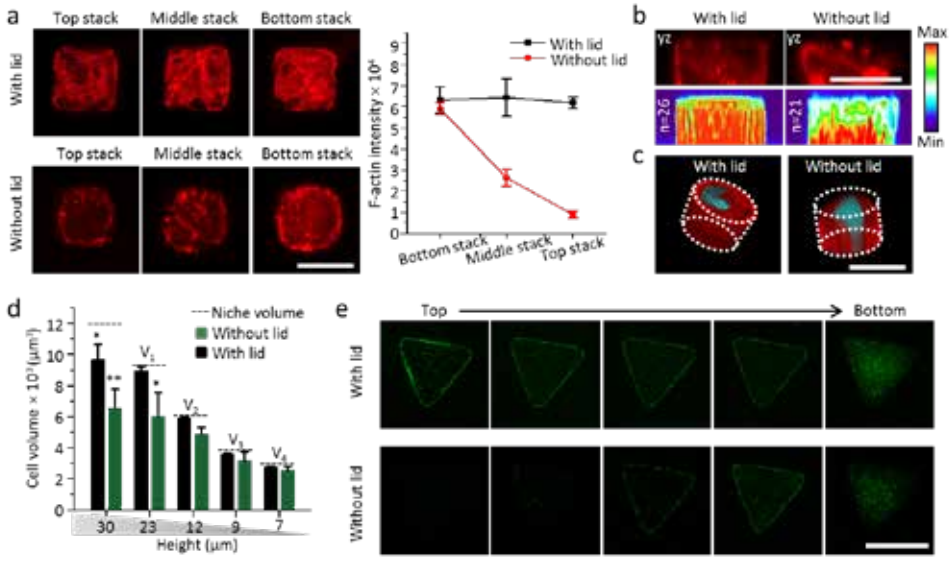


**Figure 3.6. 3D microniches to control cell volume.** a) F-actin staining for cells cultured in 3D microniche with and without lid on top. Scale bar 20 µm. To visualize the altered actin organization in microniche with and without lid on top, the fluorescent signals of actin (phalloidin 633) were quantified after 24 hours. mean ± s.d., n = 30-50 cells analysed. b) Side view and fluorescent heat maps of actin organization in a microenvironment with and without lid, red: F-actin, scale bar: 20 µm. c) 3D organization of actin cytoskeleton in a microenvironment with and without lid, red: F-actin, blue: nuclear, scale bar: 20 µm. d) Quantification of cell volume after 24-h culture in a microenvironment with and without lid; n = 50–60 cells analyzed for each data point. The microniche volume was controlled by changing the height (from 7 to 30 µm), with a constant value for project area (400 µm$^2$). e) β1 integrin staining for cells in microniche with and without lid on top. The height of microwells is 23 µm and the lateral dimension is 400 µm$^2$. The scale bar is 20 µm. The lid was not removed during integrin staining. Scale bar 20 µm. Data are shown as mean ± s.d. for all panels, and *P < 0.05, **P < 0.01 (ANOVA using a Tukey post-test), compared to theoretical niche volume.

## 3.3 Conclusion

In this chapter, we presented a robust method to control cell volume and shape of individual human mesenchymal stem cells (hMSCs) inside 3D microniches with a range of different geometries (e.g., cylinder, triangular prism, cubic, and cuboid) based on HA hydrogels. HA microwells could be selectively coated with cell-adhesion proteins, the shape, size, and stiffness of microwells could be well-controlled as well, giving a targeted investigation of the synergy between cell shape, biophysical, and chemical signals. The MeHA hydrogel lid allows nutrients and waste to pass through, leading to a cell viability as high as 70% after 10 days culture. Unlike previously developed cellular microarray platforms, microwells or 2D micropatterned substrates, our 3D microniches fully enclose cells, providing a completely non-polarized microenvironment of precisely defined volume. We therefore conclude that our 3D microniches will provide a platform to culture cell and probe single stem cell fate (i.e. differentiation), and has potential applications in investigating cell-cell or cell-matrix communication in local 3D environment.

## 3.4 Acknowledgements

We are grateful to Stéphanie M. C. Bruekers for helpful discussions, Aigars Piruska for preparing silicon masks and writing the FIJI scripts for analysis, José M. A. Hendriks for assistance with cell cultures and Dr. Liesbeth Pierson for assistance with confocal microscopy. The department of General Instruments of the Radboud University is acknowledged for providing confocal and light microscopy services.

## 3.5 Experimental section

### 3.5.1 3D microniche fabrication

*3.5.1.1 MeHA synthesis*

MeHA was synthesized following a previously described procedure[27, 28.] Briefly, methacrylic anhydride (MA) (Sigma) was added to a 1% w/v solution of sodium hyaluronate (HA, Lifecore, 70 kD) (2.4 ml MA per gram of HA) at pH 8.0 on ice for 8 h, and subsequently reacted with MA (1.2 ml MA per gram of HA) at pH 8.0 on ice for 4 h. The pH was adjusted with 5 M NaOH. The reaction mixture was dialyzed in deionized water (Spectrapor, molecular weight cutoff 3.5 kDa) at 4˚C for 3 days and lyophilised. 1H NMR (Bruker Avance III 400 MHz) was used to confirm methacrylation of hydroxyl groups on HA.

*3.5.1.2 Fabrication of MeHA microwells and lid*

Microwells with different geometries and different dimensions were produced on a silicon mask using standard photolithography and inductively coupled plasma etching (ICP). The

silicon master was silanized with 1H,1H,2H,2H-Perfluordecyltriethoxysilan (Sigma). The photoinitiator for the hydrogel, lithium phenyl-2,,4,6-trimethylbenzoylphosphinate (LAP) was synthesized following a previously described procedure[29]. MeHA macromer and LAP were separately dissolved in PBS (pH 7.4) and mixed at room temperature to a final weight percentage of 9:1 respectively. Crosslinking of the gel was initiated by irradiation with a UV lamp (ABM, USA) at 25 mW/cm$^2$ for 5 minutes with a light output of 30%. The gel was peeled off the silicon master and washed two times 30 minutes in PBS buffer to remove LAP. A lid was produced in a 24 microwell plate. A thin layer of the MeHA pre-solution (200 µL) with photoinitiator described above was crosslinked with the UV lamp for 5 min at 30% intensity. To visualize the MeHA lid cover on the microwells, 0.1 wt% rhodamine (Sigma) was added to pre-solution to form MeHA hydrogel lid.

*3.5.1.3 Fabrication of polyacrylamide (PAAm) gel containing PLL-g-PEG*

PAAm gel containing PLL-g-PEG was made on a glass coverslip (13 mm, thickness no 1, borosilicate glass), in order to make PAAm gel attach on the glass coverslip, coverslips were oxidised using oxygen plasma (Diener electronic) and then incubated in a 0.3 wt/vol% solution of 3-(trimethoxysilyl)propyl methacrylate (Sigma Aldrich) in dry toluene overnight. The slides were washed thoroughly with ethanol and water. Solutions of acrylamide (AA) at final concentrations of 30 wt/vol% and bis-acrylamide (BA) at 0.5 wt/vol% was prepared. 30 µL of 1 mg/mL PLL-g-PEG (Sigma-Aldrich) in PBS was added to 1 mL polyacrylamide (PAAm) pre-gel, polymerization was initiated by the addition of 10 µL of 10 wt/vol% ammonium persulfate (Sigma Aldrich) and 3 µL TEMED (Sigma Aldrich) to the AA/BA solutions in PBS. 5 µL of the gel precursor solution was immediately pipetted onto de methacrylated glass coverslips and a 20 mm glass coverslip, washed but untreated, was carefully placed on top of the polymerizing solution. After 2 h, the samples were soaked in PBS buffer overnight to remove the remaining monomer and crosslinker. The top coverslips were peeled off to obtain the PAAm gels containing PLL-g-PEG adhering to the glass coverslips.

*3.5.1.4 MeHA hydrogel functionalization with fibronectin*

The space in between the microwells on the MeHA hydrogel was made resistant to protein adsorption and cell adhesion with PLL-g-PEG. The PLL-g-PEG was attached to the hydrogel following a microcontact printing procedure. The MeHA hydrogel containing microwells was placed upside down on the PAAm gel (fully dried) containing PLL-g-PEG for 1 h with a 10 g weight. To increase the amount of transferred PLL-g-PEG, the procedure was repeated up to 6 times. Afterwards, fibronectin (Fn, Sigma-Aldrich) solution at 100 µg/mL was added on the surface of the MeHA gel for 1 hour at room temperature, followed by washing three times with PBS to remove extra Fn solution. Fn inside microwells was stained with anti-fibronectin antibody (Abcam, ab2413, 1:1000). For MeHA hydrogel lid preparation, same protocol was used but without PLL-g-PEG treatment.

*3.5.1.5 Permeability of MeHA hydrogel cover*

MeHA microwells covered with MeHA hydrogel was placed under a SP8 confocal microscope, and then immersed in cell culture medium containing 0.1 mg/mL GFP for 10 min. Images were taken at various time points and photon counting mode was used for quantitative analysis of the fluorescence intensity.

### 3.5.2 Hydrogel mechanical characterization

In order to show the possibility of changing stiffness for MeHA hydrogel, different MeHA concentration was used to obtain gels with a range of crosslinking densities. Stiffness of gels were measured by nanoindentation under an atomic force microscope (Bruker Nanoscope) using the "point and shoot" procedure (Nanoscope software, Bruker) as we reported previously[30]. A fluorescent polystyrene bead with 10 µm diameter (Invitrogen) was glued to silicon nitride cantilevers with nominal spring constants of 0.06 N/m (NP-S type D, Bruker). We calibrated the system in cell-free medium at 37 °C prior to each experiment by measuring the deflection sensitivity when pressing the cantilever onto a glass coverslip, which allowed the cantilever spring constant to be determined using the thermal noise method. For each MeHA gel, indentation force curves at six different locations on the gels were acquired. Before and during indentation experiments gels were kept in PBS in 37°C. To obtain stiffness values from force curves we used the PUNIAS software (http://punias.free.fr). Specifically, we corrected for baseline tilt, and used the linear fitting option for the Hertz model with a Poisson ratio of 0.5 on the indentation curve.

### 3.5.3 Culturing of hMSCs and seeding into 3D microniche

hMSCs were obtained from Lonza and cultured in DMEM low glucose (Gibco) supplemented with 10% FBS (Gibco), 1% L-glutamine and 1% Pen/Strep (Thermo fisher scientific). Cells were passaged before confluency and used at passage 6. Cells were seeded on the MeHA-Fn substrate containing microwells at a certain density in DMEM high glucose (GE healthcare) and incubated for 10~15 minutes, subsequently the MeHA hydrogel was washed several times with a gentle flow of medium to remove non-adherent cells, and placed on top of a thin MeHA-Fn hydrogel lid (~ 30 µm height).

### 3.5.4 Cell staining

hMSC cells that adhered within MeHA-Fn microniches were fixed with 4% paraformaldehyde (Sigma) for 10 min, and then the lid of microniches was carefully removed, followed by washing three times with PBS and then permeabilised with 0.2% Triton-X100 (Sigma) in reverse osmotic $H_2O$, washed two times with PBS and incubated with 1% bovine serum albumin (BSA) in PBS for 1 h. Subsequently the cells were stained with phalloidin tetramethyl-rhodamine B isothiocyanate (TRITC) (Millipore, R415, 1:1000 in 1% BSA) for 1 h to visualize F-actin and 4,6-diamidino-2-phenylindole (DAPI) (Millipore,

28718-90-3, 1:1000 in 1% BSA) to visualize nucleus for 1 h at room temperature, followed by three times PBS wash and one $H_2O$ wash. Images were taken within 24 hours after staining using a Leica SP8 confocal laser scanning microscope (Leica, Germany).

### 3.5.5 Cell viability analysis

To analyze cellular viability, a Live/Dead assay was performed with calcein AM and ethidium homodimer (Molecular Probes, Invitrogen detection technologies). These components were added to PBS at a concentration of 2 µg/mL and 4 µg/mL respectively. After removing the lid, the hydrogels containing cells were incubated in this solution for 30 min at room temperature and visualized under a Leica SP8 confocal microscope. Live cells stain green while dead cells take up the red dye.



### 3.5.6 Cell proliferation assay

Cell proliferation was determined by EdU labeling. hMSCs were seeded in 3D microniches for 2 and 9 days, followed by treatment with 1× EdU solution. When the incubation up to 3 and 10 days, cells were fixed and permeabilized with 4% PFA and 0.1% Triton X-100, respectively. Following these processes, samples were treated according to the manufacturer's protocol of Click-iT EdU Alexa Fluor-488 HCS Assay (Thermo Fisher Scientific). All images were collected by a Leica SP8 confocal microscope (Leica, Germany) with filters for DAPI and Alexa Fluor-488. For quantification, lower magnification (10 × objective) fields were collected within regions of interest.

### 3.5.7 Microscopy data analysis

All confocal images were taken with different Z-stacks and overlaid in Fiji software with Image 5D plugin. The distance between two z-stacks was the same (1 µm) for all the sample. For quantification of cell volume, project area (Aproject) of single cells were calculated by averaging the F-actin area of different z-stacks, the height (H) of cells were quantified from cross-section view of >30 cells, the volume was then calculated as: $A_{project} \times H$.

### 3.5.8 Statistics

Statistical analysis was performed with Origin software and one-way analysis of variance (ANOVA) using a Tukey post-test for more than two variables was carried out. "Significant" and "very significant" differences were indicated by * ($P < 0.05$) or ** ($P < 0.01$), respectively. All results were expressed as mean ± standard error.

## 3.6 References


1. Scadden, D.T. The stem-cell niche as an entity of action. *Nature* **441**, 1075 (2006).
2. Cosgrove, B.D. *et al.* N-cadherin adhesive interactions modulate matrix mechanosensing and fate commitment of mesenchymal stem cells. *Nat. Mater.* **15**, 1297-1306 (2016).
3. Engler, A.J., Sen, S., Sweeney, H.L. & Discher, D.E. Matrix elasticity directs stem cell lineage specification. *Cell* **126**, 677-689 (2006).
4. McBeath, R., Pirone, D.M., Nelson, C.M., Bhadriraju, K. & Chen, C.S. Cell shape, cytoskeletal tension, and RhoA regulate stem cell lineage commitment. *Dev. Cell* **6**, 483-495 (2004).
5. Théry, M. *et al.* Anisotropy of cell adhesive microenvironment governs cell internal organization and orientation of polarity. *Proc. Natl. Acad. Sci.* **103**, 19771-19776 (2006).
6. Chen, C.S., Mrksich, M., Huang, S., Whitesides, G.M. & Ingber, D.E. Geometric control of cell life and death. *Science* **276**, 1425-1428 (1997).
7. Lee, J., Abdeen, A.A., Wycislo, K.L., Fan, T.M. & Kilian, K.A. Interfacial geometry dictates cancer cell tumorigenicity. *Nat. Mater.* **15**, 856-862 (2016).
8. Ginzberg, M.B., Kafri, R. & Kirschner, M. On being the right (cell) size. *Science* **348**, 1245075 (2015).
9. Connelly, J.T. *et al.* Actin and serum response factor transduce physical cues from the microenvironment to regulate epidermal stem cell fate decisions. *Nat. Cell Biol.* **12**, 711-718 (2010).
10. Schiller, H.B. *et al.* β1-and αv-class integrins cooperate to regulate myosin II during rigidity sensing of fibronectin-based microenvironments. *Nat. Cell Biol.* **15**, 625-636 (2013).
11. Jain, N., Iyer, K.V., Kumar, A. & Shivashankar, G. Cell geometric constraints induce modular gene-expression patterns via redistribution of HDAC3 regulated by actomyosin contractility. *Proc. Natl. Acad. Sci.* **110**, 11349-11354 (2013).
12. Kassianidou, E., Brand, C.A., Schwarz, U.S. & Kumar, S. Geometry and network connectivity govern the mechanics of stress fibers. *Proc. Natl. Acad. Sci.*, 201606649 (2017).
13. Kilian, K.A., Bugarija, B., Lahn, B.T. & Mrksich, M. Geometric cues for directing the differentiation of mesenchymal stem cells. *Proc. Natl. Acad. Sci.* **107**, 4872-4877 (2010).
14. Gjorevski, N. *et al.* Designer matrices for intestinal stem cell and organoid culture. *Nature* **536**, 560-564 (2016).
15. Caliari, S.R. & Burdick, J.A. A practical guide to hydrogels for cell culture. *Nat. Methods* **13**, 405-414 (2016).
16. Gobaa, S. *et al.* Artificial niche microarrays for probing single stem cell fate in high throughput. *Nat. Methods* **8**, 949-955 (2011).
17. DeForest, C.A. & Tirrell, D.A. A photoreversible protein-patterning approach for guiding stem cell fate in three-dimensional gels. *Nat. Mater.* **14**, 523-531 (2015).

18. Mosiewicz, K.A. *et al.* In situ cell manipulation through enzymatic hydrogel photopatterning. *Nat. Mater.* **12**, 1072-1078 (2013).
19. Chaudhuri, O. *et al.* Hydrogels with tunable stress relaxation regulate stem cell fate and activity. *Nat. Mater.* **15**, 326 (2016).
20. Caliari, S.R., Vega, S.L., Kwon, M., Soulas, E.M. & Burdick, J.A. Dimensionality and spreading influence MSC YAP/TAZ signaling in hydrogel environments. *Biomaterials* **103**, 314-323 (2016).
21. Burdick, J.A. & Prestwich, G.D. Hyaluronic acid hydrogels for biomedical applications. *Adv. Mater.* **23** (2011).
22. Chopra, A. *et al.* Augmentation of integrin-mediated mechanotransduction by hyaluronic acid. *Biomaterials* **35**, 71-82 (2014).
23. Gerecht, S. *et al.* Hyaluronic acid hydrogel for controlled self-renewal and differentiation of human embryonic stem cells. *Proc. Natl. Acad. Sci.* **104**, 11298-11303 (2007).
24. Jin, J. *et al.* A triggered DNA hydrogel cover to envelop and release single cells. *Adv. Mater.* **25**, 4714-4717 (2013).
25. Ochsner, M. *et al.* Micro-well arrays for 3D shape control and high resolution analysis of single cells. *Lab Chip* **7**, 1074-1077 (2007).
26. Beachley, V.Z. *et al.* Tissue matrix arrays for high-throughput screening and systems analysis of cell function. *Nat. Methods* **12**, 1197-1204 (2015).
27. Burdick, J.A., Chung, C., Jia, X., Randolph, M.A. & Langer, R. Controlled degradation and mechanical behavior of photopolymerized hyaluronic acid networks. *Biomacromolecules* **6**, 386-391 (2005).
28. Khetan, S. *et al.* Degradation-mediated cellular traction directs stem cell fate in covalently crosslinked three-dimensional hydrogels. *Nat. Mater.* **12**, 458-465 (2013).
29. Fairbanks, B.D., Schwartz, M.P., Bowman, C.N. & Anseth, K.S. Photoinitiated polymerization of PEG-diacrylate with lithium phenyl-2, 4, 6-trimethylbenzoylphosphinate: polymerization rate and cytocompatibility. *Biomaterials* **30**, 6702-6707 (2009).
30. Xie, J., Bao, M., Bruekers, S.M. & Huck, W.T. Collagen gels with different fibrillar microarchitectures elicit different cellular responses. *ACS Appl. Mater. Interfaces* **9**, 19630–19637 (2017).

# Chapter 4

## 3D microniches reveal the importance of cell size and shape

This chapter has been published in:
Bao, M., Xie, J., Piruska, A., & Huck, W. T. 3D microniches reveal the importance of cell size and shape. Nature Communications **2017**, 8(1), 1962.

## Abstract

Geometrical cues have been shown to alter gene expression and differentiation on 2D substrates. However, little is known about how geometrical cues affect cell function in 3D. In this chapter, we encapsulate individual human mesenchymal stem cells (hMSCs) into 3D microniches with a range of different geometries (e.g., cylinder, triangular prism, cubic and cuboid) and volumes. We demonstrate that the cell volume, instead of the aspect ratio, project area or shortest axis, is the main factor to regulate cell stress fiber formation. Furthermore, we find focal adhesions, nuclear shape, YAP/TAZ localization, cell contractility, nuclear accumulation of HDAC3, and lineage selection, are all sensitive to cell volume (and to a lesser extent geometry). Our 3D microniches enable fundamental studies into the impact of biophysical cues on cell fate, and have potential applications in investigating how multicellular architectures organize within geometrically well-defined 3D spaces.

## 4.1 Introduction

*In vivo*, stem cells reside in a three-dimensional (3D) dynamic and complex microenvironment or niche, which is critical to maintain stem cell self-renewal and differentiation[1, 2]. The geometry has emerged as an important cue that can be transduced into biochemical signals and result in cell responses[3-8]. The influences of a wide range of geometrical cues that regulate cell function at the single cell level in 2D culture have been well documented in the last decade[5-13]. Early work demonstrated how the shape of cells could be engineered by micro-contact printed adhesive islands[11], and how cell shape and size can play a very important role in directing growth, death and differentiation of mesenchymal stem cells (MSCs)[7, 8]. Cells cultured in mixed media and on large islands preferred to differentiate towards osteoblasts, while small round cells typically showed adipogenesis[7]. Substrates with defined geometry have also been used to study cytoskeletal dynamics[6, 12], and cell tension distribution at a single cell level, where strong stretching or spreading led to a higher degree of cytoskeletal tension and promoted bone differentiation[9, 13, 14]. However, all of these findings are based on 2D substrates and how 3D geometry affects cell function remains elusive. One major reason for this lack of understanding is rooted in the difficulties of controlling cell morphology in a complex 3D setting for long periods of culture. Although significant progress has been made in encapsulating and culturing cells in a variety of synthetic hydrogels (PLGA[15], PEG[16, 17], agarose[18, 19], supramolecular materials[20]) as well as natural materials (such as collagen[21], fibrin[22], hyaluronic acid[23], polysaccharide[24]), there have only been a few reports on controlling the shape of the 3D environment with μm precision[25-33]. However, these methods were technologically challenging, limiting the number of cells that could be studied, or were incompatible with cell culture due to lack of porosity or biocompatibility of the well materials used, did not encapsulate single cells, or were only pseudo 3D as the cells were not fully encapsulated.

We have introduced in chapter 3 that we could constrain stem cell volume and geometry in a systematic and quantitative manner, by encapsulating cells in 3D hydrogel microniches. In this chapter, we will present results on how volume and geometry of 3D microniches affect actin polymerization, protein localization, gene expression, and lineage selection in hMSCs with systematically increasing volumes and geometries with different aspect ratios (cubic and cuboid) and shapes (cylinder and triangular prism).

## 4.2 Results and discussion

### 4.2.1 Stress fibers and F-actin polymerization in 3D microniche

Experiments on 2D micropatterned islands have shown strong correlations between

island geometry (shape, presence of sharp angles) and the organization of the actin cytoskeleton and focal adhesions[9]. However, on such islands, cells are spread, volumes are not controlled, and the actin fibers are confined within a thin layer. We investigated the influence of cell volume on the organization of the cytoskeleton, by systematically varying the height of 3D microniches (23, 12, 9 and 7 μm, respectively. Denoted as $V_1$, $V_2$, $V_3$ and $V_4$) while keeping the lateral dimensions fixed (400 $\mu m^2$). All these sizes were bigger than the average starting diameter and volume of hMSCs (~6.5 μm and ~2100 $\mu m^3$), which means cells were able to spread and expand in the microniches and cell nuclei were not compressed initially in any of the microniches. Surprisingly, as shown in **Figure 4.1a**, in the largest volume cells ($V_1$), F-actin staining showed few stress fibers and no apparent organization. With the volume of cells decreasing, increasingly clear and

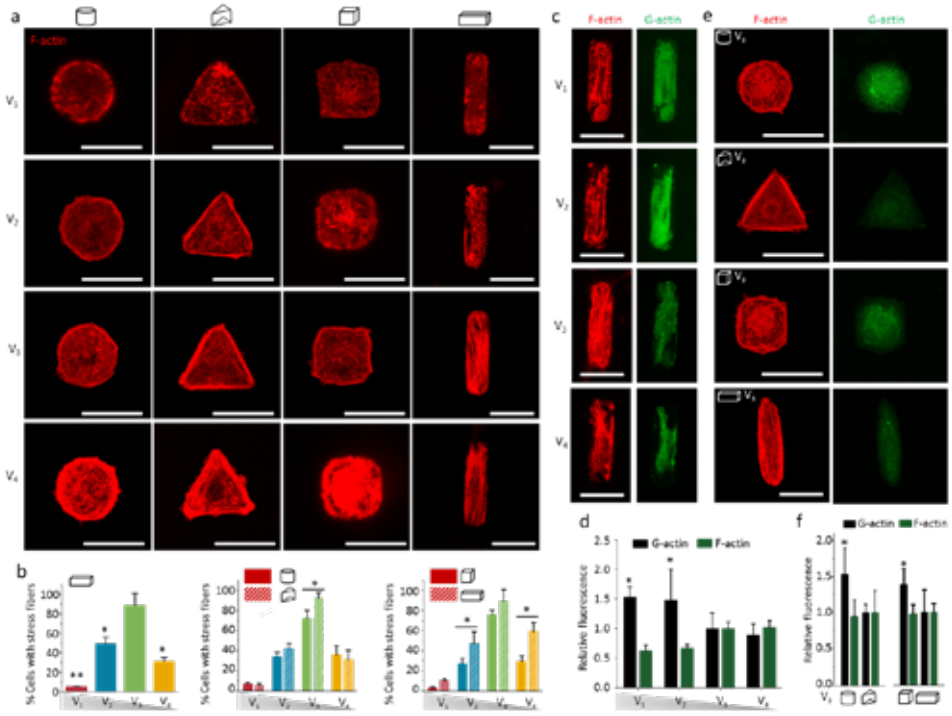


**Figure 4.1**. **F-actin filaments formation and polymerization in 3D microniche.** (**a**) Representative images of F-actin staining for hMSCs with different cell volumes and cell geometries after 24 h. (**b**) Quantification of the number of cells forming stress fibers in 3D microniche with different sizes and geometries. *n* = 50-60 cells analyzed for each data point. (**c**) Immunofluorescence images of F-actin and G-actin for hMSCs with different volumes after 12 h. (**d**) Quantification of F- and G-actin levels 12 h after seeding in 3D microniches with different volumes. Total integrated fluorescence of phalloidin (F-actin) and DNaseI (G-actin) was normalized to the fluorescence of $V_3$ cells. *n* = 40-45 cells analyzed for each data point. (**e**) Immunofluorescence images of F-actin and G-actin for hMSCs with different geometries with $V_3$ volume after 12 h. (**f**) Comparison of normalized mean F- and G-actin intensity in cells with different shapes (cylinder and triangular prism) and aspect ratios (cubic and cuboid). *n* = 40-45 cells analyzed for each data point. Data are shown as mean ± s.d. for all panels, and *P < 0.05, **P < 0.01. Scale bar for all images is 20 μm.

organized stress fibers were observed, and the number of cells that formed stress fibers increased significantly in 3D microniches with $V_3$ volume. However, fewer stress fibers were observed in the smallest size cells ($V_4$).

In addition to cell volume, cell geometry also impacted on F-actin organization. Cells cultured in 3D microniches with the same volume ($V_3$) but different shapes (triangular prism and cylinder) and aspect ratios (cuboid 1:4 and cube 1:1) showed markedly different F-actin organization, with more stress fibers observed in triangular prism and cuboid cells. It is interesting to note that F-actin organization became insensitive to changes in cellular shape (triangular prism and cylinder) in cells with greater ($V_1$) or smaller volumes ($V_4$) (**Figure 4.1a and b**).



It was previously reported that the ratio between F- and G-actin was an important determinant of cell fate in keratinocytes on micropatterned islands[10]. Quantification of phalloidin (F-actin) and DNaseI (G-actin) fluorescence revealed significantly higher levels of F-actin and lower levels of G-actin in cells with niche heights of 9 μm compared to cells in microniches with larger heights ($V_3$ vs $V_1$ and $V_2$; **Figure 4.1c and d**). For a fixed cell volume ($V_3$), the G and F-actin levels were also dependent of cellular shape or aspect ratio. Cells with triangular prism and cuboid geometry displayed 55% and 42% lower signals for monomeric G-actin and comparable signals for F-actin compared with cells cultured in cylindrical and cubical microniches (**Figure 4.1e and f**).

Next, we seeded cells in microniches with different project areas (1022, 533, 400, 311 $\mu m^2$) and different geometries, but the same height (9 μm), where the project area of 400 $\mu m^2$ corresponds to the original $V_3$ microniches. We evaluated the cellular responses by investigating stress fiber formation. We found that when the project area (and corresponding volume) was too large (1022 and 533 $\mu m^2$) or too small (311 $\mu m^2$), F-actin staining showed few stress fibers, and little organization of the cytoskeleton – in contrast to the original $V_3$ microniches with a 400 $\mu m^2$ project area (**Figure 4.2a and b**).

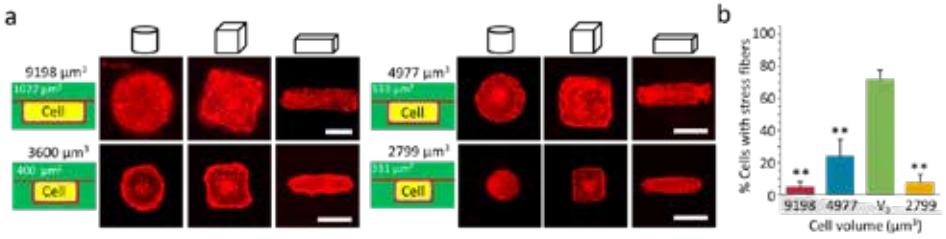


**Figure 4.2. F-actin filaments formation in 3D microniche with different volumes (same height but different project areas).** a) F-actin (red) staining for cells seeded in microniches with different project area (1022, 533, 400, 311 $\mu m^2$) and different geometries (cylinder, cubic and cuboid) but the same height (9 μm). Scale bar 20 μm. b) Quantification of the number of cells forming stress fibers in 3D microniche with different volumes (different project areas but the same height). Data are shown as mean ± s.d. n=25-31 cells analyzed for each data point and $**P < 0.01$.

To further confirm that cell volume, and not aspect ratio, project area or shortest axis, is the main factor in determining actin filaments formation in 3D, we mapped the stress fiber formation in cells seeded in microniches with different project areas (1022, 533, 400, 311 μm$^2$) and different heights (7, 9, 12, 23 μm) (**Figure 4.3**). Remarkably, clear stress fibers were found in volume ranges around 3600-3700 μm$^3$ (close to $V_3$), up to approx. 4800 μm$^3$ (with fewer cells showing clear stress fibers), irrespective of project area or height. When microniches were too large (6393, 7153 or 7154 μm$^3$) or too small (2177 μm$^3$), very few cells with clear stress fibers were found. In summary, we found the remarkable impact of cell volume on F-actin self-organization, and our results on 3D microniches with different aspect ratios but similar volumes clearly showed the decisive influence of cell volume on stress fiber formation, within the range of sizes studied.

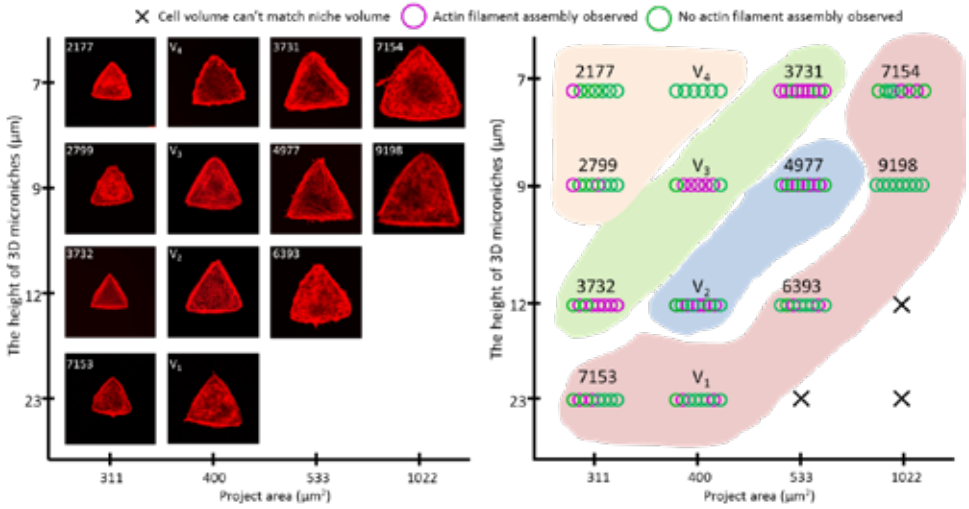


**Figure 4.3. Cell volume affect F-actin formation.** Left: F-actin staining for single hMSCs cultured in 3D microniches with different volumes. Representative cells were selected for each condition. Right: Quantification of the number of cells forming stress fibers in 3D microniche with different volumes. Colored regions show cells volumes between 2000 ~ 3000, 3000 ~ 4000, 4000 ~ 5000 and > 5000 μm$^3$ , respectively. The value of cell volumes were presented on each images.

### 4.2.2 Size and geometry affect FAs formation and cell tension

We expect that the dependency of the formation of stress fibers on cell volume, and to a lesser extent geometry, will at least partially result from the localization of focal adhesions (FAs). Unlike previous studies on 2D substrates, where more FAs are found in larger and spreading cells[34], we only observed distinct FAs in $V_3$ cells, and localization of vinculin (a FA-associated protein) to the periphery of the cells with different geometries was not observed in relatively large ($V_1$) or small cells ($V_4$) (**Figure 4.4a**). To assess differences in patterns of focal adhesion between cells with different geometries, immunofluorescent

heat maps were generated for >20 cells per geometry (**Figure 4.4b**). Similar to findings on 2D substrates[9], FAs were predominantly formed in regions of curvature in triangular prism cells or at the edge of cuboid cells with increasing aspect ratio. Immunofluorescent staining of myosin IIa, the primary motor protein assembly that is responsible for cell contractility and tension, was performed for hMSCs after 24 h culture. Cells with $V_3$ and $V_4$ were found to have higher levels of myosin IIa compared with $V_1$ and $V_2$ cells (**Figure 4.4c and d**). For cells with a fixed volume ($V_3$), myosin IIa intensity was strongly dependent on cell shape and aspect ratio (**Figure 4.4e and f**). Perturbation of myosin IIa activity by 50 μM Blebbistatin (Bleb) resulted in decreased formation of stress fibers (**Figure 4.4g**), indicating that the enhanced stress fiber formation in niches with optimal size and geometry, was regulated by cell contractility.



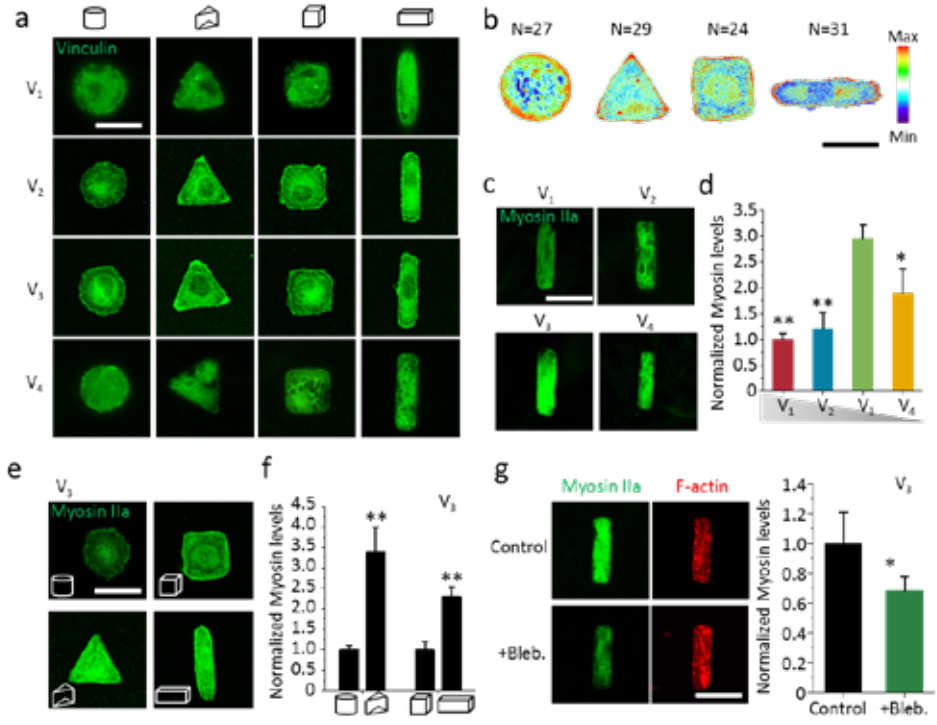


**Figure 4.4 Focal adhesions formation and cell tension in 3D microniche.** (**a**) Representative images of vinculin staining for single hMSCs cultured in 3D microniche with different volumes and geometries. (**b**) Fluorescent heatmaps of ≥ 20 cells with the same volume ($V_3$) but different geometries stained for vinculin. (**c**) Representative images of myosin IIa in cells of same geometry but different volumes. (**d**) Myosin IIa levels (per cell) as a function of cell volume. (**e**) Representative images of cells with different geometries but same volume ($V_3$). (**f**) Myosin IIa levels as a function of cell shape (cylinder and triangular prism) or aspect ratio (cubic and cuboid). (**g**) Representative images of Myosin IIa and F-actin before and after cells with $V_3$ treated with 50 μM Blebbistatin (Bleb), bar graph shows quantitation of changes in the level of Myosin IIa after treatment with 50 μM Blebbistatin (Bleb). Data are shown as mean ± s.d. for all panels, $n$ = 45-60 cells analyzed for each data point. and *P < 0.05, **P < 0.01 (ANOVA using a Tukey post-test). Scale bar for all images is 20 μm.

### 4.2.3 Size and geometry affect nuclear function and TF activity

Previous studies have shown that actin filaments play an important role in modulating nuclear shape and function[35]. We therefore expect to see nuclear deformation in cells with significant organization of actin filaments. **Figure 4.5a** shows the decreasing height of nuclei as a function of decreasing niche height from 23 to 7 μm. The volume of the nucleus was the largest (228 $\mu m^3$) in cells of volume $V_1$ and $V_2$ (no significant difference), while the nucleus volume decreased significantly with decreasing cell size from $V_2$ to $V_4$. We examined the chromatin condensation by using a quantitative procedure based on DAPI staining[35, 36]. **Figure 4.5b** shows a marked reorganization of chromatin distribution associated with nuclear deformation, as the uptake of DAPI depends on the total amount of DNA, but also on its level of condensation. The average spatial density of nuclei first increased with decreasing niche heights from 23 to 9 μm, then decreased when the niche height reached 7 μm (**Figure 4.5b**). To confirm the role of actomyosin filaments in the modulation of the nuclear architecture, we treated cells with cytochalasin D (Cyto D) or Blebbistatin (Bleb). As shown in **Figure 4.5c**, both treatments significantly decreased the average spatial density of nuclei by ~50%, indicating actin filaments play an important role in modulating nuclear shape and function.

Next, we examined nuclear localization of the YAP/TAZ transcriptional regulator, which is thought to be the key regulatory element controlling the gene expression of cells in response to physical cues[37]. Surprisingly, fluorescence staining (**Figure 4.5d**) showed that YAP/TAZ remained cytosolic in cells in microniches with $V_1$ and $V_2$ volume, but located into the nuclear region when the cell volume was $V_3$ and $V_4$. Nuclear translocation of YAP/TAZ increased from 52% to 70% with increasing cell volume from $V_4$ to $V_3$, but decreased to 5% with increasing cell volume to $V_1$.

In cells with $V_3$, YAP/TAZ localization was also strongly dependent on cell geometry (shape and aspect ratio), cells with triangular prism and cuboid geometry showing 82% and 73% nuclear YAP/TAZ localization, compared with 46% and 57% nuclear YAP/TAZ localization in cells with cylinder and cubic geometry, respectively (**Figure 4.5e**). Previous studies have shown nuclear histone acetylation is regulated by actomyosin contractility and nuclear morphology[36]. We investigated the effect of cells in different 3D microniches on histone acetylation levels by analyzing HDAC3[38], and found that nuclear levels of HDAC3 were lower in cells of $V_3$ compared larger ($V_1$ and $V_2$) ones (**Figure 4.5f**). Perturbation of actomyosin contractility results in nuclear accumulation of HDAC3 (**Figure 4.5g**), indicating nuclear HDAC3 localization is sensitive to changes in actomyosin contractility, which is consistent with literature reports[36]. It should be noted that previous literature reported that HDAC3 activity will give rise to chromatin condensation[36], the apparent correlation between HDAC3 levels and chromatic condensation in this study might indicate that other factors are altering chromatin condensation against the observed trend for HDAC3.

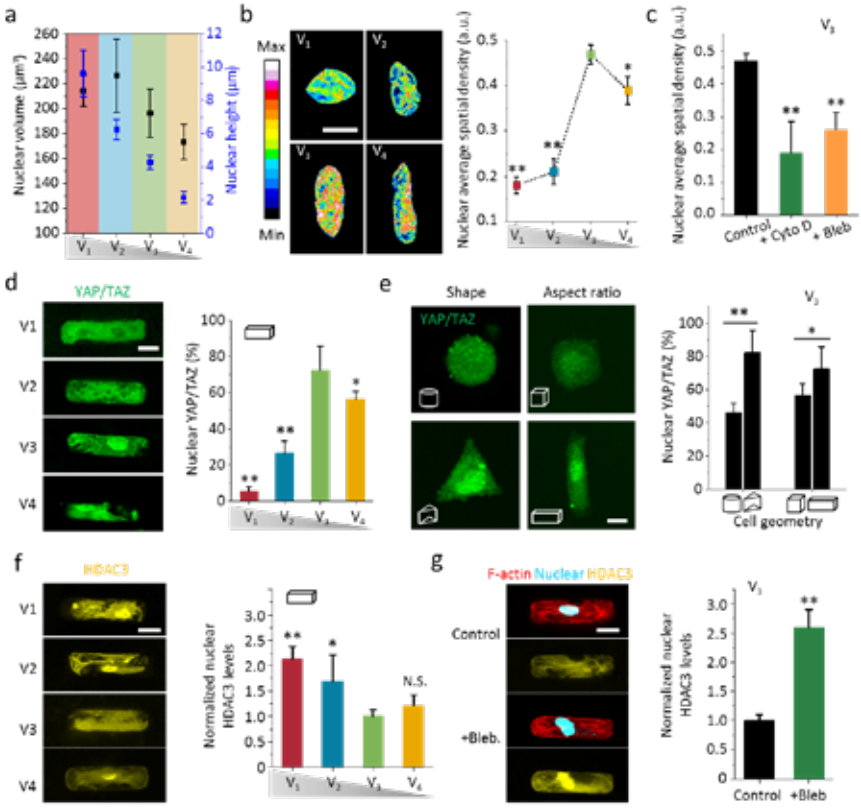


**Figure 4.5**. **Nuclear function and transcription factor activity** (**a**) Nucleus volume and height as a function of cell volume. The volume of nucleus was calculated by fitting the morphology of nucleus to an ellipsoidal shape. Data are given as mean ± s.d. with 12≤n≤15. (**b**) Quantitation of nucleus average spatial density (total DAPI intensity per nuclear volume) as a function of cell volume. Highly condensed domains show higher fluorescence intensity. The scale bar is 5 μm. (**c**) Quantitation of changes in the level of nucleus average spatial density for cells with$V_3$ after treatment with 1 μM cytochalasin D (Cyto D) or 50 μM Blebbistatin (Bleb). (**d**) Representative images and quantification of YAP/TAZ localization in hMSCs with different cell volumes but same geometry after 24 h. Scale bar 10 μm. (**e**) Representative images and quantification of YAP/TAZ localization in hMSCs with different cell geometries but same volume after 24 h. Scale bar 10 μm. (**f**) Representative images of hMSCs stained for HDAC3 on cells with different volumes but same geometry. Histogram shows nuclear HDAC3 levels as a function of cell volumes. (**g**) Representative images and quantitation of cells with $V_3$ treated with 50 μM Blebbistatin (Bleb). Data are shown as mean ± s.d. for all panels, $n$ = 50-60 cells analysed for each data point. *P < 0.05, **P < 0.01 (ANOVA using a Tukey post-test). N.S. means no significant difference.

Next, we studied nuclear YAP/TAZ localization in cells in microniches of 9 μm height, but different volumes. Consistent with stress fiber results above, nuclear YAP/TAZ localization was strongly dependent on cell volume (**Figure 4.6**).

In summary, changes in volume and geometry directly impinge on the distribution of YAP/TAZ: we observed maximum nuclear localization of YAP/TAZ in cells with $V_3$ volume

(by changing the height or aspect ratio of 3D microniches), and in cells with more anisotropic or sharp-angle-containing geometries, correlating with the fact that in those cells the presence of stress fibers, FAs localization, and cell tension were all highest.

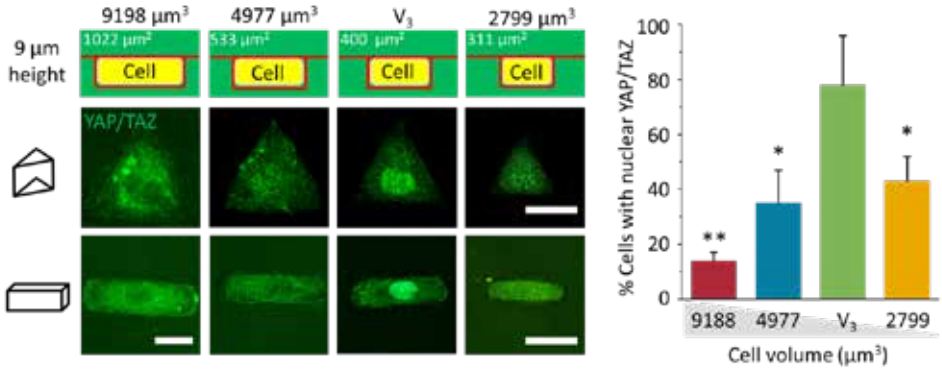


**Figure 4.6. Representative images and quantification of YAP/TAZ localization in hMSCs with different cell volumes (different project areas but the same height) after 24 h.** Scale bar 20 μm. Data are shown as mean ± s.d. with totals of 20~30 cells analyzed, and *P < 0.05, **P < 0.01.

### 4.2.4 Size and geometry affect mRNA concentration in cells

Biochemical reaction rates depend on the concentration of reactants and enzymes[39]. To maintain proper cellular function, concentrations must be buffered against fluctuations in volume. Experiments above have shown that we can change the confinement in one dimension by changing the height of the microniches, but we can also compare cells with similar aspect ratios yet different volumes. To study the impact of changes in cellular concentrations of key components in cells with different volumes, we quantified gene expression levels of specific genes using single-molecule multicolor mRNA fluorescence in situ hybridization (RNA FISH). Specifically, we monitored the expression of RhoA, Arp2/3 and TEAD1. RhoA is a protein that can stimulate formation of actin stress fibers, focal adhesions and cytoskeletal tension, and shape-dependent control of lineage commitment is mediated by RhoA activity[7, 40]. We found that copy numbers of RhoA mRNA increased with increasing cell volume from $V_4$ to $V_1$ (**Figure 4.7a and b**), and also depend on cell geometry (**Figure 4.7d**), a similar effect was found on 2D substrates[7]. However, the concentration of RhoA mRNA was significantly lower in larger cells (**Figure 4.7c**), indicating that RhoA was diluted in large cells. The actin-related protein-2/3 (Arp2/3) complex is a central protein in regulating actin filament formation[41], and the activity of Arp2/3 has been shown to strongly depend on RhoA[42]. Consistent with the results for RhoA, we find that cells with prism and cuboid shape have higher Arp2/3 mRNA copy numbers (**Figure 4.7e**). Thirdly, we studied mRNA levels of TEAD1, a nuclear transcription factor that forms ternary complexes with YAP/TAZ[43]. We found

highest TEAD1 mRNA copy numbers in smaller cells, while the concentration of TEAD1 mRNA in $V_3$ cells reach the highest level (**Figure 4.7f**). Previous studies have shown that mRNA concentration is typically higher in smaller cells, sometimes by a factor of two or more[39]. By detecting polyA tails, we found that the total mRNA intensity (which in this experiment equals concentration) in $V_3$ cells was four times higher than cells with $V_1$ cells (**Figure 4.7g**).

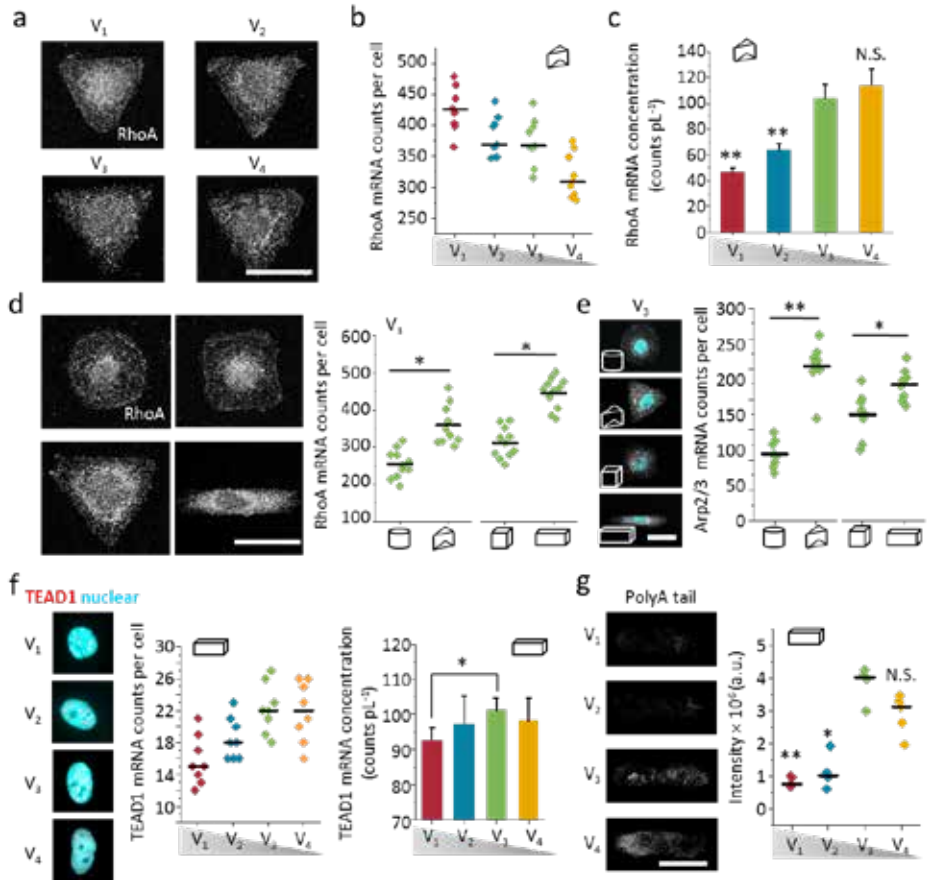


**Figure 4.7. Size and geometry affect mRNA concentration in cells.** (**a**) Representative images of RhoA mRNA in cells with different volumes. (**b, c**) Counts and concentration (divided by cell volume) of RhoA mRNA in cells with different volumes, narrow lines represent the mean within an individual donor, n=10 cells per donor and condition. (**d**) Representative images and total counts of RhoA mRNA in cells with different geometries but same volume ($V_3$). (**e**) Representative images and total counts of Arp2/3 mRNA in cells with different geometries but same volume ($V_3$). (**f**) Representative images, counts and concentration (divided by nuclear volume) of TEAD1 in cells with different volumes. (**g**) Total mRNA in middle stack of cells with different volumes, we measured total mRNA by quantifying total fluorescence intensity from a mRNA FISH probe that detect poly(A) tail. Data are shown as mean ± s.d. for all panels, $n$ = 30-35 cells analyzed for each data point. *P < 0.05, **P < 0.01 (ANOVA using a Tukey post-test), N.S. means no significant difference. Scale bar for all images is 20 µm.

To further confirm this, we stained RhoA-GTPase with active RhoA-GTP monoclonal antibody. Consistent with the mRNA result, we found total RhoA-GTPase intensity decreased (slightly, by a maximum of some 20%) with decreasing cell volume from $V_1$ to $V_4$. However, the intensity of RhoA per stack was the largest for cell volume $V_3$ (**Figure 4.8a and b**), indicating that RhoA was diluted in larger cells. To explore the function of Rho in regulating cell behavior, C3-exoenzyme was used as a specific inhibitor of Rho GTPase, inhibition of Rho activity resulted in decreased formation of stress fibers (**Figure 4.8c**). The diluted RhoA in larger cells might thus impact cell behavior.

Our results on Rho-GTP and mRNA levels within cells of different volume indicates that although cells may have similar amounts of protein or mRNA, their concentration might be different. Volume changes, possibly as a result of the influx of water[44], can thus lead to differences in interactions between key regulatory proteins in the cell. Previous studies have shown that mRNA concentration is typically higher in smaller cells, sometimes by a factor of two or more[39], however, the consequences of this effect, in particular on cell function, are not very clear. We found that RhoA, Arp2/3, TEAD, and total mRNA concentration, were diluted in large cells. It is interesting to note that this dilution of RhoA and Arp2/3, which both play a role in the formation of actin fibers, correlates with a much less pronounced organization of the actin cytoskeleton and higher proportion of G-actin in larger cells.

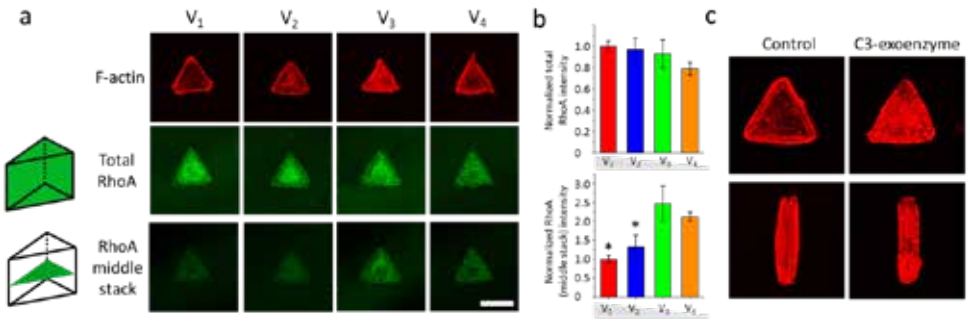


**Figure 4.8. The role of RhoA-GTP on cell behavior.** a) Representative images of F-actin and RhoA staining for cells seeding in microniches with different volumes, total RhoA images were taken with different Z-stacks and overlaid in Fiji software with Image 5D plugin. The distance between two z-stacks was the same (1 µm) for all the sample. The middle stack for different cells was selected to compare RhoA intensity per stack. Scale bar: 20 µm. b) Quantification of total RhoA and middle stack RhoA intensity, normalized to $V_1$ cells. Data are shown as mean ± s.d. with totals of 15-26 cells analyzed, and *P < 0.05. c) Representative images of F-actin staining for $V_3$ cells treated with 10 µM C3-exoenzyme.

### 4.2.5 Size and geometry affect single hMSC fate

Finally, we studied differentiation of hMSCs in 3D microniches. 82% and 67% of $V_1$ and $V_2$ cells, respectively, exhibited adipogenic differentiation, as indicated by staining for

neutral lipids, and very low levels (less than 26%) of osteogenic differentiation, as indicated by alkaline phosphatase staining (**Figure 4.9a and b**). Osteogenic differentiation was significantly enhanced (87%) in cells of $V_3$; however, when cell size decreased to $V_4$, decreased osteogenesis and increased adipogenesis were observed, and compared with $V_1$ and $V_2$ cells, adipogenic differentiation in $V_3$ cells was significantly decreased (**Figure 4.9b**). For hMSCs with fixed cell volume ($V_3$), but different geometries, we found that cylinder and cubic geometry induced more differentiation into adipocytes, compared with cells in triangular prism and cuboid microniches (**Figure 4.9c**). In cylinder and cubic cells, approximately 40-60% and 30-50%, respectively, of cells stained positive for neutral lipids (**Figure 4.9d**). These experiment illustrate that 3D geometry and size play a very important role in regulating cell fate.



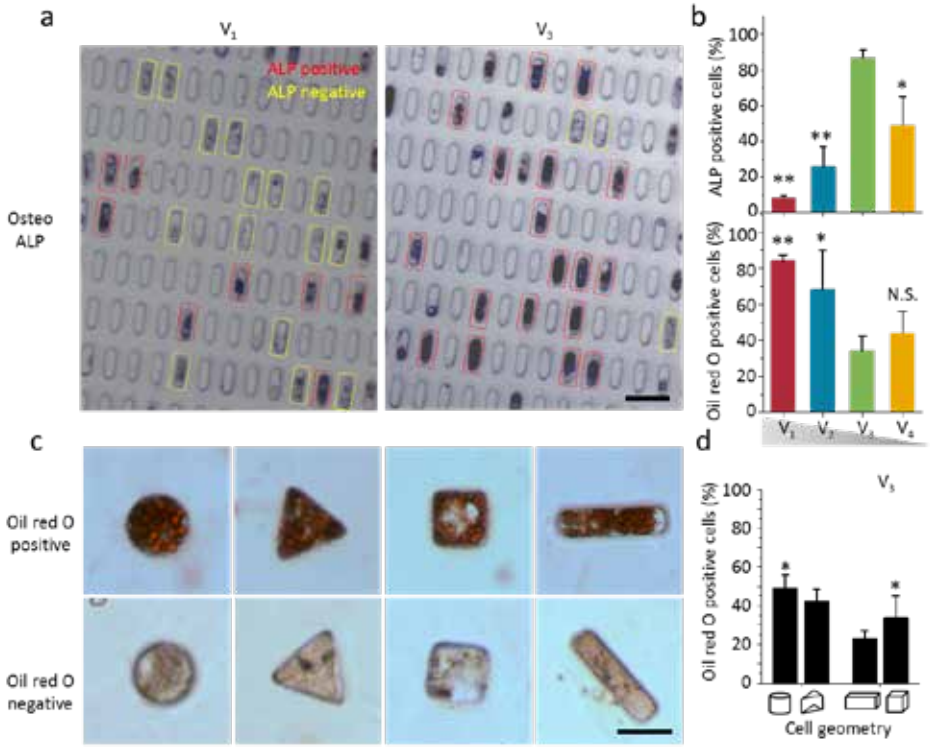


**Figure 4.9. Size and geometry affect single hMSC fate.** (a) Alkaline Phosphatase (ALP) staining for cells with different $V_1$ and $V_3$ volume. The ALP positive cells were determined by applying an optimal threshold to the image, ALP intensity above the threshold were determined as ALP positive. (**b**) Quantification of differentiation after 7 d (ALP) and 10 d (Oil Red O) for cells with different volumes. (**c**) Representative images show Oil red O positive and negative staining for cells with volume ($V_3$) but different geometries. (**d**) Quantification of adipo differentiation after 10 d for cells with different geometries. Mean ± SD, ANOVA oneway analysis followed by Tukey post hoc test shows significance levels of *: $p<0.05$, **: $p<0.01$, N.S. means no significant difference. N ≥ 6 regions of interest (ROI) with totals of 150-200 cells analyzed. Scale bar 20 µm.

## 4.3 Conclusion

The control over cell volume and geometry, and the option to alter the mechanical properties of the gels, as indicated in the chapter 3, enables further studies on the role of biophysical cues. Here, we have focused on single cells, but also at the tissue-level, geometry and biophysical factors play a significant role[45-47]. It is straightforward to investigate a range of other geometries, including asymmetric ones and it will be very interesting to compare the response to geometrical cues between different cell types. We also foresee further broadening of the use of our platform by studying cell division[48] and exploiting the ability to culture multiple cells, which makes it possible to explore how multicellular architectures such as tumor spheroids, organoids, or microtissues, organize within geometrically well-defined 3D spaces.

## 4.4 Acknowledgements

We are grateful to Stéphanie M. C. Bruekers for helpful discussions, José M. A. Hendriks for assistance with cell cultures and Dr. Liesbeth Pierson for assistance with confocal microscopy. Jing Xie is acknowledged for performing some of the experiments and discussions. The department of General Instruments of the Radboud University is acknowledged for providing confocal and light microscopy services.

## 4.5 Experimental section

### 4.5.1 3D microniches preparation and cell seeding

3d microniches were prepared as described in section 3.5.1 of this thesis, cell seeding procedure is also as mentioned in section 3.5.3, the stiffness of MeHA gel in this chapter is ~10 kPa.

### 4.5.2 Differentiation Assays

Differentiation medium was composed of proliferation medium and osteogenic and adipogenic chemical supplements (5 × 10−7 M dexamethasone, 5 mM β-glycerolphosphate, 0.1 mM ascorbic acid-2-phosphate, 250 μM 3-isobutyl-1-methylxanthine, 5 μg/mL insulin, and 5 × 10−8 M rosiglitazone maleate, all from Sigma). hMSCs were cultured for 7 or 10 days in differentiation medium for osteogenic and adipogenic differentiation, respectively. Subsequently, all cells in microniches with different sizes and geometries were fixed with 4% PFA, the lid was removed afterwards and cells were penetrated with 0.2% Triton-X 100 for 10 min. ALP staining was performed by Fast Blue assay (naphthol-AS-MSC phosphate and Fast Blue RR, Sigma) in Tris–HCl

buffer (pH 8.9) and incubated at 37 °C for 1 h. Oil Red O staining was performed by incubating cells with 1.8 mg/mL Oil Red O (Sigma) for 30–60 min at room temperature and then rinsing with 60% isopropanol (Sigma). Images were acquired on a Zeiss inverted microscope (Photometrics, USA).

### 4.5.3 Cell staining

hMSC cells that adhered within MeHA-Fn microniches were fixed with 4% paraformaldehyde (Sigma) for 10 min, and then the lid of microniches was carefully removed, followed by washing three times with PBS and then permeabilised with 0.2% Triton-X100 (Sigma) in reverse osmotic $H_2O$, washed two times with PBS and incubated with 1% bovine serum albumin (BSA) in PBS for 1 h. Subsequently the cells were stained with phalloidin tetramethyl-rhodamine B isothiocyanate (TRITC) (Millipore, R415, 1:1000 in 1% BSA) for 1 h to visualize F-actin, Alexa fluor488–DNaseI (Invitrogen, D12371, 1:500) to visualize G-actin, anti-vinculin (Abcam, AB18058, 1:500) for focal adhesions, anti-myosin IIa (Sigma, 150M4764, 1:500) for cell contractility, YAP/TAZ (Cell signalling, D24E4, 1:500), HDAC3 (Abcam, ab32369, 1:100) or active RhoA-GTP monoclonal antibody (NewEast Biosciences, 26904, 1:100), washed three times with PBS and stained with 4,6-diamidino-2-phenylindole (DAPI) (Millipore, 28718-90-3, 1:1000 in 1% BSA), Alexa-488 labeled goat anti-mouse (Thermo Fisher Scientific, A11029, 1:200) or anti-rabbit IgG (Thermo Fisher Scientific, A10040 or A21071, 1:200) for 1 h at room temperature, followed by three times PBS wash and one $H_2O$ wash. Images were taken within 24 hours after staining using a Leica SP8 confocal laser scanning microscope (Leica, Germany). Myosin-IIa motor activity was inhibited by treating cells with Blebbistatin (Sigma) for 40 min. C3-exoenzyme (Cytoskeleton, Inc.) was used as an inhibitor of Rho GTPase. For quantitative imaging (F-actin, G-actin and Myosin II-a), images were taken with photon counting mode to make sure the intensity of fluorescent settings for all the images were the same.

### 4.5.4 RNA fluorescence in situ hybridization and imaging

To examine the mRNA expression in cells with different geometries and sizes, single-molecule mRNA FISH was performed on different samples. hMSCs in 3D microniches with different geometries and sizes were fixed with 4% paraformaldehyde (sigma) for 10 min, after removing the lid, samples were permeabilized with 70% ethanol before in situ hybridization. Afterwards, samples were stained with oligonucleotide probes for RhoA labelled with Quasar 570 Dye, Arp2/3 mRNA with Atto 647 and TEAD mRNA with Quasar 570 Dye (Stellaris oligonucleotides, Biosearch Technologies). Oligonucleotide probe sequences used to assay RhoA, Arp2/3 and TEAD RNA abundance are RhoA: 5′-CCTGAAGAAGGCAGAGATATGGCAAACAGGATTGGCGCTTTTGGGTACAT-3′, Arp2/3: 5′-CAGCCAGCGCCCGCGATGAC-3′ and TEAD: 5-CTAGCTAGCAACATGGAAAGGATGAGCGACT-3. The poly(dT) probe that detect total mRNA poly A tails was purchased from GeneDetect. Subsequently, samples were washed with 2 × saline sodium citrate buffer (SSC) with 10%

formamide (Ambion), and then 2 × SSC supplemented with DAPI to stain the cell nuclei. Cells in microniches were mounted in 2 × SSC and compressed between two cover slips for imaging. Single mRNA molecules were imaged using a 63x HC PL APO CS2, Na 1.40 objective on the DMi8 microscope of the Leica sp8 automated widefield fluorescence microscope equipped with a cooled DFC 420C, a cooled DFXC365 FX camera and filter sets specific for each fluorophore. Images were taken as a series of optical z-sections (1 microns per section) spanning the vertical extent of each cell.

### 4.5.5 Microscopy data analysis

All confocal images were taken with different z-stacks and overlaid in Fiji software with Image 5D plugin. The distance between two z-stacks was the same (1 μm) for all the sample. For quantitative analysis of the fluorescence intensity, images were taken by confocal microscope with photon counting mode to make sure all camera setting was identical. For generating heat maps of focal adhesions staining, raw fluorescent images were aligned in Fiji and incorporated into a Z stack, the total average intensity per pixel of each cell in microwells was measured afterwards to generate fluorescent heat map. Nuclear volume and spatial chromatin organization was measured by FIJI as described previously[35, 36]. For quantification of copy number from RNA fish images, on collecting images of mRNA FISH samples, total mRNA spots were counted from different z-stacks using custom plugin in Fiji software. The mRNA concentration was calculated by diving the total mRNA spots into cell volume (RhoA, Arp2/3, poly A tails) or nuclear volume (TEAD), depending on the localization of mRNA.

### 4.5.6 Statistics

Statistical analysis was performed with Origin software and one-way analysis of variance (ANOVA) using a Tukey post-test for more than two variables was carried out. “Significant” and “very significant” differences were indicated by * ($P < 0.05$) or ** ($P < 0.01$), respectively. All results were expressed as mean ± standard error.

## 4.6 References


1. Morrison, S.J. & Spradling, A.C. Stem cells and niches: mechanisms that promote stem cell maintenance throughout life. *Cell* **132**, 598-611 (2008).
2. Watt, F.M. & Huck, W.T. Role of the extracellular matrix in regulating stem cell fate. *Nat. Rev. Mol. Cell Biol.* **14**, 467-473 (2013).
3. Vogel, V. & Sheetz, M. Local force and geometry sensing regulate cell functions. *Nat. Rev. Mol. Cell Biol.* **7**, 265-275 (2006).
4. Lutolf, M.P., Gilbert, P.M. & Blau, H.M. Designing materials to direct stem-cell fate. *Nature* **462**, 433-441 (2009).
5. James, J., Goluch, E.D., Hu, H., Liu, C. & Mrksich, M. Subcellular curvature at the perimeter of micropatterned cells influences lamellipodial distribution and cell polarity. *Cell motility and the cytoskeleton* **65**, 841-852 (2008).
6. Théry, M., Pépin, A., Dressaire, E., Chen, Y. & Bornens, M. Cell distribution of stress fibres in response to the geometry of the adhesive environment. *Cell motility and the cytoskeleton* **63**, 341-355 (2006).
7. McBeath, R., Pirone, D.M., Nelson, C.M., Bhadriraju, K. & Chen, C.S. Cell shape, cytoskeletal tension, and RhoA regulate stem cell lineage commitment. *Dev. Cell* **6**, 483-495 (2004).
8. Chen, C.S., Mrksich, M., Huang, S., Whitesides, G.M. & Ingber, D.E. Geometric control of cell life and death. *Science* **276**, 1425-1428 (1997).
9. Kilian, K.A., Bugarija, B., Lahn, B.T. & Mrksich, M. Geometric cues for directing the differentiation of mesenchymal stem cells. *Proc. Natl. Acad. Sci.* **107**, 4872-4877 (2010).
10. Connelly, J.T. *et al.* Actin and serum response factor transduce physical cues from the microenvironment to regulate epidermal stem cell fate decisions. *Nat. Cell Biol.* **12**, 711-718 (2010).
11. Singhvi, R. *et al.* Engineering cell shape and function. *Science*, 696-696 (1994).
12. Parker, K.K., Tan, J., Chen, C.S. & Tung, L. Myofibrillar architecture in engineered cardiac myocytes. *Circulation research* **103**, 340-342 (2008).
13. Schiller, H.B. *et al.* β1-and αv-class integrins cooperate to regulate myosin II during rigidity sensing of fibronectin-based microenvironments. *Nat. Cell Biol.* **15**, 625-636 (2013).
14. Gautrot, J.E. *et al.* Mimicking normal tissue architecture and perturbation in cancer with engineered micro-epidermis. *Biomaterials* **33**, 5221-5229 (2012).
15. Uematsu, K. *et al.* Cartilage regeneration using mesenchymal stem cells and a three-dimensional poly-lactic-glycolic acid (PLGA) scaffold. *Biomaterials* **26**, 4273-4279 (2005).
16. Phelps, E.A. *et al.* Maleimide cross-linked bioactive peg hydrogel exhibits improved reaction kinetics and cross-linking for cell encapsulation and in situ delivery. *Adv. Mater.* **24**, 64-70 (2012).

17. McKinnon, D.D., Domaille, D.W., Cha, J.N. & Anseth, K.S. Biophysically defined and cytocompatible covalently adaptable networks as viscoelastic 3D cell culture systems. *Adv. Mater.* **26**, 865-872 (2014).
18. Luo, Y. & Shoichet, M.S. A photolabile hydrogel for guided three-dimensional cell growth and migration. *Nat. Mater.* **3**, 249-253 (2004).
19. Aizawa, Y., Wylie, R. & Shoichet, M. Endothelial cell guidance in 3D patterned scaffolds. *Adv. Mater.* **22**, 4831-4835 (2010).
20. Tong, X. & Yang, F. Sliding Hydrogels with Mobile Molecular Ligands and Crosslinks as 3D Stem Cell Niche. *Adv. Mater.* (2016).
21. Chevallay, B. & Herbage, D. Collagen-based biomaterials as 3D scaffold for cell cultures: applications for tissue engineering and gene therapy. *Medical and Biological Engineering and Computing* **38**, 211-218 (2000).
22. Ho, W., Tawil, B., Dunn, J.C. & Wu, B.M. The behavior of human mesenchymal stem cells in 3D fibrin clots: dependence on fibrinogen concentration and clot structure. *Tissue engineering* **12**, 1587-1595 (2006).
23. Burdick, J.A. & Prestwich, G.D. Hyaluronic acid hydrogels for biomedical applications. *Adv. Mater.* **23** (2011).
24. Tam, R.Y., Fisher, S.A., Baker, A.E. & Shoichet, M.S. Transparent Porous Polysaccharide Cryogels Provide Biochemically Defined, Biomimetic Matrices for Tunable 3D Cell Culture. *Chemistry of Materials* (2016).
25. Zorlutuna, P. *et al.* Microfabricated biomaterials for engineering 3D tissues. *Adv. Mater.* **24**, 1782-1804 (2012).
26. Ochsner, M. *et al.* Micro-well arrays for 3D shape control and high resolution analysis of single cells. *Lab Chip* **7**, 1074-1077 (2007).
27. Jin, J. *et al.* A triggered DNA hydrogel cover to envelop and release single cells. *Adv. Mater.* **25**, 4714-4717 (2013).
28. Gurkan, U.A. *et al.* Simple precision creation of digitally specified, spatially heterogeneous, engineered tissue architectures. *Adv. Mater.* **25**, 1192-1198 (2013).
29. Fennema, E., Rivron, N., Rouwkema, J., van Blitterswijk, C. & de Boer, J. Spheroid culture as a tool for creating 3D complex tissues. *Trends in biotechnology* **31**, 108-115 (2013).
30. Gallego-Perez, D. *et al.* High throughput assembly of spatially controlled 3D cell clusters on a micro/nanoplatform. *Lab Chip* **10**, 775-782 (2010).
31. Eng, G. *et al.* Assembly of complex cell microenvironments using geometrically docked hydrogel shapes. *Proc. Natl. Acad. Sci.* **110**, 4551-4556 (2013).
32. Neto, A.I. *et al.* Fabrication of Hydrogel Particles of Defined Shapes Using Superhydrophobic-Hydrophilic Micropatterns. *Adv. Mater.* (2016).
33. Gobaa, S. *et al.* Artificial niche microarrays for probing single stem cell fate in high throughput. *Nat. Methods* **8**, 949-955 (2011).
34. Rape, A.D., Guo, W.-h. & Wang, Y.-l. The regulation of traction force in relation to cell shape and focal adhesions. *Biomaterials* **32**, 2043-2051 (2011).

35. Versaevel, M., Grevesse, T. & Gabriele, S. Spatial coordination between cell and nuclear shape within micropatterned endothelial cells. *Nat. Commun.* **3**, 671 (2012).
36. Jain, N., Iyer, K.V., Kumar, A. & Shivashankar, G. Cell geometric constraints induce modular gene-expression patterns via redistribution of HDAC3 regulated by actomyosin contractility. *Proc. Natl. Acad. Sci.* **110**, 11349-11354 (2013).
37. Dupont, S. *et al.* Role of YAP/TAZ in mechanotransduction. *Nature* **474**, 179-183 (2011).
38. Bhaskara, S. *et al.* Deletion of histone deacetylase 3 reveals critical roles in S phase progression and DNA damage control. *Molecular cell* **30**, 61-72 (2008).
39. Padovan-Merhar, O. *et al.* Single mammalian cells compensate for differences in cellular volume and DNA copy number through independent global transcriptional mechanisms. *Molecular cell* **58**, 339-352 (2015).
40. Amano, M. *et al.* Formation of actin stress fibers and focal adhesions enhanced by Rho-kinase. *Science* **275**, 1308-1311 (1997).
41. Welch, M.D., Iwamatsu, A. & Mitchison, T.J. Actin polymerization is induced by Arp2/3 protein complex at the surface of Listeria monocytogenes. *Nature* **385**, 265 (1997).
42. Chimini, G. & Chavrier, P. Function of Rho family proteins in actin dynamics during phagocytosis and engulfment. *Nat. Cell Biol.* **2**, E191-E196 (2000).
43. Varelas, X. The Hippo pathway effectors TAZ and YAP in development, homeostasis and disease. *Development* **141**, 1614-1626 (2014).
44. Guo, M. *et al.* Cell volume change through water efflux impacts cell stiffness and stem cell fate. *Proc. Natl. Acad. Sci.*, 201705179 (2017).
45. Heisenberg, C.-P. & Bellaïche, Y. Forces in tissue morphogenesis and patterning. *Cell* **153**, 948-962 (2013).
46. Friedl, P. & Gilmour, D. Collective cell migration in morphogenesis, regeneration and cancer. *Nat. Rev. Mol. Cell Biol.* **10**, 445-457 (2009).
47. Nelson, C.M., VanDuijn, M.M., Inman, J.L., Fletcher, D.A. & Bissell, M.J. Tissue geometry determines sites of mammary branching morphogenesis in organotypic cultures. *Science* **314**, 298-300 (2006).
48. Minc, N., Burgess, D. & Chang, F. Influence of cell geometry on division-plane positioning. *Cell* **144**, 414-426 (2011).

# Chapter 5

## Mechanical tension mediated by geometric confinement impacts on self-organization of mouse ESCs

*Manuscript in preparation*

## Abstract

The ability of embryonic stem cells (ESCs) to differentiate into geometrically organized tissues with three different germ layers is vital to morphogenesis. While soluble signals are important regulators of this self-organization, we show that gradients of mechanical forces are also involved in controlling this process. We developed a 3D microenvironment to geometrically confine mouse ECS colonies and present mechanical stress patterns, for which we show that ESC colonies underwent self-organization in the presence of soluble factors permitting ESC colony differentiation. Interestingly, changing the shape of the colonies modulated the shape of different germ layers, with CDX2 positive population highly expressed around the edge and in high curvature regions. The gradients of cell tension, mediated by cell migration and proliferation, preceded and mirrored the patterns of differentiation, where regions of high tension resulted in extraembryonic mesoderm differentiation, while cells in the center of low tension regions differentiated to ectodermal lineages. Inhibiting cytoskeletal tension suppressed ESC self-organization. These findings demonstrate a role for mechanical forces in linking multicellular organization to spatial differentials of cell differentiation, and hint at an important guiding principle in tissue patterning.

## 5.1 Introduction

Morphogenesis, the self-organization of the embryo into geometrically organized tissues with three different germ layers (ectoderm, mesoderm and endoderm), is a remarkable demonstration of biology's ability to organize matter in time and space[1]. Replicating this embryonic self-organization in vitro would allow us to investigate the intercellular communication that is responsible for embryonic patterning, and help us to better understand early embryonic development[2-6]. Therefore, there is a need for the development of in vitro methods reconstituting the spatial organization of embryonic germ layers. Recently, Harrison and colleagues showed that embryonic stem cells (ESCs) and trophoblast stem cells (TSCs) cultured in a 3D Matrigel matrix have the ability to self-organize into an embryo architecture[5]. By co-culturing ESCs and TSCs in microwells, a blastocyst-like structure can be generated[6]. A number of groups have shown the use of micro-patterning technologies to control ESC colonies in a circular geometry, demonstrating improved consistency in the cellular response compared to what is achieved in conventional adherent cultures[7-10]. Micropatterned colonies in 2D that recapitulate the spatial organization of germ layers have been demonstrated in both human[11] and mouse ESC[12].

A number of methods have been successfully developed to mimic the self-organization of the embryo, but the underlying mechanisms that induce the self-organization remain unclear. It has been shown that morphogen gradients play a dominant role during gastrulation and that the self-organization of homogenously distributed morphogens into complex, asymmetric patterns provides spatial information to developing tissues [13-16]. Etoc et al. recently reported a reaction diffusion model to explain the role of morphogens gradients in lithographically prepared circular differentiation domains[14]. It is known that, at the signaling level, self-organization in embryoid bodies depends on local activation of the Wnt pathway[15], and control over endogenous signaling profiles is crucial to robustly regulate cell fate and spatial tissue organization. During development, cells not only become patterned into distinct cell fates through the activity of morphogens, but also physically interact to modulate the large-scale geometric architecture of their tissues, including size, shape, and curvature[17-19]. However, unlike morphogen gradients patterning, the fundamental mechanisms that allow embryoids to sense and control their geometric properties are arguably poorly understood. It has been reported that geometrical signals play an important role in cell tension and stem cells differentiation[20-23], but most of the current understanding on the effects of mechanics and geometry in human stem cell fate specification is based on studies with adult human stem cells. Fundamental questions such as how mechanical signals affect spatial organization of different germ layers, how morphogen gradients interact with mechanical force field to create spatially organized differentiation patterns and how

local geometric information is integrated and coordinated within cell collectives to achieve global organization at the level of a tissue, remain unanswered

Here we present a method for generating embryoid colonies in 3D confined environment with organized germ layers from mouse ESC and show that cell tension mediated by geometrical signals can strengthen and alter the influence of morphogen gradients in controlling germ layer position. We find that cells at the edges, high curvature and aspect ratio regions of colonies experience a different mechanical niche than cells in the interior of the colony, and cells at the edge and high curvature region have stronger mechanical interactions. These local high mechanical forces, linked to β1 integrin expression, RhoA activity and E-cadherin expression of the cells, promote cell proliferation, and improve trophoblast-like population differentiation efficiency. In contrast, cells in the center can migrate towards the edge, show decreased cell tension, and interaction between cells leads to activation of N-cadherin and ESC differentiation into different germ layers. Together, this study describes a new method to generate self-organization in ESC colonies and provide evidence of a link between local cellular mechanical tension and spatial organization of ESCs.

## 5.2 Results and discussion

### 5.2.1 Patterned hyaluronic acid -based 3D microniches spatially organize ESCs

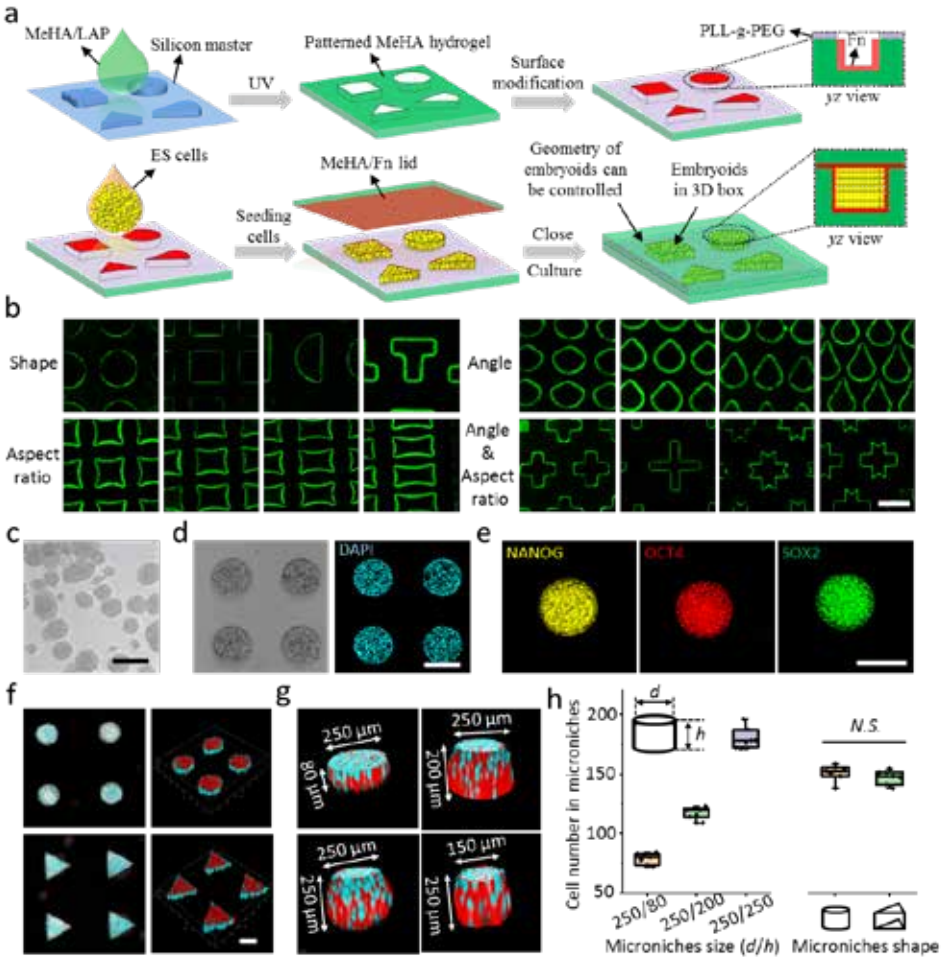


**Figure 5.1 Generation patterned mouse embryoids in a 3D microenvironment.** (a) Schematic of the fabrication of patterned mouse embryoids in 3D microenvironment. (b) Confocal images show homogeneous Fn distribution within 3D microniches with different geometries. Images were taken from the middle stack of 3D microniches. (c) Transmission image show mouse ESCs grown under standard culture. (d) Transmission image and DAPI staining for mouse ESCs grown inside 3D microniches. (e) Immunostaining images of pluripotency makers (NANOG, OCT4 and SOX2) in patterned colonies in growth medium. (f) Confocal images show DAPI (blue) and F-actin (red) staining for patterned colonies after 24 hours culture. (g) High magnification images show DAPI and F-actin of 3D patterned colonies structure with different heights and project areas. (h) Cell number quantification (from DAPI staining) in microniches with different sizes (same shape) or shapes (same size). Scale bar in all figures is 200 μm.

We first patterned and confined ESCs in 3D for an extended period of culture using an approach we previously described[24]. Briefly, we formed microwells in hydrogels of

methacrylated hyaluronic acid (MeHA), a known biocompatible material that allows the diffusion of macromolecules and support self-renewal and differentiation of embryonic stem cells[25], by photopolymerizing MeHA against a silicon photoresist master with different patterns. To prevent cells from adhering to the surface area between the microwells, the outside surface was passivated using poly(L-lysine)-grafted-poly(ethylene glycol) (PLL-g-PEG), and inside microwells was functionalized with fibronectin (Fn) to promote cell adhesion and spreading. ESCs could be selectively seeded into the microwells and an un-patterned hydrogel, prepared from the MeHA and having identical functionalization, can be put over the microwells to function as a lid and fully close the micro-compartments. In this manner, the encapsulated ESCs will be confined in a truly 3D microenvironment with the same adhesions from every sides (**Figure 5.1a**). Fn staining shows selective and uniform Fn deposition on the inside surface of the microwells with different geometries (shapes, angles and aspect ratios) (**Figure 5.1b**). Under standard culture conditions, ESCs grew in colonies that exhibited a wide range of sizes and shapes (**Figure 5.1c**), the heterogeneity in colony geometries could affect cell-cell signaling and result in a loss of reproducible spatial order upon differentiation[11]. By using 3D microniche technology, we were able to create patterns of ESCs in colonies of precisely controlled size and geometry (**Figure 5.1d**). The cells were maintained in the presence of the self-renewal factor (leukemia inhibitory factor, LIF) and homogeneously expressed NANOG, OCT4 and SOX2 across all the patterns (**Figure 5.1e**), suggesting that these ESCs maintained pluripotency and self-renewing capacity. After 12 hours culture, ESCs completely filled 3D microniches with clear actin cytoskeleton. Unlike 2D monolayer cell culture, cells cultured in 3D microniches assemble into 3D constructs with dimensions determined by the gel mould, as shown by 3D confocal images (**Figure 5.1g**). Cells were seeded at same cell density (~50000 cells/cm$^2$), therefore, the number of cells after spreading was almost the same for a fixed microniche volume, for example, one colony contained ~120 cells in a cylinder shape with 250 μm in diameter and 200 in height, increasing microniche volume give rise to increased cell number, regardless of the microniche shape (**Figure 5.1h**).

### 5.2.2 Self-organization of mouse ESCs in 3D micropatterned colonies

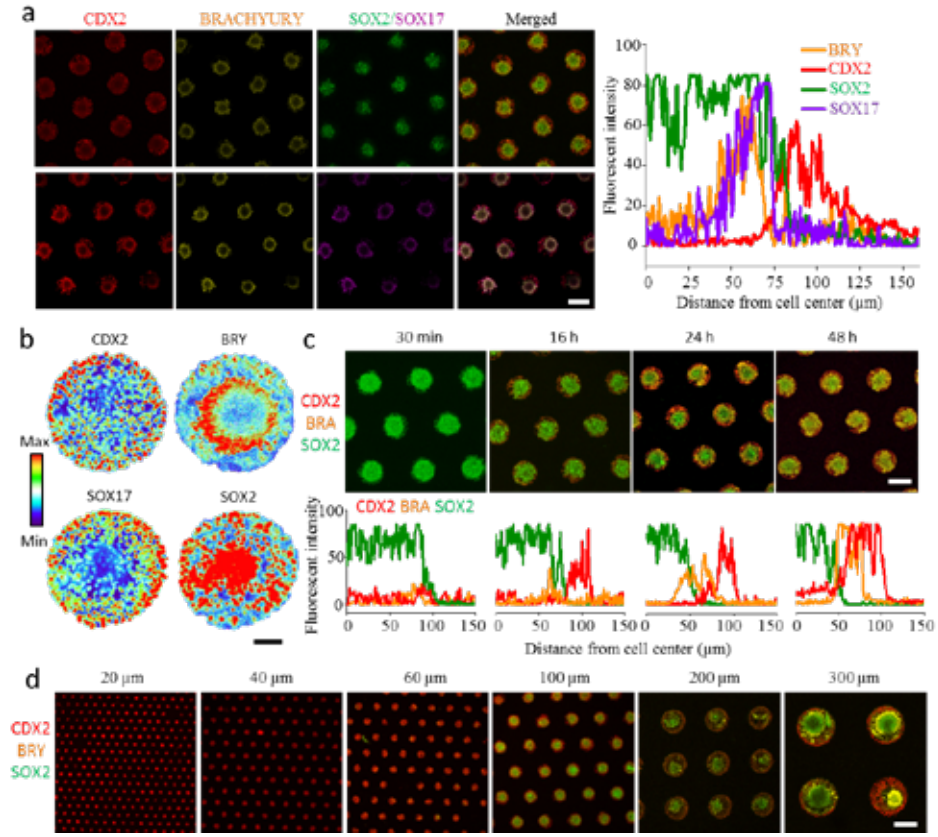


**Figure 5.2 Mouse ESCs differentiated in 3D microniches form self-organized spatial patterns** (a) immunofluorescence images show different germ layer markers, CDX2 for trophectoderm, brachyury (BRY) for mesoderm, SOX2 for ectoderm and SOX17 for endoderm. The plots show quantified immunofluorescence data for the indicated fate markers. (b) Fluorescent heat maps of ≥20 colonies stained for different germ layer marker. (c) Time course of formation of patterned germ layers. Colonies were fixed at different time points after differentiation and stained for CDX2, BRY and SOX2. The plots show quantified immunofluorescence data for different markers at corresponding time spots. (d) Effect of colony size on cell fate. As the colony radius decreased from 300 to 20 μm, the central fate was gradually lost. The height (40 μm) was the same for all the colonies. Scale bar is 200 μm in all figures.

We next examined whether the reproducible cell geometries led to organized germ layer differentiation. After cells proliferated in LIF-containing medium to fill the patterns (~ 1 day), we cultured the patterned colonies in the absence of LIF for 3 days, and we found that mouse ESCs differentiated into organized and radially symmetric rings resembling embryonic patterning. Specifically, we observed a SOX2-positive layer indicative of ectoderm in the center region, a CDX2-positive layer indicative of a trophectoderm-like population at the edge of the colony, and a BRY-positive layer indicative of mesoderm in between (**Figure 5.2a**). Much of the CDX2 positive region also expressed SOX17, the

definitive endoderm marker. As shown in immunofluorescence heatmaps, cells confined to circular geometries differentiated into all three germ layers and a trophoblast-like population in an ordered sequence along the radial axis of the colony (**Figure 5.2b**). In comparison, it has been reported that by using a conventional hanging drop assay or 2D standard culture to generate EBs, ES cells failed to form distinct patterns of germ layers[26-28]. To dynamically monitor the status of lineage differentiation of patterned colonies, we used a mouse ES cell line that stably expresses green fluorescent protein (GFP) driven by the SOX2 promoter. SOX2 expression falls initially at the colony edge and then rises at the center of the colony. After 24 h of self-organization, SOX2 was expressed only at the center of the colonies (**Figure 5.2c**). It has previously been shown that different colony sizes of human ESCs give rise to different differentiation patterns[9-11, 14].We asked whether colony diameter also influenced cell fate specification and patterning in mouse ESCs. After 48 hours of differentiation of mouse ESC in 3D microniches with 100-300 μm in diameter, three concentric domains could be discerned showing SOX2, BRY and CDX2 expression, respectively. However, as the colony size decreased to 60 μm, the SOX2-expressing population at the interior of the colonies was lost, indicating mouse ESCs may specify fates as a function of distance from the colony edge (**Figure 5.2d**).

### 5.2.3 The effect of geometric cues on self-organization of mouse ESC colonies

In addition to gradients of chemical cues, it is clear that tissue development and homeostasis are fundamentally influenced by mechanical cues. Tension-dependent signaling has been widely investigated in single cells[22, 29, 30]. Cell geometry has recently been found to direct lineage commitment of human mesenchymal stem cells[23, 24, 31]. We then ask whether ESC pattern formation is also determined by the interplay between cell-generated forces and the geometry of the local microenvironment. To answer this question, we extended the micro-patterned ESC colonies to different geometries, including semicircles, "L" and "T" shapes, as wells as cross shapes with different aspect ratios and "drop" shapes with different angles. Note that all patterns generated colonies with the same volume, height and project area with the same number of cells (~150 cells in one colony). We found that all patterns resulted in SOX2 expression in the interior, CDX2 expression at the edges and BRY expression in between, regardless of whether the edges were straight, cornered or curved (**Figure 5.3a**). Interesting, cells at sharp curvature and high aspect ratio regions showed elevated expression levels of CDX2. In colonies with "cross" shapes, we found that decreasing the arm lengths impacted on the expression patterns of BRY and SOX2 positive cells. To better understand these gastrulation-like processes, we examined the three-dimensional (3D) structure of the colonies. We found cells at vertical direction express same markers (**Figure 5.3a**). For example, cells from top to bottom around the edge and sharp corner always express CDX2. By systematically changing the angles of a drop shape, we found more cells differentiating into trophoblast-like populations with decreasing angles, but the width

of BRY positive clusters remained the same (**Figure 5.3a and b**). These experiments are striking because subtle geometric differences resulted in significant differences in spatial organization in EBs.

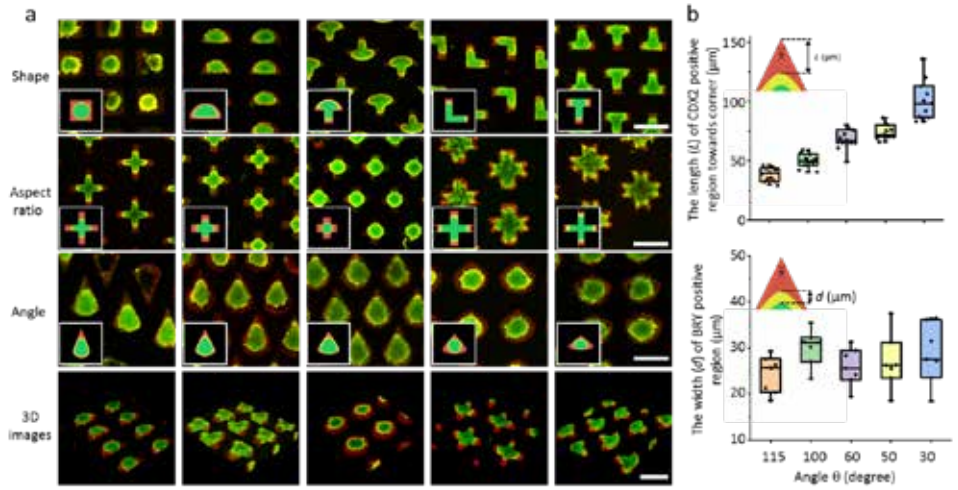


**Figure 5.3 Self-organization of mouse ESC colonies in 3D microniches with different geometries.** (a) CDX2 (red), BRY (yellow) and SOX2 (green) staining for ESC colonies in 3D microniches with different geometries. The size for all colonies is the same, with 250 x 250 μm$^2$ in project area and 250 μm in height. The inset images show schematic drawing of patterning in colonies with different geometries. Scale bar is 200 μm. (b) Quantification results show the effect of angles on the length of CDX2 positive cells towards the corner and the width of BRY positive cells.

### 5.2.4 Geometrical confinement induces cell tension gradients

Previous studies have provided strong evidence that geometrical signals can affect cell adhesion and cell tension[21-23, 32]. Cells adhere to the ECM through several different cell surface receptors including integrins which are involved in mechanosensing and bi-directional transmission of mechanical force[33]. Immunofluorescent staining of β1 integrin (the primary protein involved in cell adhesions) and RhoA (a central regulator of cell contractility) was performed for ESCs with different geometries (**Figure 5.4a**). We found higher intensity of RhoA and β1 integrin at sharp corners and regions with high aspect ratios, indicating higher cell tension in these regions. Cadherins play a vital role in forming adherents junctions with neighboring cells[34] and the regulation of spatial patterning of a variety of responses such as proliferation and gastrulation[35-38]. We stained cells for E-cadherin and N-cadherin in patterned colonies with different sizes (**Figure 5.4b**). We found cells at the perimeter showed higher expression of E-cadherin compared with the center, indicating that cells around the perimeter have more cell-cell interactions and more tension, while cells in the center express more N-cadherin allowing for greater cell motility. Previous studies have shown that cell segregation by active migration away from neighboring cells, a process triggered by N-cadherin, led

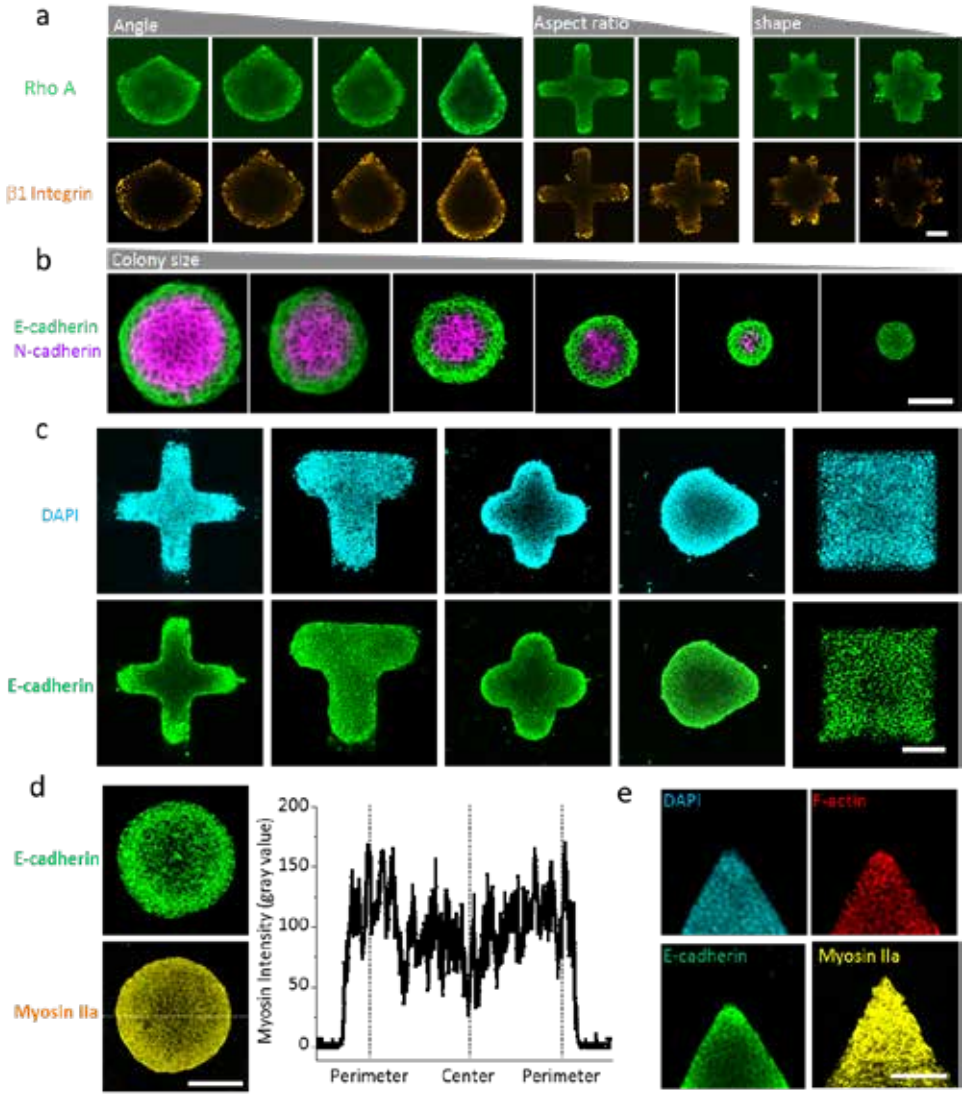


**Figure 5.4 The effect of cell tension on self-patterning formation.** (a) Confocal images (middle stack) show RhoA and β1 integrin staining for ESC colonies with different geometries. (b) E-cadherin and N-cadherin staining for ESC colonies with same geometries but different sizes. (c) DAPI and E-cadherin staining for ESC colonies with different geometries. (d)E-cadherin and Myosin IIa staining for ESCs. Quantification shows myosin IIa intensity across the dotted line. (e) DAPI, F-actin, E-cadherin and Myosin IIa staining for ESC colonies with a sharp corner geometry. Scale bar in all images is 100 μm.

to the formation of endodermal layer forms[35], which is consistent with our findings. With pattern size decreasing, cells in the center gradually lost N-cadherin expression, suggesting that size of colony can affect cell fate, as shown also in **Figure 2e**. E-cadherin

staining for different geometries shows that cells always generate more interactions and higher tension in sharp comers and in high aspect ratio regions (**Figure 5.4c**). E-cadherin expression is also related to myosin-generated cytoskeletal tension[39]. By staining for E-cadherin and mysion IIa, we found that cells around the perimeter (**Figure 5.4d**) and sharp corners (**Figure 5.4e**) expressed higher mysion IIa.

**5.2.5 Synergies between migration and proliferation induces cell density variations**

High cell tension in sharp corners may result from high cell-cell interactions. In order to better understand cell behavior inside 3D microniches and elucidate the triggers for cell tension gradients, we used time-lapse microscopy to monitor and analyze in vitro cell migration during self-organization within cylinder and quadrangle patterns. We found that cells in the center of the colonies with different geometries (cylinder and quadrangle) migrated towards the colony perimeter, resulting in a higher cell density (~2.5cells/100μm$^2$) at the pattern perimeter (**Figure 5.4a**), especially in the corners, which is coincident with a region of higher CDX2 expression. Tissue formation can provide feedback to regulate patterns of proliferation[40]. Therefore, we investigated cell proliferation in colonies with different geometries (cylinder and quadrangle) by performing an EdU incorporation study, and we found more EdU positive cells at the perimeter (~55%) and sharp corners (~72%) than in the center (~16%) (**Figure 5.4b**), indicating cells at the perimeter and in sharp corners can proliferate faster than cells in the center. To confirm that increasing cell number at the pattern perimeter and sharp corner resulted from the combination of biased cell migration of cells to the pattern perimeter and enhanced cell proliferation of cells at the perimeter, we investigated cell density in different colony geometries, we always found a higher cell density at the pattern perimeter and in sharp corners after 24 hour culture, as shown from DAPI staining images and fluorescent heat-map images (**Figure 5.4c**).

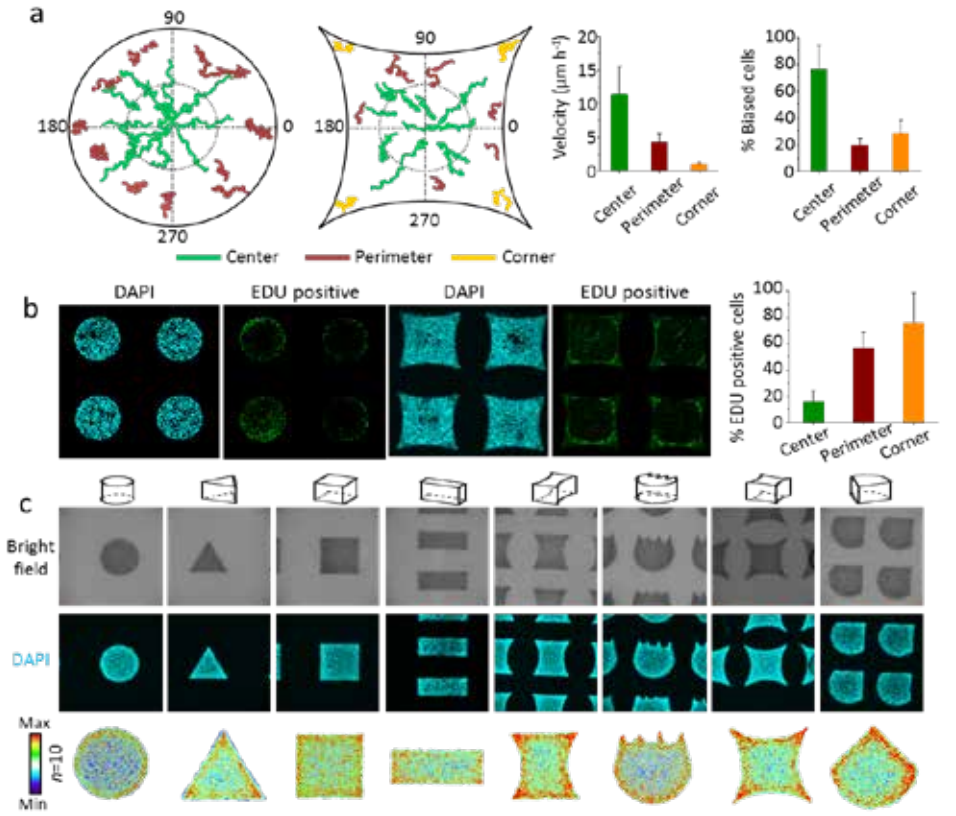


**Figure 5.5 Cell migration and proliferation induce cell density variations.** a. Single-cell tracking showed that cells in the center of the pattern had higher potential to migrate directionally towards the perimeter and corner with a higher migratory velocity and percentage of biased cell migration. Solid outline of cell migration trajectory figure shows the shape of ESC pattern. Data represent as the means with error bars s.d. with n = 40 for four individual patterns multiplied by 10 cells within each pattern. b. EdU staining to visualize the cell proliferation. Quantification figure shows EdU positive cells were located at the corner and near the pattern perimeter compared with the center. Data represent as the means with error bars s.d. with n = 10 individual patterns. c. DAPI staining and fluorescent heat maps of nucleus in ESC colonies with different geometries.

## 5.2.6 Biophysical cues and morphogen gradients direct self-organization of ESCs

We have shown that the expression levels of cell tension related proteins (E-cadherin, RhoA, Myosin IIa) are strongly influenced by geometric cues, and the pattern of tension gradients is the same as the pattern of different germ layers, suggesting that self-organization is (at least in part) dependent on cell tension gradients. To address this possibility, we evaluated the effect of several pharmacological agents that are known to modulate the cells' response to biophysical cues. Two drugs that directly inhibit contractility—Blebbistatin, which inhibits myosin II and Y-27632, which inhibits RhoA/

ROCK pathway — disrupted the organization and removed the influence of shape on differentiation (**Figure 5.6a**). To further investigate whether the tension gradient is important for the correct positioning of different germ layers, we blocked E-cadherin adhesion with anti-E-cadherin antibody to disrupt cadherin-mediated cell–cell adhesion. We were careful to use a concentration of antibody that does not block spreading of the cell to fill the patterned island. Blocking E-cadherin adhesions completely abrogated the organization of the germ layers (**Figure 5.6a**). These results establish the apparent requirement for actomyosin contractility in shape-dependent influence on ESC self-organization.

Previous work suggested that contractile cells may be poised in a state of higher susceptibility to soluble factors and demonstrated the importance of Wnt signaling gradients in regulating patterning formation[14, 15, 20, 41]. To determine the extent to which morphogen gradients play a role in shape-dependent differentiation we used IWP2 to disrupt Wnt-dependent signaling[42], resulting in a complete loss of patterned differentiation in different shapes (**Figure 5.6b**). We also used a GSK3 inhibitor CHIR99021 (CHIR) to activate the canonical WNT/β catenin pathway for mesoderm induction[43]. We found that self-organization was maintained, although treatment with CHIR caused a significant decrease in trophoblast differentiation but an increase in mesoderm differentiation (**Figure 5.6c**). We also probed the role of Wnt signaling by supplementing the media with the recombinant extracellular Wnt3a[44], and we found trophoblast differentiation is no longer sensitive to angles or aspect ratios, as shown in quantification figure, the length of CDX2 population towards the corner was almost the same after adding Wnt3a, indicating that increased morphogen concentration can override the effect of geometrical cues on patterned differentiation (**Figure 5.6d**). From these results we conclude that mechanical signals cannot regulate patterned differentiation independently.

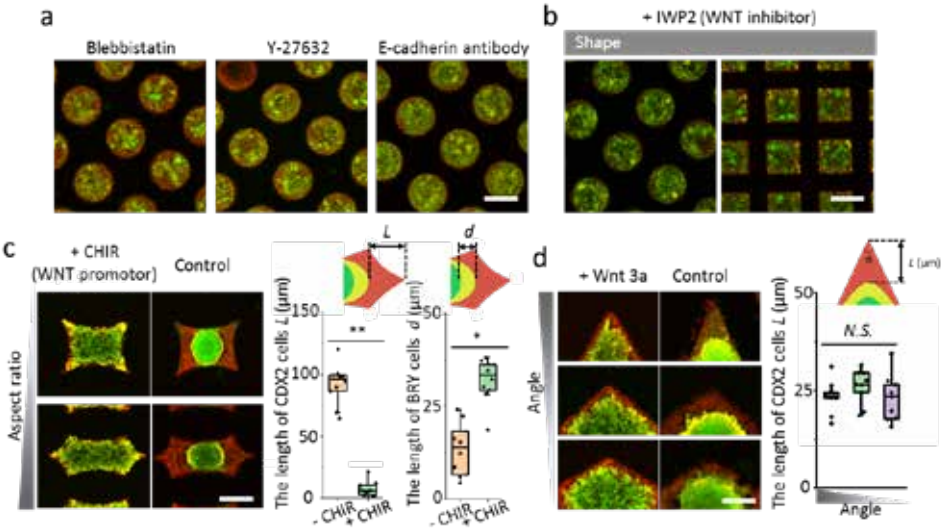


**Figure 5.6. Cell tension and morphogen gradients influence patterned formation.** (a) Confocal images show CDX2 (red), BRY (yellow) and SOX2 (green) staining for ESC colonies treated with different compounds that modulate cell mechanotransduction (b) CDX2, BRY and SOX2 staining for ESC colonies treated with IWP2 (a WNT inhibitor) (c) CDX2, BRY and SOX2 staining for ESC colonies treated with CHIR (a WNT promoter). Quantification data show the length of CDX2 and BRY cells with and without CHIR treatment in same shape. (d) Confocal images show CDX2, BRY and SOX2 staining for ESC colonies after treated with with the recombinant extracellular Wnt3a. Quantification data show the length of CDX2 cells with and without Wnt3a treatment. The size for all colonies is 250 x 250 $\mu m^2$ in project area and 200 μm in height.

## 5.3 Conclusion

Together, these results show that mouse ESCs confined in our 3D microniches can self-organize into different germ layers that resemble the mouse embryo during gastrulation (E5.5) stages (**Figure 5.7a**). The number of cells in mouse embryos at this stage is comparable to that in our microniches. A confined environment is sufficient to induce cells to differentiate to all three germ layers and a trophoblast-like population in an ordered sequence. However, in natural mouse embryo development, gastrulation results in the three germ layers adopting a trilaminar structure with the mesoderm between the ectoderm and endoderm (**Figure 5.7a**), whereas in our study, these layers are positioned differently. In addition, embryos have a well-defined anterior–posterior axis, but micro-patterned colonies do not. By using our microniches, we found the gradients of cell tension, mediated by cell migration and proliferation, preceded and mirrored the patterns of differentiation, where regions of high tension resulted in trophectoderm-like population while cells in the center and at low tension differentiated to ectoderm (**Figure 5.7b**). Future studies should focus on investigating morphogen gradients in

colonies with different geometries as well as getting a better understanding about how mechanics (for example, matrix stiffness) affect self-organization.

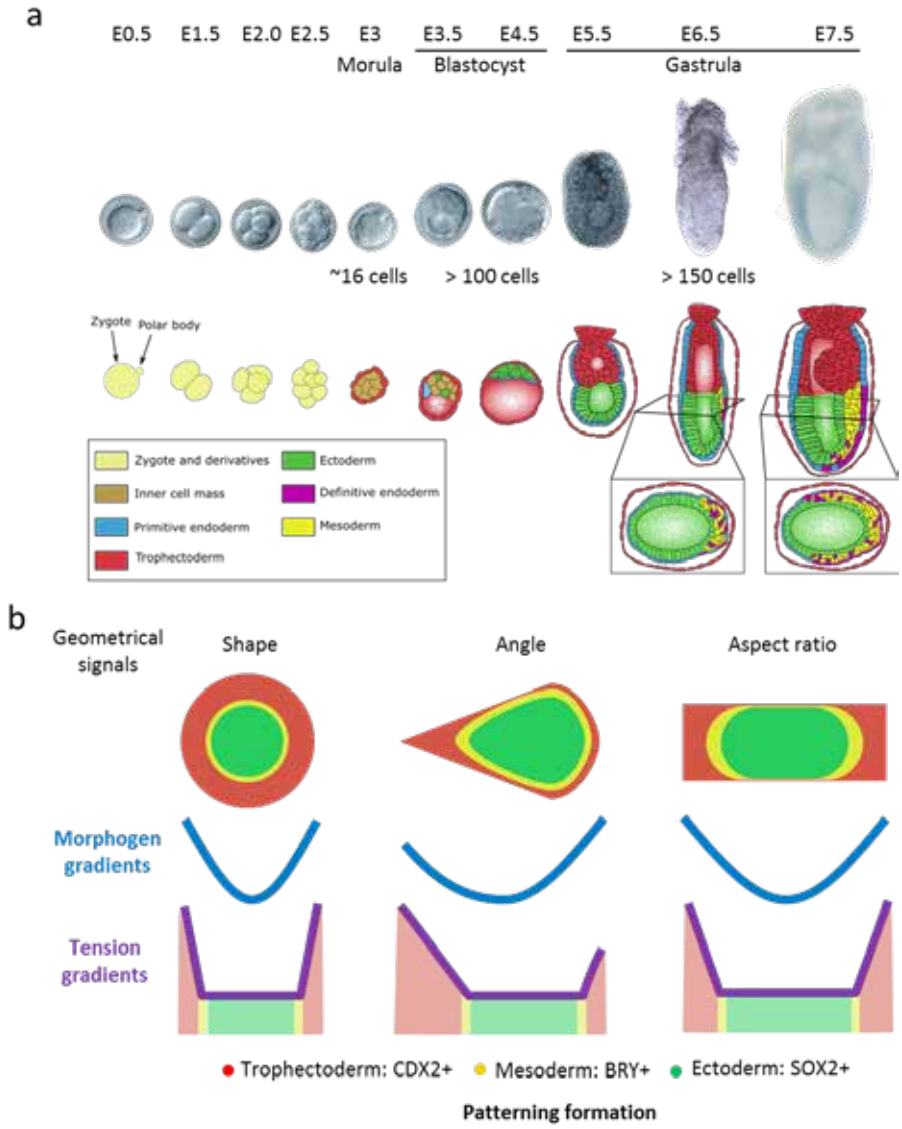


**Figure 5.7 Mechanism of gastrulation-like fate patterning in geometrically confined mouse ESC colonies.** (a) Cartoon illustrating early mouse embryo development. During gastrulation (E5.5-E7.5), Some cells of the posterior region of the epiblast start to change, making an epithelial–mesenchymal transition, that gives the primitive streak. The primitive streak advances to the dorsal, left and right regions of the epiblast. Some primitive streak's cells will intercalate and displace the primitive endoderm. The rest of epiblast gives the ectoderm, the cells that intercalate with the primitive endoderm give the definitive endoderm and the cells in the middle give the mesoderm. (b) Mechanism of fate patterning in geometrically confined mouse ESC colonies. Geometry confinement induces a radial and periodic cell tension gradient.

## 5.4 Acknowledgements

We are grateful to Asst. Prof. Hendrik Marks and Guido van Mierlo for helpful discussions and providing assistance with ES cell cultures. Jose Hendrik is acknowledged for helping with ES cell expansion, Dr. Liesbeth Pierson for assistance with confocal microscopy. We appreciate the help from Aigars Piruska for preparing silicon masks and designing different shapes, Gerard Castro for helping with immunostainings and making gels. The department of General Instruments of the Radboud University is acknowledged for providing confocal and light microscopy services.

## 5.5 Experimental section

### 5.5.1 3D microniches preparation and cell seeding

3d microniches were prepared as described in section 3.5.1 of this thesis, cell seeding procedure is also as mentioned in section 3.5.3. Cell seeding density ($5 \times 10^4/cm^2$) was the same for all experiments. It took 1 day for mESCs to fill up patterns.

### 5.5.2 mESC culture and differentiation

mESC and SOX-2 mESC in this study were obtained from Hendrik Marks's group in Radboud university. These cells were further used to grow inside the microniches and immunostained for endoderm, mesoderm or ectoderm germ layers. The undifferentiated mESCs were cultured and maintained in the medium consisting of high glucose-Dulbecco's Modified Eagles Medium (Invitrogen) supplemented with 15% ES-qualified fetal bovine serum (Invitrogen), 2mM L-glutamine (Invitrogen), 1mM sodium pyruvate, 0.1mM nonessential amino acids (Invitrogen), 1% penicillin–streptomycin, 0.1mM beta-mercaptoethanol (Sigma) and 500 U/mL recombinant leukemia inhibitory factor (LIF, Millipore) at 37 $^oC$ in 5% $CO_2$. Cells were passaged every 2~3 days using 0.05% Trypsin/EDTA. Culture medium was changed daily and 0.1% gelatin-coated plates were used for cell culture. For differentiation assays, cells were cultured in 3D microniches in growth medium for 1 day and then in a medium without LIF (-LIF) for up to 2 days. For WNT signaling experiments, recombinant Wnt3a (10 μM) or CHIR (10 μM) (obtained from R&D Systems) were added to differentiation medium.

### 5.5.3 Immunofluorescence staining

mESCs cultured in microniches were fixed 4% formaldehyde (Sigma) for 10 min at room temperature. Cells were then permeabilized with 0.5% Triton X-100 (Sigma) for 10 min and treated with blocking buffer made of 10% BSA in PBS for 1 h. To visualize the nucleus and cytoskeleton, cells were stained with DAPI (Millipo) and Phalloidin-Atto 633 (Sigma). To investigate cell tension, cell were stained with anti-RhoA (Abcam Ltd.) primary antibody, anti-myosin IIa primary antibody (Sigma). To visualize cell adhesions,

cells were stained with anti-β1 integrins primary antibody (Abcam). Anti-E-cadherin (R&D Systems Europe Ltd.) and anti-N-cadherin (Bio Connect B.V.) primary antibodies were used for investigating cell-cell interactions. To examine the presence of different germ layers, anti-CDX2 primary antibody was used to label trophectoderm, an anti-SOX17 primary antibody (Santa Cruz Biotechnology) was used to label endoderm; an anti-Brachyury primary antibody (Abcam) was used to label mesoderm; and an anti-Sox2 primary antibody (Abcam) was used to label ectoderm. Detection of germ layer types was performed using appropriate Alexa-conjugated secondary antibodies (Invitrogen). Cells were incubated with all primary antibodies (diluted with 2% BSA buffer at a ratio of 1:500) 1 hour at room temperature. After being washed to remove unbound primary antibodies with PBS for three times, cells were incubated with the secondary antibody for 1 h under dark conditions.



### 5.5.4 Inhibition assays

Inhibitors were added to differentiation medium at the following concentrations: Blebbistatin (10 μM), and Y-27632 (2 M) (Calbiochem). E-cadherin blocking antibody (R&D Systems Europe Ltd.) was added to cells in cell culture medium at 1 μg/mL. For Wnt inhibition, medium was supplemented daily with IWP2 (5 nM) (R&D systems).

### 5.5.5 Confocal imaging

After colonies were fixed and immunofluorescent labelled, confocal microscopy was performed using a Leica SP8 microscope to obtain 3D reconstructive images or images with different stacks of the colonies. Different stacks were then merged into a single image by Image 5D - Fiji software. For generating heat maps of staining, raw fluorescent images were aligned in Fiji and incorporated into a Z stack, the total average intensity per pixel of each cell colony in microwells was measured afterwards to generate fluorescent heat map.

### 5.5.6 EdU incorporation study

To inversigate cell proliferation, EdU assay was performed in cell colonies. The protocol is the same as described in section 2.5.8 of this thesis.

## 5.6 References


1. Karsenti, E. Self-organization in cell biology: a brief history. *Nat. Rev. Mol. Cell Biol.* **9**, 255 (2008).
2. Bedzhov, I. & Zernicka-Goetz, M. Self-organizing properties of mouse pluripotent cells initiate morphogenesis upon implantation. *Cell* **156**, 1032-1044 (2014).
3. Deglincerti, A. *et al.* Self-organization of the in vitro attached human embryo. *Nature* **533**, 251-255 (2016).
4. Eiraku, M. *et al.* Self-organizing optic-cup morphogenesis in three-dimensional culture. *Nature* **472**, 51 (2011).
5. Harrison, S.E., Sozen, B., Christodoulou, N., Kyprianou, C. & Zernicka-Goetz, M. Assembly of embryonic and extraembryonic stem cells to mimic embryogenesis in vitro. *Science* **356**, eaal1810 (2017).
6. Rivron, N.C. *et al.* Blastocyst-like structures generated solely from stem cells. *Nature* **557**, 106-111 (2018).
7. Stevens, K. *et al.* InVERT molding for scalable control of tissue microarchitecture. *Nat. Commun.* **4**, 1847 (2013).
8. Nazareth, E.J. *et al.* High-throughput fingerprinting of human pluripotent stem cell fate responses and lineage bias. *Nat. Methods* **10**, 1225 (2013).
9. Deglincerti, A. *et al.* Self-organization of human embryonic stem cells on micropatterns. *Nat. Protoc.* **11**, 2223-2232 (2016).
10. Bauwens, C.L. *et al.* Control of human embryonic stem cell colony and aggregate size heterogeneity influences differentiation trajectories. *Stem cells* **26**, 2300-2310 (2008).
11. Warmflash, A., Sorre, B., Etoc, F., Siggia, E.D. & Brivanlou, A.H. A method to recapitulate early embryonic spatial patterning in human embryonic stem cells. *Nat. Methods* **11**, 847-854 (2014).
12. Morgani, S.M., Metzger, J.J., Nichols, J., Siggia, E.D. & Hadjantonakis, A.-K. Micropattern differentiation of mouse pluripotent stem cells recapitulates embryo regionalized cell fate patterning. *Elife* **7**, e32839 (2018).
13. Tewary, M. *et al.* A stepwise model of Reaction-Diffusion and Positional-Information governs self-organized human peri-gastrulation-like patterning. *Development*, dev. 149658 (2017).
14. Etoc, F. *et al.* A balance between secreted inhibitors and edge sensing controls gastruloid self-organization. *Dev. Cell* **39**, 302-315 (2016).
15. ten Berge, D. *et al.* Wnt signaling mediates self-organization and axis formation in embryoid bodies. *Cell stem cell* **3**, 508-518 (2008).
16. Li, P. *et al.* Morphogen gradient reconstitution reveals Hedgehog pathway design principles. *Science*, eaao0645 (2018).
17. Shyer, A.E. *et al.* Villification: how the gut gets its villi. *Science* **342**, 212-218 (2013).

18. He, B., Doubrovinski, K., Polyakov, O. & Wieschaus, E. Apical constriction drives tissue-scale hydrodynamic flow to mediate cell elongation. *Nature* **508**, 392 (2014).
19. Sasai, Y. Cytosystems dynamics in self-organization of tissue architecture. *Nature* **493**, 318 (2013).
20. Przybyla, L., Lakins, J.N. & Weaver, V.M. Tissue mechanics orchestrate Wnt-dependent human embryonic stem cell differentiation. *Cell Stem Cell* **19**, 462-475 (2016).
21. McBeath, R., Pirone, D.M., Nelson, C.M., Bhadriraju, K. & Chen, C.S. Cell shape, cytoskeletal tension, and RhoA regulate stem cell lineage commitment. *Dev. Cell* **6**, 483-495 (2004).
22. Vogel, V. & Sheetz, M. Local force and geometry sensing regulate cell functions. *Nat. Rev. Mol. Cell Biol.* **7**, 265-275 (2006).
23. Kilian, K.A., Bugarija, B., Lahn, B.T. & Mrksich, M. Geometric cues for directing the differentiation of mesenchymal stem cells. *Proc. Natl. Acad. Sci.* **107**, 4872-4877 (2010).
24. Bao, M., Xie, J., Piruska, A. & Huck, W.T. 3D microniches reveal the importance of cell size and shape. *Nat. Commun.* **8**, 1962 (2017).
25. Gerecht, S. *et al.* Hyaluronic acid hydrogel for controlled self-renewal and differentiation of human embryonic stem cells. *Proc. Natl. Acad. Sci.* **104**, 11298-11303 (2007).
26. Hayashi, K., de Sousa Lopes, S.M.C., Tang, F. & Surani, M.A. Dynamic equilibrium and heterogeneity of mouse pluripotent stem cells with distinct functional and epigenetic states. *Cell stem cell* **3**, 391-401 (2008).
27. Graf, T. & Stadtfeld, M. Heterogeneity of embryonic and adult stem cells. *Cell stem cell* **3**, 480-483 (2008).
28. Poh, Y.-C. *et al.* Generation of organized germ layers from a single mouse embryonic stem cell. *Nat. Commun.* **5** (2014).
29. Parsons, J.T., Horwitz, A.R. & Schwartz, M.A. Cell adhesion: integrating cytoskeletal dynamics and cellular tension. *Nat. Rev. Mol. Cell Biol.* **11**, 633 (2010).
30. Halder, G., Dupont, S. & Piccolo, S. Transduction of mechanical and cytoskeletal cues by YAP and TAZ. *Nat. Rev. Mol. Cell Biol.* **13**, 591-600 (2012).
31. Jain, N., Iyer, K.V., Kumar, A. & Shivashankar, G. Cell geometric constraints induce modular gene-expression patterns via redistribution of HDAC3 regulated by actomyosin contractility. *Proc. Natl. Acad. Sci.* **110**, 11349-11354 (2013).
32. Kassianidou, E., Brand, C.A., Schwarz, U.S. & Kumar, S. Geometry and network connectivity govern the mechanics of stress fibers. *Proc. Natl. Acad. Sci.*, 201606649 (2017).
33. Na, S. *et al.* Rapid signal transduction in living cells is a unique feature of mechanotransduction. *Proc. Natl. Acad. Sci.* **105**, 6626-6631 (2008).
34. Cosgrove, B.D. *et al.* N-cadherin adhesive interactions modulate matrix

mechanosensing and fate commitment of mesenchymal stem cells. *Nat. Mater.* **15**, 1297-1306 (2016).

35. Giger, F.A. & David, N.B. Endodermal germ-layer formation through active actin-driven migration triggered by N-cadherin. *Proc. Natl. Acad. Sci.* **114**, 10143-10148 (2017).
36. Tepass, U., Truong, K., Godt, D., Ikura, M. & Peifer, M. Cadherins in embryonic and neural morphogenesis. *Nat. Rev. Mol. Cell Biol.* **1**, 91 (2000).
37. García-Castro, M.n.I., Vielmetter, E. & Bronner-Fraser, M. N-Cadherin, a cell adhesion molecule involved in establishment of embryonic left-right asymmetry. *Science* **288**, 1047-1051 (2000).
38. Ranscht, B. Cadherins and catenins: interactions and functions in embryonic development. *Curr. Opin. Cell Biol.* **6**, 740-746 (1994).
39. Borghi, N. *et al.* E-cadherin is under constitutive actomyosin-generated tension that is increased at cell–cell contacts upon externally applied stretch. *Proc. Natl. Acad. Sci.* **109**, 12568-12573 (2012).
40. Nelson, C.M. *et al.* Emergent patterns of growth controlled by multicellular form and mechanics. *Proc. Natl. Acad. Sci. U. S. A.* **102**, 11594-11599 (2005).
41. Chen, Q., Shi, J., Tao, Y. & Zernicka-Goetz, M. Tracing the origin of heterogeneity and symmetry breaking in the early mammalian embryo. *Nat. Commun.* **9**, 1819 (2018).
42. Chen, B. *et al.* Small molecule–mediated disruption of Wnt-dependent signaling in tissue regeneration and cancer. *Nature chemical biology* **5**, 100 (2009).
43. Bennett, C.N. *et al.* Regulation of Wnt signaling during adipogenesis. *Journal of Biological Chemistry* **277**, 30998-31004 (2002).
44. Berendsen, A.D. *et al.* Modulation of canonical Wnt signaling by the extracellular matrix component biglycan. *Proc. Natl. Acad. Sci.* **108**, 17022-17027 (2011).

# Chapter 6

## Summary and Perspective

## 6.1 Summary

In order to better understand the interactions between cells and ECM in vitro, techniques are urgently needed for the engineering of microenvironments that recapitulate many aspects of the natural extracellular matrix with precisely controlled biophysical and chemical properties. In this thesis, we demonstrate the utility of extracellular properties in regulating cell fate decisions, and study the importance of cell shape and size in determining cell function as well as how geometrical and mechanical signals affect tissue organization in 3D microenvironments.

**In Chapter 1,** we discussed the role of the microniche in regulating cell function, with the emphasis on the importance of ECM properties. We provided a short overview on different properties of the ECM that regulate cell fate, and then examined the differences between 2D and 3D cell culture. We also gave an overview of the techniques used for investigating the interactions between ECM and stem cells in 3D, and discussed current advances toward designing 3D engineered niches.

**In Chapter 2,** we investigated how local architecture and mechanical properties from the fibrillar microenvironment of collagen gels influence cell behavior. We systematically polymerized collagen gels at different temperatures, providing substrates with tunable mechanics and defined local micro-architecture. Specifically, we found lower polymerization temperatures lead to shorter, thicker and stiffer collagen fibers. We demonstrated the ability of cells to remodel the collagen fibers is a major factor in determining cell spreading, proliferation and migration. High fiber stiffness together with limited connectivity between bundles due to short fiber lengths limited the transfer of cellular traction forces to nearby fibers, resulting in cells devoid of long-range and continuous force transmission, and suppressed cell spreading, proliferation and migration. Cells on such fibers also showed limited focal adhesion formation and promoted adipogenic differentiation of hMSCs. Our findings in this chapter highlight the importance for a better understanding of the role of fiber architecture of the natural ECM on cellular behavior.

**In Chapter 3,** we have developed a methacrylated hyaluronic acid microwell array with a lid on top to construct a 3D microniche, where the internal surfaces of the wells, but not the intervening plateau regions, were coated with fibronectin. Thus, this cell culture platform enables the 3D presentation of adhesive ligands in a controlled microenvironment in which shape, size, stiffness and protein density could be independently controlled. The lid of MeHA hydrogel allows nutrients and waste to pass through, resulting in a high cell viability after 10 days culture. Cells could form integrins and homogenously distributed F-actin inside 3D microniches, indicating

that our 3D microniches fully enclosed cells, providing a completely non-polarized environment of precisely defined volume.

**In Chapter 4,** we further investigated how cell shape and size affect cell function in 3D by using our 3D microniches. We demonstrated that the cell volume, instead of the aspect ratio, project area or shortest axis, was the main factor regulating cell stress fiber formation. Furthermore, we found focal adhesions, nuclear shape, YAP/TAZ localization, cell contractility, nuclear accumulation of HDAC3, and lineage selection, are all sensitive to cell volume (and to a lesser extent geometry). By using RNA-FISH techniques, we shown that concentrations of key components (RhoA, Arp2/3 and TEAD1) were diluted in larger cells, which might impact cell behavior.

**In Chapter 5,** we generated mouse embryonic stem cell colonies in our 3D microniches with organized germ layers, and we showed that cellular mechanical tension plays a major role in controlling germ layer organization. The layering of tissues as they express gastrulation markers could be controlled by minor alterations in colony geometry. We found that cells at the edges and high curvature region of colonies experience a different mechanical niche than cells in the interior of the colony, where cells at the edge and high curvature region have stronger mechanical interactions. These local high mechanical forces, linked to RhoA activity and E-cadherin expression of the cells, promote cell proliferation, and improve trophoblast differentiation efficiency. In contrast, cells in the center have  migrate towards the edge, show decreased cell tension, and interaction between cells leads to activation of N-cadherin and ESC differentiation into different germ layers. Together, this chapter described a new method to generate homogenous self-organization in ESC colonies in 3D and provide evidence of a link between local cellular mechanical tension and spatial organization of ESCs.

Overall, the work presented in this thesis demonstrates the importance and utility of extracellular properties in regulating cell programming and reprogramming, and should aid in the development of biomaterials for more efficiently directing distinct cellular states for the development of synthetic model systems that more accurately recapitulate the in vivo microenvironment.

## 6.2 Perspective

The use of engineered 3D cellular microenvironments enable us to look into the way in which cells interact and react to the external environment. We conclude with some suggestions and thoughts on future directions in this field.

### 6.2.1 Cell dynamics

Cells are not in equilibrium, and understanding how cells accumulate information about their environment over time, how external stimuli are translated molecularly into cell face decisions, and how these decisions manifest themselves in changes in cell phenotype remain core questions for cell biology. Controlling the environment as much as possible can help answer these questions. Future work should focus on developing new ways to track and observe single cell dynamics over extended periods of time, while building up a molecular picture of the changes occurring in the cell.

### 6.2.2. Hydrogel dynamics

It should be noted that changes do not only occur inside cells, cells also modify their surroundings. A very promising development there is the engineering of biomimetic materials with time-regulated properties that react to external stimuli[1-5]. However, most of these dynamic materials only result in mechanical or topographical changes, which is oversimplified when compared to the in vivo cell microenvironment dynamics. Therefore, future work should focus on developing new materials that allow the real-time control of cell microenvironments and fully capture cell dynamics. We can also prepare some multi-functional hydrogel lids (for example, encapsulating some drugs) to realize spatial-temporal control of cell behavior. Ultimately, we need all of this information to understand how we can engineer synthetic microenvironments for developing and maintaining living tissues inside synthetic compartments.

### 6.2.3 Developing real embryo structure or functional organoids

The spatial organization structure of mESCs we developed in chapter 5 is not truly resembling the natural embryo. Recently, by mixing trophoblast stem cells and ESCs, people have shown that these two cells can self-organized into a structure that really mimic embryognesis[6, 7]. A lot of studies have shown that different functional organoids can be achieved in different materials[8-10]. However, separate stages of these processes may require different mechanical environments and ECM components, therefore, synthetic hydrogel networks can be prepared to define the key ECM parameters that govern cell function at different stages. Biochemical and biophysical components can be varied to promote or regulate this process, and their influence on biological processes can be tested systematically.

## 6.3 References


1. Stowers, R.S., Allen, S.C. & Suggs, L.J. Dynamic phototuning of 3D hydrogel stiffness. *Proc. Natl. Acad. Sci.* **112**, 1953-1958 (2015).
2. Guvendiren, M. & Burdick, J.A. Stiffening hydrogels to probe short-and long-term cellular responses to dynamic mechanics. *Nat. Commun.* **3**, 792 (2012).
3. DeForest, C.A. & Tirrell, D.A. A photoreversible protein-patterning approach for guiding stem cell fate in three-dimensional gels. *Nat. Mater.* **14**, 523-531 (2015).
4. Rosales, A.M. & Anseth, K.S. The design of reversible hydrogels to capture extracellular matrix dynamics. *Nat. Rev. Mater.* **1**, 15012 (2016).
5. Rosales, A.M., Vega, S.L., DelRio, F.W., Burdick, J.A. & Anseth, K.S. Hydrogels with reversible mechanics to probe dynamic cell microenvironments. *Angew. Chem.* **129**, 12300-12304 (2017).
6. Rivron, N.C. *et al.* Blastocyst-like structures generated solely from stem cells. *Nature* **557**, 106-111 (2018).
7. Harrison, S.E., Sozen, B., Christodoulou, N., Kyprianou, C. & Zernicka-Goetz, M. Assembly of embryonic and extraembryonic stem cells to mimic embryogenesis in vitro. *Science* **356**, eaal1810 (2017).
8. Eiraku, M. *et al.* Self-organizing optic-cup morphogenesis in three-dimensional culture. *Nature* **472**, 51 (2011).
9. Lancaster, M.A. *et al.* Guided self-organization and cortical plate formation in human brain organoids. *Nature Biotechnology* (2017).
10. Shao, Y. *et al.* Self-organized amniogenesis by human pluripotent stem cells in a biomimetic implantation-like niche. *Nat. Mater.* **16**, 419 (2017).

## Acknowledgement

时间似乎有加速度，进入研究生阶段后，它的速度已经让人追之不及。在荷兰博士求学的一千五百余天如此匆匆，随着毕业论文的完成，我的博士阶段也行将结束。回首过去的四年博士生涯里，我很庆幸的发现我的所得、命运对我的赐予并没有因为时间加快脚步而减少。博士毕业意味着离开，在即将告别的时候，不舍与感激在心头涌动。衷心感谢这四年时间里陪伴我、帮助我的导师们、亲人们和朋友们。因为你们的存在，我枯燥的留学生活才有一份收获、一份乐趣、一份色彩。

At the outset, I would like to thank my advisor, Wilhelm Huck, for giving me an opportunity to do my PhD study in your group, for your guidance and mentoring on my research, and for your support and suggestions on my academic career. I have learnt a lot from you during my PhD study. Your enthusiasm, physical intuition, and ability to approach complex problems with clarity and simplicity, have very much shaped the type scientist that I aspire to be. It's amazing how many ideas can emerge from your office! After each discussion we had there, understanding and inspiration were often amplified and the growth rate of my *"to do list"* always showed a sharp increase. You helped me come up with the thesis topic, and always provide a lot of unique insights for my results. When I made any mistakes, you never blame me, but taught me how to get there in the right way. I also admire your speed in reviewing and submitting my papers, I feel very lucky to be here and I wish you all the best in the future.

Next, I'd like to thank the members of the reading committee: Prof. dr. A. Cambi, Prof. dr. E.H.J. Danen and Dr. J. Gautrot. Thank you very much for your time and efforts in reading and approving this thesis. Your valuable comments helped me improve the manuscript.

I would like to show my grateful appreciation to Professor Yanzhong Zhang, who was my supervisor when I was a Master. He brought me into scientific career. Without him, I may not be able to start my PhD study in the Netherlands. I really appreciate their great support and for providing letters of recommendation for awards, PhD and postdoctoral applications.

All former and current colleagues in HUCK group are acknowledged for your great help during the past years. In particular, I would like to thank the members in the "cells and gels subgroup" for every discussions, useful suggestions and coffee breaks. Stephanie Bruekers, thanks a lot for your contributions to this thesis and your help during my PhD study. You taught me how to make collagen, fibrin, polyacrylamide gels in the first week when I came to the lab, we have been working in close collaboration for my first 2 years, I will never forget the hundreds of gels and experiments that we did together. I hope you don't regret it: this is fun science and according to the promising results and

the rich discussions we had, it seems to work! Jose Hendrik, I was so lucky to have you around during my PhD. Thanks a lot for your experience and assistance in cell culture, the projects wouldn't go smoothly without your help. Jing Xie, one of the greatest joys of my time in Radboud University in Nijmegen was working with you. Without you, I don't have enough space to share my non-scientific and scientific life every day. Thanks for always sharing ups and downs and lots of "grapevine" with me, which I think truly established and reinforced our friendship. As a brother, I do hope that you will find a right person at right time in the near future. Xinyu, you recently joined our group and definitely brought fresh blood and new energy into our team, your positive attitude towards life and rigorous attitude towards science are something that I have to learn, I am sure these characteristics will give you a successful PhD, let's keep in touch in the future and may our friendship last forever. Baoxiu, you are such a kind girl, always willing to help everyone around you, and you are a very hardworking girl, every time when I come to the lab, I know you must be already there. I can't forget the time that we played with microwells, cells, gels and squash together. I wish you all the best in your scientific career and your daily life with Kangkang.

My time in the Netherlands was made enjoyable in large part due to the Chinese community here. Lifei Zheng, every time when I talk to you make me feel on the high speed train, you are not only an "experienced driver", but also a diligent, hard-working and dedicated scientist with broad scientific knowledge, and of course a good father. I hope you will feel like a fish in water when you are working in Germany, and I wish all the best with your little princess. Nannan Deng, I was convinced by your experienced experimental skills in making beautiful liposomes. Enjoy your time in Boston. Yingfeng Tu and Fei Peng, your credits during PhD study were impressive for me. Efficient in work, self-disciplined in lifestyle, and persistent in your dreams, all these made you extraordinary and outstanding from general Chinese guys. At a certain point, you two look like a mirror to remind me to improve myself. Yingfeng, especially thanks for you to help me with lots of PhD graduation stuff. I hope you are doing well with Fei in Guangzhou. Dayong Yang, Hui Zhao, Yongjun Men, Hailong Che, Yang Zhang. And also the "hot-pot" and "player unknown's battlegrounds" community, Wei Li, Zhaobao Zhang and Jieqiong Qu, it is a treasure to meet all of you guys.

I acknowledge all the research facilities in the Institute for Molecules and Materials, in particularly, Liesbeth Pierson, you were always warm-hearted and patient, every time when I asked you a simple question, you will explain me as much as you can, your experiences in confocal microscope contributed a lot to this thesis.

I would like to thank administrative and technical staff members of our lab who have been kind enough to advise and help in their respective roles. Desiree van der Wey, you

were the first person that I met in this building, I think our group were lucky to have you around, and thanks a lot for your daily matters and for translating numerous Dutch letters for me. Theo Peters and Peter van Dijk, you were always efficient in helping me order different antibodies and chemicals from different companies.

The following master students that were working under my supervision for their internship are kindly acknowledged: Nando Katoele and Gerard Castro. Thanks for your hard-working, I was happy to supervise you guys, as much as I learnt from you, I wish you all have a fruitful PhD study.

I also wish to heartily thank my collaborators. Aigars Piruska, I really appreciate your help, I couldn't start any experiments without you. I don't remember how many masters you draw for me and how many wafers you made for me. You were always patient, careful and friendly, and I think that sets an good example to me. I wish you and your family all the best in the future. Guido van Mierlo, you taught me the basics of embryonic stem cell culture, and your background in cell biology was really helpful in many respects, thanks a lot for your contributions to embryonic story. Sjoerd van Helvert, I spent three month with you to learn the principles of atomic force microscopy, without your patience and rigorous, everything would not have gone as smoothly.

I am grateful for the financial support afforded by Radboud Nanomedicine Alliance during my Ph.D. thesis.

A special mention goes to Mum and Dad: your support was determining all along my education and encouraging me to live my life, wherever it is, is certainly the best demonstration of love you could give me. Every time when we meet online, I know you miss me very much. I am very grateful to you for your understanding and supporting.

Finally, I would like to close this thesis with a big THANK to my wife Liyuan Zhang. Thank you for accompanying me through each moment. Thank you for your love! I'm looking forward to our future adventures.

Min Bao, Nijmegen

## About the author

Min Bao was born on 29 May 1990 in Anhui, China. He received the B.Sc. degree in bioengineering from Bengbu College (Anhui, China) in 2011. After this, he moved to Donghua University (Shanghai, China) and obtained his Master's degree in biochemistry and molecular biology in 2014. During his master's, he focused on developing advanced biomaterials for tissue regeneration. In the same year, he received a PhD fellowship from Radboud Nanomedicine Alliance to start his PhD research in the group of Physical Organic Chemistry under the supervision of Prof. Wilhelm Huck at Radboud University (Nijmegen, The Netherlands). His project is mainly about understanding cell-matrix interactions in 3D and micro-tissue engineering based on hydrogels.

## List of publications

Related to this thesis:

- ✓ Min Bao, Jing Xie, Wilhelm T.S. Huck, Recent advances in engineering the stem cell microniche in 3D, *Advanced Science,* 2018, 1800448.

- ✓ Min Bao, Jing Xie, Aigars Piruska, Wilhelm T. S. Huck, 3D microniches reveal the importance of cell size and shape, *Nature Communications*, 2017, 8, 1962.

- ✓ Jing Xie*, Min Bao*, Stephanie Bruekers, Wilhelm T.S. Huck, Collagen Gels with Different Fibrillar Microarchitectures Elicit Different Cellular Responses, *ACS Applied Materials & Interface, 2017,* 9 (23): 19630–19637 (* Co-first author)

- ✓ Min Bao, Jing Xie, Guido van Mierlo, Xinyu Hu, Gerard Castro, Aigars Piruska, Hendrik Marks, and Wilhelm T.S. Huck, Mechanical tension mediated by geometric confinement drives mouse ESC patterned differentiation, manuscript in preparation.

Related to PhD projects:

- ✓ Stephanie Bruekers*, Min Bao*, José Hendriks, Klaas W. Mulder, Wilhelm T. S. Huck, Adaptation trajectories during adhesion and spreading affect future cell states, *Scientific Reports*, 2017, 7, 12308. (* Co-first author)

- ✓ Sjoerd G.J. Postma, Ilia N. Vialshin, Casper Y. Gerritsen, Min Bao, Wilhelm T.S. Huck, Preprogramming complex hydrogel responses using enzymatic reaction networks, *Angewandte Chemie International Edition*, 2017, 56 (7), 1794-1798.

- ✓ Hatice Imran, Min Bao, Sjoerd van Helvert, John A. Jansen, Sander Leeuwenburgh, Frank Walboomers, Differentiation-specific effects of mechanical loading and substrate elasticity on mesenchymal stem cell behavior, *ACS Biomaterials Science & Engineering,* In revision

- ✓ Shuanhong Ma, Mingming Rong, Peng Lin, Min Bao, Jing Xie, Xiaolong Wang, Wilhelm T.S. Huck, Feng Zhou, Weimin Liu, Fabrication of 3D tubular hydrogels materials through on-site surface free radical polymerization, *Chemistry of Materials*, In revision

- ✓ Min Bao, Jing Xie, Xinyu Hu, Baoxiu Wang, Nando Katoele, Aigars Piruska, Wilhelm T.S. Huck, Cellular volume regulation and matrix stiffness direct stem cell behavior in a 3D microniche, submitted.

- ✓ Jing Xie, Min Bao, Wilhelm T.S. Huck, Intracellular energy fluctuations due to cytoskeleton organization trigger AMPK-mediated stem cell fate decisions, manuscript in preparation.